UNIVERSITEIT VAN PRETORIA
UNIVERSITY OF PRETORIA
YUNIBESITHI YA PRETORIA

Electrical characterization of ZnO and metal ZnO contacts

by

WILBERT MTANGI

Submitted in partial fulfilment of the requirements for the degree

MAGISTER SCIENTIAE

in the Faculty of Natural and Agricultural Science at the University of Pretoria

Supervisor/Promoter: Professor F. D. Auret

Co-supervisor: Dr. J. M. Nel

October 2009

© University of Pretoria

UNIVERSITEIT VAN PRETORIA
UNIVERSITY OF PRETORIA
YUNIBESITHI YA PRETORIA

Electrical characterization of ZnO and metal ZnO contacts

By Wilbert Mtangi

Supervisor: Prof. F. D. Auret

Co-supervisor: Dr. J. M. Nel

SUMMARY

The electrical properties of ZnO and contacts to ZnO have been investigated using different techniques. Temperature dependent Hall (TDH) effect measurements have been used to characterize the as-received melt grown ZnO samples in the 20 – 330 K temperature range. The effect of argon annealing on hydrogen peroxide treated ZnO samples has been investigated in the 200 – 800°C temperature range by the TDH effect measurement technique. The experimental data has been analysed by fitting a theoretical model written in Matlab to the data. Donor concentrations and acceptor concentrations together with the associated energy levels have been extracted by fitting the models to the experimentally obtained carrier concentration data by assuming a multi-donor and single charged acceptor in solving the charge balance equation. TDH measurements have revealed the dominance of surface conduction in melt grown ZnO in the 20 – 40 K temperature range. Surface conduction effects have proved to increase with the increase in annealing temperature. Surface donor volume concentrations have been determined in the 200 – 800°C by use of theory developed by D. C. Look.

Good rectifying Schottky contacts have been fabricated on ZnO after treating the samples with boiling hydrogen peroxide. Electrical properties of these Schottky contacts have been

investigated using current-voltage (*IV*) and capacitance-voltage (*CV*) measurements in the 60 – 300 K temperature range. The Schottky contacts have revealed the dominance of predominantly thermionic emission at room temperature and the existence of other current transport mechanisms at temperatures below room temperature.

Polarity effects on the Schottky contacts deposited on the O-polar and Zn-polar faces of ZnO have been demonstrated by the *IV* technique on the Pd and Au Schottky contacts at room temperature. Results obtained indicate a strong dependence of the Schottky contact quality on the polarity of the samples at room temperature. The quality of the Schottky contacts have also indicated their dependence on the type of metal used with the Pd producing contacts with the better quality as compared to the Au.

Schottky barrier heights determined using temperature dependent *IV* measurements have been observed to increase with increasing temperature and this has been explained as an effect of barrier inhomogeneities, while the ones obtained from *CV* measurements have proved to follow the negative temperature coefficient of the II – VI semiconductor material, i.e. a decrease in barrier height with increasing temperature. However, the values have proved to be larger than the energy gap of ZnO, an effect that has been explained as caused by an inversion layer.

Acknowledgements

For the success of this study, I wish to extend my sincere gratitude to the following people for their support:

- My academic supervisor and promoter, Prof F. D. Auret for his social and financial support. I would also like to thank him for the fruitful discussions and encouragement.
- The Head of the Physics department, Prof. J. B. Malherbe for the part time teaching jobs which he organised for me to supplement my finances.
- My co-supervisor Dr. J. M. Nel for the discussions we had and suggestions in the compilation of this thesis.
- Dr. W. E. Meyer, and my seniors (PhD students), C. Nyamhere, P. J. Janse van Rensburg, A. Chawanda, M. Diale and Sergio Coelho for the discussions we had.
- Hannes de Meyer and Louwrens van Schalkwyk for the support they gave in the drawing of the diagrams used in this thesis and moral support.
- Financial assistance provided by the National Research Foundation (NRF)
- My late mother Mrs E. Mtangi for the love and support.
- My family and friends for their faith in my abilities, continuous support and encouragement.

UNIVERSITEIT VAN PRETORIA
UNIVERSITY OF PRETORIA
YUNIBESITHI YA PRETORIA

Table of contents

CHAPTER 1: **Introduction**……………………………………………………... 1

CHAPTER 2: **Properties of ZnO as a semiconductor**…………………… 5

2.1: Introduction……………………………………………….…... 5

2.2: Crystal structure ……………………………………….. 5

2.3: Band structure……………………………………………….. 6

2.4: Carrier transport phenomena……………………………… 7

2.4.1: Introduction……………………………………….…… 7

2.4.2: Mobility……………………………………………… 8

2.4.3: Scattering mechanisms……………………………… 10

CHAPTER 3: **Electrical characterization techniques**…………………… 14

3.1: Introduction……………………………………………….. 14

3.2: **The Hall effect technique**……………………………... 14

3.2.1: Introduction…………………………………………. 14

3.2.2: The Hall effect theory………………………………. 14

3.2.3: The Hall coefficient determination…………………. 17

3.2.4: Resistivity determination…………………………… 19

3.2.5: Factors affecting the measured Hall voltage……….. 20

3.2.5.1: The IR effect……………………………… 20

3.2.5.2: Galvanomagnetic effects………………….. 20

3.2.5.2.1: The Ettingshausen effect……….. 21

3.2.5.2.2: The Nernst effect………………. 21

3.2.5.2.3: The Righi-Leduc effect………… 21

3.2.6: Correction of IR and Galvanomagnetic effects……. 21

3.2.7: Effect of contact size, geometry, and position……… 23

3.2.8: Impurity concentration determination……………… 25

3.2.9: Surface conduction…………………………………. 26

3.3: ***IV* measurements on Schottky Barrier Diodes…………** 27

3.3.1: Introduction………………………………………… 27

3.3.2: Metal semiconductor contacts……………………… 27

3.3.2.1: Introduction……………………………… 27

3.3.2.2: Band bending …………………………… 28

3.3.2.3: Ohmic contacts …………………………… 29

3.3.2.4: Schottky contacts ………………………… 31

3.3.2.4.1: Forward biasing………………… 32

3.3.2.4.2: Reverse biasing………………….. 32

3.3.3.1: Surface cleanliness………………………… 33

3.3.3.2: Surface states……………………………… 34

3.3.3.3: Fermi level pinning………………………… 35

3.4: **Temperature dependence of *IV* measurements on Schottky barrier diodes…………………………………** 36

3.4.1: Introduction………………………………………… 36

3.4.2: Current transport processes………………………… 37

3.4.2.1: Thermionic emission current……………… 37

3.4.2.2: Generation recombination current………… 40

3.4.2.3: Quantum mechanical tunneling…………… 41

3.4.3: The Richardson constant……………………………. 43

3.4.3.1: Barrier Height inhomogeneities…………… 44

3.4.3.2: The modified Richardson constant……… 46

3.5: ***CV* measurements on Schottky Barrier Diodes ………** 47

3.5.1: Introduction…………………………………………. 47

3.5.2: The depletion width approximation…………………. 47

3.5.3: The built in potential………………………………… 47

3.5.4: The depletion capacitance…………………………… 48

3.5.5: The image charge and image force………………….. 50

3.5.6: Barrier height determination………………………… 52

3.5.7: Frequency dependence of the Schottky barrier height.. 53

CHAPTER 4: **Experimental Techniques**………………………………… 57
4.1: Temperature dependent Hall measurements………………. 57
4.2: *IV*, *CV* measurements: …………………………………… 59
4.2.1: Sample preparation………………………………….. 59
4.2.2: Contact fabrication..………………………………… 59
4.3: Temperature dependent *IV* measurements…..…………… 60
4.4: Temperature dependent *CV* measurements………………. 61

CHAPTER 5: **Results and discussions**…………………………………… 62
5.1: **Hall effect measurements on ZnO** …………………….. 62
5.1.1: Temperature dependent Hall measurements (TDH) .. 62
5.1.1.1: Carrier concentration-temperature analysis…………………………………… 62
5.1.1.2: Mobility-temperature analysis…………….. 66
5.1.1.3: Annealing studies of ZnO………………… 69
5.1.1.3.1: Introduction…………………….. 69
5.1.1.3.2: Carrier concentration-temperature analysis…………………………. 69
5.1.1.3.3: Mobility-temperature analysis…… 72
5.1.2: Conclusions…………………………………………… 73
References…………………………………………………… 74
Publications……………………………………………………………… 75

5.2: ***IV* measurements on ZnO Schottky Barrier Diodes..…..** 82
5.2.1: General *IV* characteristics of Pd/ZnO Schottky diode.. 82
5.2.1.1: The ideality factor………………………….. 85
5.2.1.2: Series resistance……………………………. 86
5.2.1.3: Saturation current …………………………. 87
5.2.1.4: Barrier height determination……………….. 88

5.2.1.5: Reverse leakage current…………………… 88
5.2.2: Conclusions……………………………………….. 89
References…………………………………………………… 91
Publications……………………………………………………………… 92

5.3: **Temperature dependent *IV* measurements on ZnO Schottky Barrier Diodes** ..……………………… 96
5.3.1: The general *IV* characteristic………………………… 96
5.3.2: Temperature dependence of the ideality factor……… 98
5.3.3: Temperature dependence of series resistance………... 100
5.3.4: Temperature dependence of saturation current……… 101
5.3.5: Temperature dependence of *IV* barrier height……….. 102
5.3.6: Determination of the effective Richardson constant for ZnO…………………………………… 104
5.3.7: Conclusions…………………………………………… 106
References…………………………………………………… 107
Publications……………………………………………………………….. 108

5.4: ***CV* measurements on ZnO Schottky Barrier Diodes …..** 113
5.4.1: *CV* characteristics of Pd/ZnO Schottky diodes……… 113
5.4.1.1: The built in potential…………..………… 114
5.4.1.2: Determination of the barrier height………… 116
5.4.1.3: Depth profiling……………………………… 118
5.4.2: Temperature dependence of *CV* barrier height……….. 120
5.4.3: Conclusions…………………………………………… 121
References…………………………………………………… 123
Publications……………………………………………………………….. 124

CHAPTER 6: **Conclusions……………………………………………………..** 128

CHAPTER 1.

Introduction

Zinc Oxide (ZnO) has become the second most widely studied material after Si. It is presently used in many diverse products, such as phosphors, paints, piezoelectric transducers, varistors and transparent conducting layers for the photovoltaic industry. Due to its superior electronic properties that include its high exciton binding energy of 60 meV, its wide, direct bandgap of 3.37 eV and excellent radiation hardness, it has attracted the attention of many researchers as it can be used considerably in electronic and optoelectronic devices that can operate in the blue and ultraviolet (UV) spectrum, though not very efficient as yet [1]. Other advantages of ZnO lie in the availability of fairly high quality bulk single crystals [2] and amenability to conventional wet chemistry etching, compatible with Si technology. The ease of etching ZnO with all acids and alkalis provides an opportunity for the fabrication of small-size devices [2].

Knowledge of the electrical properties of semiconductor material is of vital importance in device fabrication as it determines the use of the material in both electronic and optoelectronic applications. To date, several studies to find information about the electrical properties of ZnO have been performed using different techniques. Reports on the existence of native and unintentionally introduced defects have been published from photoluminescence (PL) measurements [2]. Hall Effect measurements have also been used to study the shallow defects in ZnO [3,4,5], while deep level transient spectroscopy (DLTS) has been widely used to study the deep level defects [6]. Temperature dependent Hall effect measurements can also give valuable and important information pertaining to the current transport mechanisms that are likely to occur in a material by analysing the values of carrier concentration. The frequency response together with the conductivity of a semiconductor material can also be deduced from the Hall Effect measurements by considering the mobility of the carriers in a material.

In the study of deep level defects using DLTS, a simple p-n junction or a metal-semiconductor (MS) contact can be used. A Schottky contact good enough for DLTS measurements must ideally have low leakage currents, and low series resistance that does not

affect capacitance determination. The quality of a Schottky contact in terms of stability at different temperatures is also crucial as DLTS is a temperature dependent technique. High quality Schottky contacts are also important in device fabrication. The first Schottky contacts to ZnO were reported by Mead in 1965 [7]. Since then, an increasing amount of research has been carried out using different metals as Schottky contacts. In the majority of the reported work, the contacts have produced high leakage currents and in most cases have proved to be ohmic. Reported barrier heights on MS contacts to ZnO are in the range 0.6-0.84 eV [2]. Reports from the research carried out on these MS contacts have indicated the dependence of the Schottky contact quality on the type of metals used, with high work function metals producing better quality Schottky contacts to undoped ZnO samples [2] and sample cleaning procedures prior to metal deposition, with the latter considered as a major effect. Fabrication of stable Schottky contacts to ZnO remains a challenge despite numerous investigations. In the earlier research, organic solvents have been used, and of late the contact quality has reportedly been improved by the use of oxidising treatment where etching using acids has been employed. Significant improvement in the current voltage characteristics of as-deposited gold Schottky contacts after plasma cleaning was reported by Koppa *et al* [8].

Polarity of the ZnO samples is also another factor that can adversely affect Schottky contact quality to bulk ZnO. Since ZnO has a high iconicity and a wurtzite structure with a lack of inversion symmetry along the c-axis, it produces a large spontaneous polarization with bound sheet charges of opposite sign occurring at the Zn-polar and O-polar faces [9]. It is expected that the O-polar face and the Zn-polar face of bulk grown ZnO produce contacts of different qualities and properties. This is because of the termination of the different faces. During the process of termination, electronic configurations different from the bulk material and from each other are formed, creating incomplete covalent bonds, rendering differences in the properties the two faces. The behaviour of a Schottky contact under an applied voltage is also important in electronic device technology. A lot of work has been carried out in determining the electrical properties of the semiconductor devices using current voltage and capacitance voltage techniques at room temperature. Little has been reported about the temperature dependence of the current voltage and capacitance voltage characteristics on metal ZnO contacts.

This study presents the results obtained from the electrical characterization of bulk ZnO using temperature dependent hall (TDH) effect, current-voltage (IV) and capacitance-voltage (CV)

techniques. An overview of the properties of ZnO as a semiconductor material is given in chapter 2, with particular reference to its, crystal structure, band structure and its mobility and carrier transport phenomena.

Chapter 3 provides the theory of the electrical characterization techniques and a background of the existing information on the findings from the work that has been carried out on ZnO. In chapter 3.2, theory on the Hall effect technique as a tool for semiconductor characterization is discussed explaining how the Hall coefficient, Hall voltage, carrier concentration, and mobility can be determined. In chapter 3.3, the current voltage measurements theory is outlined with particular reference to the general structure of the Schottky diode. An overview on the formation of the ohmic contacts and the Schottky contacts is given based on the existing literature and results, while chapter 3.4 provides some information on the temperature dependence of the Schottky contacts with the main focus being on the current transport mechanisms and determination of the barrier height and ideality factors. In chapter 3.5, the capacitance voltage technique is discussed as a method for barrier height determination in Schottky diodes.

Chapter 4 gives details of the experimental setups and techniques that were employed in order to obtain the results in this study. Chapter 4.1 focuses on the Hall effect technique, while chapter 4.2 deals with the current voltage and capacitance voltage measurements, chapter 4.3 addressing the temperature dependence of the IV and CV measurements.

In chapter 5, the results obtained from experiments are discussed, comparing and contrasting with what was obtained in some other research work carried out on ZnO. Chapter 5.1 gives an analysis of the Hall effect measurements, while chapter 5.2 discusses about the findings from the current voltage measurements performed at room temperature. The results from the temperature dependence of the IV measurements are discussed in chapter 5.3. Temperature dependent CV measurement results are discussed in chapter 5.4.

Chapter 6 gives a summary of all the results obtained and discussed in this study.

References

[1] F. D. Auret, M. Hayes, J. M. Nel, W. Meyer, P. J. Janse van Rensburg, W. Wesch, E. Wendler, Mater. Res. Soc. Symp. Proc. Vol 957 (2007).

[2] U. Ozgur, A comprehensive review of ZnO materials and devices, *J. Appl. Phys*. 98, 41301 (2005).

[3] G. H. Kassier, M. Hayes, and F. D. Auret, J. Appl. Phys. 102, 014903 (2007).

[4] D. C. Look, H. L. Mosbacker, Y. M. Strzhemechny, and L. J. Brillson, Superlattices and Microstruct. 38, 406 (2005).

[5] G. Brauer, W. Anwand, W. Skorupa, J. Kuriplach, O. Melikhova, J. Cizek, I. Prochazka, C. Moisson, H. von Wenckestern, H. Schmidt, M. Lorenz, M. Grundmann, Supperlattices and Microstruct. 42 259-264 (2007).

[6] F. D. Auret, S. A. Goodman, M. Hayes, M. J. Legodi, H. A. van Laarhoven, D. C. Look, J. Phys. Condens. Matter 13 8989-8999 (2001).

[7] C. A. Mead, Phys. Lett,18, 218 (1965).

[8] B. J. Koppa, R. F. Davis, and R. J. Nemanich, Appl. Phys. Lett. 82, 400 (2003).

[9] M. W. Allen, M. M. Alkaisi and S. M. Durbin.: Appl. Phys. Lett., 89. 103520,(2006).

CHAPTER 2: ZnO as a semiconductor

2.1: Introduction

ZnO is a group II-VI compound semiconductor with a wide and direct bandgap (3.37eV at room temperature). It contains some superior electronic parameters such as high breakdown voltage, high electron saturation velocity [1], high thermal conductivity [2] and high radiation tolerance [3], which are better than those of the classical semiconductors, such as Si and GaAs, and is also compatible with the wide band gap semiconductors, like SiC and GaN [4]. Since it has a high saturation velocity, ZnO can be used to fabricate devices, which can operate at very high speeds and hence improved efficiency. Due to its large exciton binding energy of about 60meV and high melting point (2250K) [5], ZnO is highly efficient in excitonic emission devices, since it enables stability at high device operating temperatures and this makes it a better material than GaN. This material also allows for band gap engineering by alloying it with MgO and CdO to increase and decrease its energy bandgap, respectively [6] thereby modifying its optoelectronic properties. From the abovementioned properties, ZnO has attracted much attention from researchers and also in commercial applications as it can be used in the manufacture of UV photodetectors, acoustic wave devices, light emitting diodes, laser diodes and high frequency electronic devices [5].

2.2: Crystal structure.

This defines the structure formed when a basis of atoms (Zn and O) is attached identically to every lattice point. For ZnO, three lattice structures can be formed. These are the rock salt, zinc blende and the wurtzite structure. Of the three structures, the wurtzite structure is the thermodynamically stable one at ambient conditions [7] i.e. for bulk ZnO. This structure can be considered as two interpenetrating hexagonal-close-packed lattices, characterized by two interconnecting sublattices of Zn^{2+} and O^{2-} such that each Zn ion is surrounded by a tetrahedral of O ions and vice versa [6]. The tetrahedral coordination gives rise to the polar symmetry along the hexagonal axis. This polarity gives rise to a number of properties of ZnO. There are four common face terminations for the wurtzite ZnO namely; the polar Zn terminated (0001) and the O terminated $(000\bar{1})$ faces (*c*-axis oriented) and the non-polar $(11\bar{2}0)$ (a-axis) and $(10\bar{1}0)$ faces which both contain an equal number of Zn and O atoms. The wurzite structure for ZnO is shown in Fig. 2.1. The polar faces possess different

chemical and physical properties with the O face having a different electronic structure from the other three [6]. The rock salt structure is stable at very high pressures while the zinc blende structure can be achieved through growth on cubic substrates.

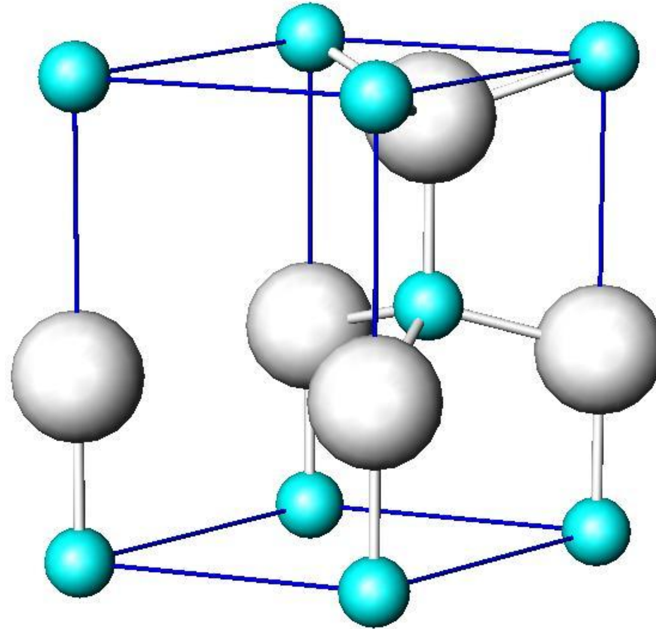

Figure 2.1. The hexagonal wurtzite structure of ZnO. O atoms are shown as large light spheres, Zn atoms as small spheres.

2.3: Band structure

This is the most important property in semiconductors since it is responsible for the wide range of electrical properties observed in various materials [8] and determines the potential application of the material [7]. In any semiconductor material, this structure is such that the filled valence band is separated from an empty conduction band by a band gap containing no allowed energy states at 0K [8]. A number of theoretical approaches using different degrees of complexity and also several experiments have been carried out to calculate the band structure and electronic states of the wurtzite structure of ZnO, respectively [7]. The experimental techniques, which can be used to determine the band structure for ZnO, include conventional x-ray and ultraviolet (UV) induced photoemission spectroscopy, as well as angular photoelectron spectroscopy. Experimental observations and theoretical calculations using pseudo potential methods on the band structure of ZnO only have a qualitative agreement [7] but the most important fact is ZnO has a direct bandgap semiconductor (i.e. the minimum of the conduction band occurs at the same momentum (**k**)-value as the maximum of the valence band in the energy-momentum (E, k) diagram shown in Fig. 2.2.

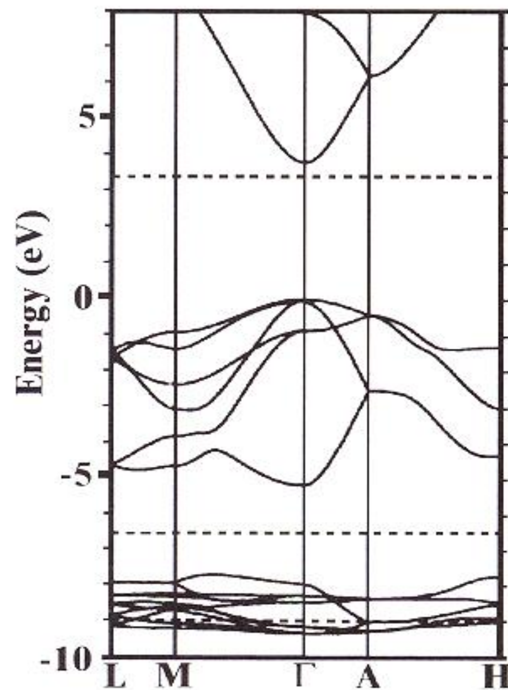

Figure 2.2. The local density approximation (LDA) band structure of bulk wurtzite ZnO calculated using dominant atomic self-interaction-corrected pseudo potentials (SIC-PP).

2.4: Carrier transport phenomena

2.4.1: Introduction

Current flow in a semiconductor material is an important statistical aspect. The ease with which the charge carriers move under an applied electric and/or magnetic field must be looked at more considerably as this is one of the important factors that contribute to the amount of current per unit area (current density). It is also imperative to know the values of the electrons and holes to account for the collisions that take place between the charge carriers and the lattice atoms as well as the impurities as this helps in determining the ease with which these carriers can drift (mobility) through the crystal [8]. Knowledge of the scattering mechanisms that take place at different temperature regimes within a material is required as it determines the thermal motion of the lattice atoms and the carrier velocities. In this subsection, I am going to give a brief outline of how carriers drift through the material and also how the atoms in the lattice as well as the impurities within the material affect this movement.

2.4.2: Mobility.

Introduction

Carrier mobility influences device behavior through its frequency response or time response in two ways. Firstly, carrier velocity is proportional to the mobility for low electric fields. So a material with a higher mobility is likely to have a higher frequency response, since carriers take less time to travel through the device. Secondly, the device current depends on the material and hence, the larger the mobility, the higher the current. These higher currents in turn affect the rate at which capacitors charge up. Higher currents charge capacitors more rapidly, resulting in higher frequency responses. This means there is need to determine the mobility of the semiconductor material in order to determine its use in device fabrication. In this section, a brief outline on how to obtain *conductivity* mobility is given.

Consider an n-type semiconductor with a uniform donor concentration in the absence of an applied electric field. At room temperature, electrons will undergo a continual random motion interrupted by collisions as shown in Fig 2.3 [8]. Since there is no preferred direction of motion of these electrons, there is no net current flow.

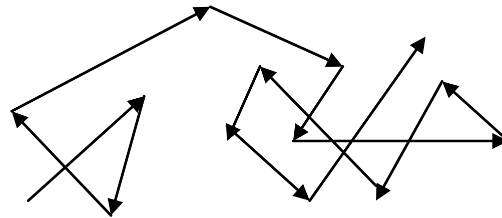

Fig 2.3. Thermal motion of an electron in a semiconductor

If an external electric field is applied, each electron will experience a net force given by $-qE_x$, insufficient to change the random motion of each individual electron significantly. However, when the effect is averaged over all the electrons, it becomes the net motion of the electrons drifting in the direction opposite that of the applied field with drift velocity, $\langle v_d \rangle$. Now taking the total momentum of these electrons to be *p*, the force of the field on the *n* electrons/cm^3 is given by,

$$-nqE_x = \frac{dp}{dt} \qquad (2.4.1)$$

Assuming that the collisions are truly random [8], there is always a constant probability of collision at any time, *t* for each electron. Suppose at time, $t = 0$ we have N_0 electrons and at

any time t, there are *N(t)* electrons which would have not undergone collisions. The rate at which *N(t)* decreases with time is proportional to the number left un-scattered at *t*, i.e.

$$-\frac{dN(t)}{dt} = \frac{1}{\bar{t}} N(t) \tag{2.4.2}$$

which has a solution $N(t) = N_0 \exp\ t/\bar{t}$

where $\bar{t}$ is the mean free time. Each electron has a probability of colliding with another one in the time interval *dt*, given by $dt/\bar{t}$. The differential change in momentum due to collisions is thus given by:

$$dp = -p\frac{dt}{\bar{t}} \tag{2.4.3}$$

The force, i.e. the rate of change of momentum due to decelerating effect of collision is

$$\frac{dp}{dt} = -\frac{p}{\bar{t}} \tag{2.4.4}$$

For a steady state condition, the sum of the decelerating and accelerating effects must be zero [8] such that the average momentum, $\langle p \rangle$ is given by,

$$\langle p \rangle = -q\bar{t}E \tag{2.4.5}$$

Thus the average velocity $\langle v_d \rangle$ is also given by,

$$\langle v_d \rangle = \frac{\langle p \rangle}{m_n^*} = -\frac{q\bar{t}}{m_n^*}E \tag{2.4.6}$$

m_n^* is the conductivity effective mass for electrons.

The current density for *n* electrons moving with drift speed, $\langle v_d \rangle$ is now given by,

$$J = -qn\langle v_d \rangle = \frac{nq^2\bar{t}}{m_n^*}E \tag{2.4.7}$$

From $J = \sigma E$ [9]**,** it follows that the conductivity, σ is,

$$\sigma = \frac{nq^2\bar{t}}{m_n^*} \tag{2.4.8}$$

which can also be written as $\sigma = q\mu_n n$, where

$$\mu_n = \frac{q\bar{t}}{m_n^*} \tag{2.4.9}$$

μ_n in equation (2.4.9) is called the electron or conductivity mobility, m_n^* is the conductivity effective mass for electrons. Equation (2.4.9) illustrates that the longer the time between collisions and the smaller the conductivity effective mass, the higher the mobility.

2.4.3: Scattering mechanisms

Carrier scattering is one of the most important factors affecting the ease with which electrons/holes drift through the crystal (mobility). Measurements have shown that in a semiconductor, mobility varies with temperature and impurity concentration [10]. In order to understand the variations in carrier movement through crystals, knowledge of the scattering mechanisms involved at different temperature conditions is necessary. A general overview of the scattering mechanisms that take place in semiconductor material, with particular reference to ZnO will be covered in this section.

During crystal growth in semiconductors, impurities are introduced into the lattice causing these crystals to be imperfect or non-ideal. Intentional doping also contributes to the imperfections within the crystal lattice. Discontinuities such as screw or edge dislocations formed during crystal growth also act as centers for charge accumulation. The perturbing potential which is created causes carrier scattering. Basically, the number of defects in properly grown crystals is low enough that this type of scattering can be overshadowed by other mechanisms and therefore can be neglected [11]. There are four main scattering mechanisms that affect the movement of mobile carriers in a semiconductor. These are: Lattice scattering, ionized impurity scattering, neutral impurity scattering and carrier-carrier scattering [12]. This thesis is going to give detailed information pertaining to each of these mechanisms. The following is a summary of each of these mechanisms.

Lattice Scattering.

This type of scattering is usually dominant under high temperature conditions. Compressions and dilations that occur within a crystal cause some lattice atoms to be squeezed up in some regions and pulled out in others. The dielectric constant is also made to change with these variations in disturbances and this in turn alters the periodic potential in the vicinity of these compressions and dilations [10]. An increase in temperature causes an increase in the amplitude of the lattice vibrations that excite normal modes of higher energies and this causes a corresponding rise in scattering since thermal agitation of the lattice becomes greater [8]. This behavior of the lattice with temperature produces a relaxation time that is dependent on

temperature, i.e. it decreases with increasing temperature [8, 10]. The resulting scattering mobility is given by [10].

$$\mu_L = B_1 T^{-3/2} \tag{2.4.10}$$

T is the temperature in Kelvin.

According to [9],

$$B_1 \equiv \frac{\sqrt{8\pi}\, q\hbar^4 C_{11}}{3E_{ds} m^{*5/2} k^{3/2}} \approx m^{*\,-5/2} \tag{2.4.11}$$

where C_{11} is the average longitudinal elastic constant of the semiconductor, E_{ds} is the displacement of the edge of the band per unit dilation of the lattice, m^* is the conductivity effective mass, k is the Boltzmann constant.

From equation (2.4.10) and (2.4.11), the mobility is given by [9],

$$\mu_L = m^{*\,-5/2} T^{-3/2} \tag{2.4.12}$$

Equation (2.4.12) shows that mobility decreases with temperature and with the effective mass.

Ionized impurity scattering

This can also be referred to as Coulomb scattering [10]. This type of scattering occurs at low temperatures, but high enough to cause the ionization of impurity atoms, leaving some charged scattering centers behind. The charged scattering centers associated with the ion impurity cause a change in the lattice potential near its location and thus produce an electric field that deflect the moving carriers. If a carrier enters the radius that is influenced by this electric field, it will be scattered by the charged ion. Instead of it following a straight path, the electron path will be bent and since at low temperatures, the thermal speed of the electron is low, it spends more time in the neighborhood of the impurity atom thereby increasing the effectiveness of the scattering. Slow moving carriers are scattered by an interaction with a charged ion that has a greater momentum. This type of scattering is thus dominant at low temperatures. As the temperature is increased, scattering decreases and thus the relaxation time increases with temperature and so the ionized impurity mobility is given by [10],

$$\mu_1 = B_2 T^{3/2} \qquad (2.4.13)$$

This can also be expressed as [9]

$$\mu_1 = \frac{64\sqrt{\pi}\varepsilon_s^2 \;\; 2kT^{\frac{3}{2}}}{N_I q^3 m^{*1/2}} \left\{ \ln\left[1 + \left(\frac{12\pi\varepsilon_s kT}{q^2 N_I^{1/3}} \right)^2 \right] \right\}^{-1} \qquad (2.4.14)$$

$$\mu_1 \sim \;\; m^{* \;\; -1/2} N_I^{-1} T^{3/2} \qquad (2.4.15)$$

where N_I is the ionized impurity density and ε_s is the semiconductor permittivity. Equation (2.4.15) illustrates that the mobility decreases with effective mass but increases with temperature.

Neutral impurity scattering

The main factor behind this type of scattering is the difference in sizes of the impurity atom and its host lattice atoms. The presence of the impurity atom will affect the lattice orientation by forcing it to strain in order to accommodate for the impurity atom. By so doing, the potential of the lattice is also affected as a bump [10] is going to be produced in the lattice, near the impurity atom. The electric field associated with this bump will in turn scatter carriers as they come closer to the impurity atom and this will affect the mobility of the carriers.

Carrier-carrier scattering

In a semiconductor, carriers interact and they deflect each other during their movement through the crystal. Electrons and holes move in opposite directions under the influence of an external electric field and so a collision would lead to complete annihilation and effectively cause a decrease in mobility. Though carriers of the same charge can interact with each other through Coulombic forces, there is no pronounced effect on the mobility since they will be moving in the same direction. These interactions, however serve to randomize the motion and have an indirect effect through the dominant scattering mechanisms. This type of mechanism becomes important when the carrier density of a material exceeds 10^{14}cm^{-3} [13].

References

[1] J. D. Albrecht, P. P. Ruden, S. Limpijumnong, W. R. L. Lambrecht and K. F. Brennan *J. Appl. Phys*.86 6864 (1999).

[2] D. I. Flourescu, L. G. Mourokh, F. H. Pollak, D. C. Look, G. Cantwell and X. Li J. *Appl. Phys*. 91 890 (2002).

[3] C. Coskun, D. C. Look, G. C. Farlow and J. R. Sizelove *Semicond. Sci. Technol*. **19** 752 (2004).

[4] H. Morkoc, S. Strite, G. B. Gao, M. E. Lin, B. Sverdlov and M. Burns *J. Appl. Phys*. **76** 1363 (1994).

[5] Q. L. Gu, C. C Ling, X. D. Chen, C. K. Cheng, A. M. C. Ng, C. D.Beling, S. Fung, A. B. Djurisic, and L. W Lu, *Appl Phys Lett*. **90** 122101 (2007).

[6] C. Jagadish and J. Pearton, Zinc Oxide Bulk, Thin Films and Nanostructures Processing, Properties and Applications, Elsevier, Oxford, UK, Amsterdam, Netherlands, (2006).

[7] U. Özgür, A comprehensive review of ZnO materials and devices, *J. Appl. Phys*. **98**, 41301 (2005).

[8] B. G. Streetman, Solid State Electronic Devices, 5th Edn, Prentice Hall, New Jersey 2000.

[9] S. M. Sze Physics of semiconductor devices, 2nd Edn. Wiley, New York (1981).

[10] M. S. Tyagi, Introduction to semiconductor materials and devices, J. Wiley and Sons, (1991).

[11] D. L. Rode, Semiconductors and semimetals, vol 10, Academic Press (1975)

[12] R. B. Adler, A. C. Smith and R. L. Longini, Introduction to Semicon. Phys, SEEC vol. 1, John Wiley, NY, (1964).

[13] B. R. Nag, Electron transport in compound semiconductors, Springer series in Solid State Sciences 11. Springer Verlag (1980).

CHAPTER 3: Electrical characterization techniques.

3.1: Introduction

With increasing interest in researchers using ZnO as a better material for electronic and optoelectronic devices compared to other wide bandgap materials, the issues of its electron mobility, Schottky contact quality, Schottky barrier height, forward and reverse leakage current, and material defects need to be addressed more quantatively. Different techniques have been used to electrically characterize ZnO. These include the Hall effect, current-voltage, (*I*-*V*) and capacitance-voltage, (*C*-*V*) measurements, deep level transient spectroscopy (DLTS), photoluminescence spectroscopy, and admittance spectroscopy. In this particular section, an outline of some of the afore-mentioned techniques, which can be used to characterize each of the above-mentioned parameters, with particular reference to the use of ZnO in electronic devices, is given.

3.2: The Hall effect technique

3.2.1: Introduction

The Hall Effect technique has found wide applications in semiconductor material characterization because it gives the resistivity, the carrier density, and the mobility [1]. If a magnetic field is applied to a current carrying semiconductor, an electric field will be produced which is perpendicular to the magnetic field. The motion of the carriers in the presence of these fields (magnetic and electric) is important and gives rise to a number of galvanometric effects [2]. This section is going to give an outline of how carriers move under the effect of magnetic and electric fields leading to the determination of the Hall coefficient and mobility.

3.2.2: The Hall Effect theory

Consider a rectangular wafer of n-type semiconductor material of length, l, width, w and thickness d. In a magnetic field, and applied electric field a current is established causing carriers to drift, opposing and following the direction of the applied field for electrons and holes respectively at a speed, v. This current flow is an important effect in as much as the drift of carriers in a material is concerned. Given that these carriers are charged particles, in

an applied magnetic field, they experience a Lorentz force that makes them move in a direction perpendicular to the magnetic field, given by [3]

$$F_L = q\left(v \times B\right) \qquad (3.2.1)$$

where q is the charge of the carriers, v is the drift velocity and B is the applied magnetic field. Taking the carriers to be negatively charged, the Lorentz force will deflect these particles in the -y-direction and a charge imbalance will be produced, which will in turn induce an electric field, $-E_y$ as shown in Fig. 3.1 below.

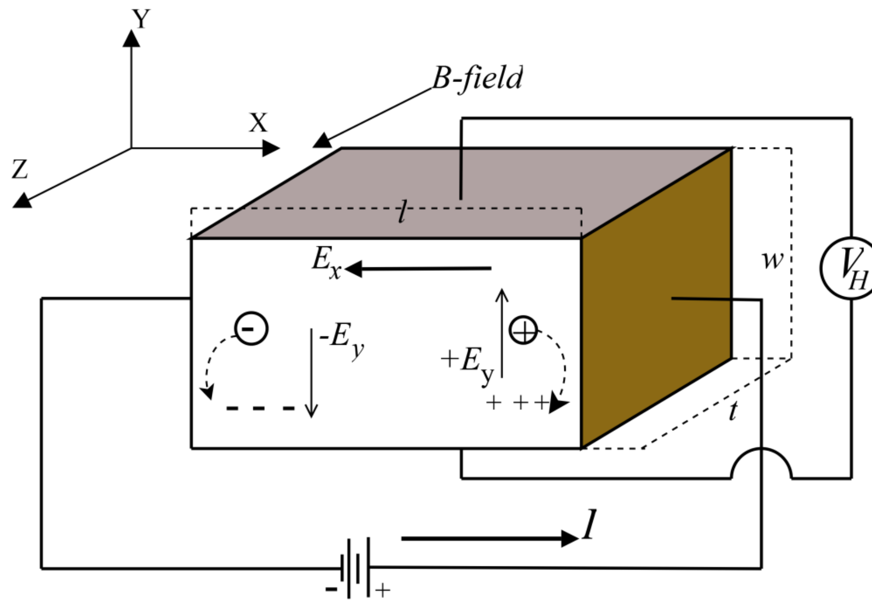

Figure 3.1: Determination of the Hall voltage on a semiconductor wafer using the Hall effect technique.

Under steady state conditions, the Lorentz force F_L must balance the downward force, F_E due to the electric force on the electrons such that there is no net acceleration of these carriers in the y-direction, i.e.,

$$F_L = -F_E \qquad (3.2.2)$$

and thus

$$q\left(v \times B\right) = -qE_y \qquad (3.2.3)$$

which can be simplified to,

$$E_y = v_x B_z \qquad (3.2.4)$$

upon evaluation of the cross product of *v* and *B*, bearing in mind that v_x, B_z and E_y point in the *x, z* and *y* directions respectively. This establishment of the electric field E_y is called the Hall effect [4]. The resulting voltage is called the Hall voltage, V_H. The velocity, v_x can be expressed in terms of the current density, J_x and carrier concentration, *n* as:

$$v_x = -\frac{J_x}{nq} \tag{3.2.5}$$

Substituting equation (3.2.5) into (3.2.4) yields

$$E_y = -\frac{J_x}{nq} B_z \tag{3.2.6}$$

From [2],

$$E_y = R_H J_x B_z \tag{3.2.7}$$

Comparing (3.2.6) and (3.2.7), gives

$$R_H = -\frac{1}{nq} \tag{3.2.8}$$

Equation (3.2.8) represents what is known as the *Hall constant*. The same analysis can be done in the case of holes, but for holes, this quantity is positive.

It is imperative to note that in deriving equation (3.2.8), we assumed that no scattering takes place and also all charge carriers move with the same velocity. However in real semiconductor materials, scattering effects randomize the velocity of carriers leading to equation (3.2.8) being an approximate relationship. The accuracy of this relationship is determined by the scattering mechanisms, carrier type, band structure of the material and temperature. The exact relationship between carrier concentration and the Hall constant is given by [5, 6].

$$R_H = -\frac{r}{nq} \tag{3.2.9}$$

where *r* is the scattering factor whose value lies between 1 and 2, depending on the scattering mechanism in the semiconductor [1]. Usually, *r* is assumed to be unity, an assumption generally introducing an error of less than 30% [7]. This scattering factor is also a function of the magnetic field and temperature. For very high magnetic fields, the limit for the scattering factor tends to 1 [1]. The determination of the Hall constant leads to the knowledge of carrier concentration as well as type.

3.2.3: Hall coefficient determination.

The Hall coefficient can be determined experimentally by the van der Pauw method. Van der Pauw in 1958 proved that for any flat, isotropic, homogeneous sample of uniform thickness, and singly connected domain, the Hall coefficient is independent of the length and thickness (irrespective of shape), when he solved the potential for a thin layer of arbitrary shape with four point-like contacts along the periphery [8].

Now consider a sample of length, l , breadth w and uniform thickness, t placed in a magnetic field, B. If a current, I is allowed to pass through the sample, perpendicular to a surface of cross-sectional area, $A=wt$, then the current density passing through the sample is given by,

$$J_x = \frac{I_x}{wt} \tag{3.2.10}$$

The electric field for this sample in terms of the measured Hall voltage and the thickness in the y-direction can also be written as

$$E_y = \frac{V_H}{w} \tag{3.2.11}$$

Substituting equation (3.2.10) into (3.2.11) yields

$$E_y = \frac{V_H J_x t}{I_x} \tag{3.2.12}$$

Substituting equation (3.2.7) into (3.2.12) gives

$$R_H = \frac{tV_H}{B_z I_x} \tag{3.2.13}$$

The correct sign of R_H can be obtained by taking I_x as positive if an electron current is flowing from left to right. Similarly, V_H is positive when a positive potential is measured at the bottom of the sample. As viewed in Fig. 3.1, the Hall voltage, will be measured directly from the experiment.

Practically, point-like contacts are critical though very difficult to realize. A good rule of thumb to adhere to is not to let the contact size exceed 10% of the smallest sample dimension [5,1].

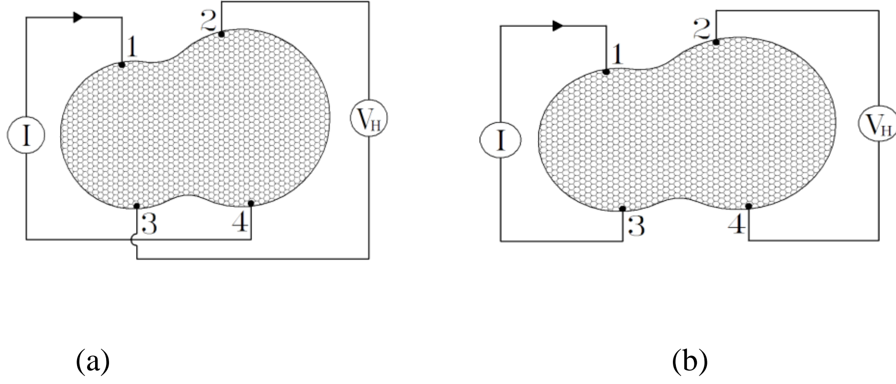

Figure.3.2. Contact configuration for (a) Hall coefficient determination and (b) resistivity measurement.

Fig. 3.2(a) shows how the sample Hall coefficient can be experimentally obtained while, Fig. 3.2(b) shows how the resistivity can be determined. Since the quantities t and B_z in equation (3.2.13) are constants, it indicates that R_H is proportional to V_H/I_x , which has units of resistance. Defining resistances $R_{14,23} = V_{23}/I_{14}$, with $V_{23} = V_3 - V_2$, the potential difference between contact *2* and *3* and I_{14} being the current flowing between contact *1* and *4*, the Hall coefficient is given by [5, 9].

$$R_H = \frac{t}{B}\left(\frac{R_{14,23} + R_{41,23}}{2}\right) \tag{3.2.14}$$

In this type of measurement, averaging over the two Hall configurations eliminates errors caused by misalignment of the four contacts. However, there are a number of thermomagnetic effects that could falsify measurements if not taken into consideration. These include the Ettingshausen effect, the Righi-Leduc and the Nernst effect [9], which produce a thermoelectric voltage caused by temperature gradients in the sample. In the Nernst effect, the temperature gradient is caused by magnetic field independent factors such as uneven sample heating (cooling) or the Peltier effect. In the other two effects, the temperature gradient is set up by the different Lorentz deflection of carriers that have different velocities. Suppose a hall resistance denoted by $R_{ij,kl}^{+}$ is measured in a magnetic field in the $+Z$ direction and a corresponding hall resistance denoted by $R_{ij,kl}^{-}$ is measured in a magnetic field pointing in the $-Z$ direction. It can be shown that the Righi-Leduc and the Nernst effects can be eliminated by the following average over current and magnetic field directions [10].

$$R_H = \left(\frac{t}{B}\right)\left[R^+_{12,34} - R^+_{21,34} + R^+_{23.41} - R^+_{32,41} + R^-_{43,21} - R^-_{34,21} + R^-_{14,32} - R^-_{41,32}\right] \quad (3.2.15)$$

Once the Hall coefficient has been determined, the carrier concentration n can be calculated using equation (3.2.9). The value of r is determined by identifying the dominant scattering mechanism.

3.2.4: Resistivity determination.

The resistivity ρ, can be defined as the constant of proportionality relating the current density, J in a conductor to the electric field, E, such that, $E = \rho J$. The inverse of the resistivity is called the conductivity, σ. According to van der Pauw's analysis [1], the resistivity of any arbitrary shape is given by,

$$\rho = \frac{\pi t}{\ln(2)}\frac{(R_{12,34} + R_{23,41})}{2}F \quad (3.2.16)$$

where $R_{12,34} = V_{34}/I_{12}$ and F is a correction factor. The current enters the sample through contact 1 and leaves through contact 2, and $V_{34} = V_4 - V_3$ is the voltage between contact 4 and contact 3 with reference to Fig. 3.2(b). Also $R_{23,41} = V_{41}/I_{23}$ in which the current enters the sample through contact 2 and leaves through contact 4 and $V_{41} = V_1 - V_4$ is the voltage between contacts 1 and 4. Current enters the sample through two adjacent terminals and the voltage is measured across the other two adjacent terminals. F is a correction factor, which is a geometric correction factor, which depends on the ratio $R_r = R_{12,34}/R_{23,41}$ only satisfying the relation,

$$\frac{R_r - 1}{R_r + 1} = \frac{F}{\ln(2)}\cosh^{-1}\left\{\frac{\exp[\ln(2)/F]}{2}\right\} \quad (3.2.17)$$

For symmetric samples (circles or squares) $F = 1$ [1]. Since F is a correction factor, it does not cause any resistivity anisotropies in the sample. If such anisotropies occur, the resistivity becomes a tensor rather than a scalar.

As in the Hall coefficient determination, thermoelectric effects can be reduced by averaging over all the different contact permutations and current directions [5]:

$$\rho = \frac{\pi t}{\ln(2)}\left[\frac{(R^{+}_{12,34} - R^{+}_{21,34} + R^{+}_{23.41} - R^{+}_{32,41})F_A}{8} + \frac{(R^{-}_{43,21} - R^{-}_{34,21} + R^{-}_{14,32} - R^{-}_{41,32})F_B}{8}\right] \quad (3.2.18)$$

In this case, F_A and F_B are determined from R_A and R_B respectively, where,

$$R_A = \frac{R_{12,34} - R_{21,34}}{R_{23,41} - R_{32,41}} \quad (3.2.19)$$

and

$$R_B = \frac{R_{43,21} - R_{34,21}}{R_{14,32} - R_{41,32}} \quad (3.2.20)$$

3.2.5: Factors affecting the measured Hall voltage.

In determining the Hall voltage, certain associated effects give rise to potentials, which must be corrected in order to avoid errors in the measured value. These effects together with the correction measures are discussed below.

3.2.5.1: The IR effect

During the process of determining the Hall voltage, electrical contacts are established by using Indium Gallium eutectic or by depositing metals as ohmic contacts on the edges of the sample. These contacts (1,2,3,4) as in Fig. 3.2 are the ones used to pass the current into and out of the semiconductor as well as for tapping the Hall voltage across the sample. A situation arises that contacts used for measuring the Hall voltage are not aligned at the same equipotential line. If this occurs, a potential will be detected between the probes used in the measuring. This potential can be of the order of the Hall voltage itself [10]. Also, thin high resistance surface layers under the current contacts cause an abnormally low Hall voltage since most of the applied voltage would be lost in the *IR* drop across the barrier [11].

3.2.5.2: Galvanomagnetic effects

Three possible thermomagnetic and galvanomagnetic effects can influence the Hall voltage measurements. These are the Ettingshausen, the Nernst, Righi-Leduc effects and have been summarized by Goodman [10]. These effects were discovered after the Hall Effect discovery as a result of intensive research on electrical conduction [12]. A brief summary of how these effects affect the movement of electrons and the measured Hall voltage is given.

3.2.5.2.1: The Ettingshausen effect

Since electrons in a semiconductor material travel at different velocities, without an external transverse temperature gradient, the sample can set up its own. Resulting from the difference in the carrier velocities, the $e\vec{v}\times\vec{B}$ force shunts the slow (cool) and fast (hot) carriers to the sides in different numbers and this causes an internally generated Seebeck effect. More energy will be deflected to one side of the sample than the other resulting in a transverse temperature gradient. Unlike in the Seebeck effect, the Ettingshausen voltage generated is proportional to both the current and the magnetic field. This leads to a modification of the Hall coefficient. However, this modification is normally less than the experimental error in the Hall coefficient [10].

3.2.5.2.2: The Nernst effect

If a longitudinal temperature gradient is established across the sample, electrons tend to diffuse from the hot end of a sample to the colder end. The diffusion current set up by these moving electrons is affected by the magnetic field, setting up a Hall voltage, V_N [5]. This voltage is proportional to the magnetic field and is not affected by the external current.

3.2.5.2.3: The Righi-Leduc effect

This effect is brought about by the differences in the carrier velocities, as does the Ettingshausen effect. From the Nernst effect, as electrons diffuse from the hot end to the colder end, they set up diffusion current. A transverse Seebeck voltage, also known as a Righi-Leduc voltage V_R, which is proportional to the magnetic field, is thus set up [12].

3.2.6: Correction of IR effects and Galvanomagnetic effects

Since all the above mentioned effects are observed at the contacts where the Hall voltage used in the calculation of the Hall coefficient is measured, there is a need to eliminate them or reduce them for a more accurate value of the Hall coefficient. Experiments have shown that the Ettingshausen effects are directly related to the magnetic field and the current flowing through the sample, whilst the Nernst and Righi-Leduc effects produce a voltage related to the magnetic field and not the current [5, 10, 12]. The IR drop is only related to the applied current and the contact quality but is independent of the magnetic field. Thus the voltage measured by using the probes considering all the effects on a semiconductor is given by,

$$E = V_H + V_E + V_{IR} + V_{RL} + V_N \qquad (3.2.21)$$

where V_H is the voltage associated with the Hall voltage, V_E is the voltage associated with the Ettingshausen effect, V_{IR} is the voltage associated with the potential drop, V_{RL} is associated with the Righi-Leduc effect and V_N is the voltage associated with the Nernst effect. Taking a series of 8 readings, by reversing the magnetic field, allowing current to pass through all the possible contact combinations, can eliminate all the other effects except the Ettingshausen effect and the Hall effect voltage [12,13].

We need to consider a square sample, with the four contacts positioned at the four corners as shown in Fig. 3.3 below.

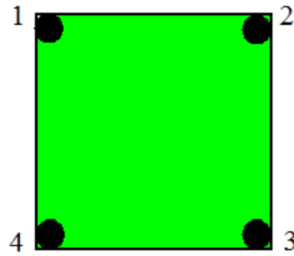

Fig. 3.3. Square sample with four contacts used to determine the Hall voltage.

If V_{ij} is the voltage drop across contacts i and j, upon application of a current I_{kl} through contacts k and l, then the following 8 combinations would be measured:

With a forward magnetic field, +B,

I_{13}; $V_{24} = V_H + V_E + V_{IR} + V_{RL} + V_N = V_1$

I_{31}; $V_{24} = -V_H - V_E - V_{IR} + V_{RL} + V_N = V_2$

I_{24}; $V_{13} = V_H + V_E + V_{IR} + V_{RL} + V_N = V_3$

I_{42}; $V_{13} = -V_H - V_E - V_{IR} + V_{RL} + V_N = V_4$

Reversing the magnetic field, -B,

I_{13}; $V_{24} = -V_H - V_E - V_{IR} - V_{RL} - V_N = V_5$

I_{31}; $V_{24} = V_H + V_E - V_{IR} - V_{RL} - V_N = V_6$

I_{24}; $V_{13} = -V_H - V_E + V_{IR} - V_{RL} - V_N = V_7$

I_{42}; $V_{13} = V_H + V_E - V_{IR} - V_{RL} - V_N = V_8$

By regrouping the measured potentials in terms of the same contact configurations but with opposite magnetic fields, we obtain

$$E_1 = V_1 - V_5 = 2V_H + 2V_E + 2V_{RL} + 2V_N$$

$$E_2 = V_6 - V_2 = 2V_H + 2V_E - 2V_{RL} - 2V_N$$

$$E_3 = V_3 - V_7 = 2V_H + 2V_E + 2V_{RL} + 2V_N$$

$$E_4 = V_8 - V_4 = 2V_H + 2V_E - 2V_{RL} - 2V_N$$

Adding up the set of equations above yields,

$$E_1 + E_2 + E_3 + E_4 = 8V_H + 8V_E$$

Such that

$$V_H + V_E = \left(E_1 + E_2 + E_3 + E_4\right)/8 \qquad (3.2.22)$$

The combination of the set of equations to produce equation (3.2.22) eliminates the potential errors caused by the IR effect, the Nernst effect and the Righi-Leduc effects in the Hall voltage measurements. Since the Ettingshausen effect is brought about by the existence of a temperature gradient due to the charge carriers' different velocities, it will still affect the measured Hall voltage but to a lesser extent if a series of readings is taken over a short period of time, and keeping the sample in good thermal contact with its surroundings [14]. This means that under close to perfectly controlled conditions, the Ettingshausen voltage is small and can be neglected.

3.2.7: Effect of contact size, position, and geometry.

Ohmic contacts deposited on the sample prior to Hall measurements can be of different sizes due to the deposition technique used. Also, because of the vibrations of the cryostat during measurements, some contacts can be knocked off from the periphery of the specimens (samples). This difference in contact size and the displacement of the probes can cause a difference in the resistance values of those particular contacts on the same sample. Due to this

difference, some errors in the determination of the sample resistivity can occur. Van der Pauw [15] studied the errors caused by finite electrodes and the displacement of the contact electrodes from the periphery of circular specimens. Weider [16] indicated that finite contacts cause errors such as short-circuiting the Hall field, thereby reducing the measured Hall voltage compared to the one obtained by point electrodes and as well as short-circuiting the current streamlines near and around the Hall electrodes, causing non-linearities of the magnetic field dependence of the Hall voltage. According to van der Pauw [17]'s evaluation, choosing an appropriate specimen contour such as the "clover leaf" shape can minimize such errors. However, such a geometrical structure requires some complex preparation procedures, to such an extent that it modifies the surface of the sample if some photolithographic processes are applied to films or epitaxial layers [16]. In this study, square specimens were preferred to the "clover-leaf" because of the latter reasons. Triangular contacts were used on the periphery of the specimens instead of circular contacts used by van Daal [18]. The correction factors for finite electrodes, relating the effective to the measured Hall voltage and resistivity are much larger for circular contacts than those for the square contacts. Triangular contacts have the least correction factors.

Consider a specimen given in Fig. 3.4.

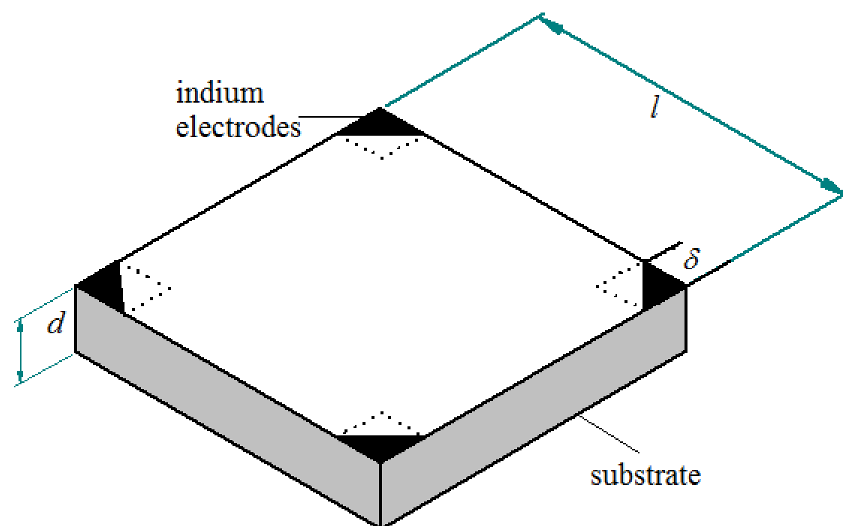

Figure 3.4. Bulk ZnO wafer of edge length l and thickness d with indium solder electrodes of length δ along the edge of a sample of length l.

For triangular electrodes, the resistivity correction appears to increase monotonically with the ratio δ/l and also the Hall voltage correction factor is smaller since $\delta/l << 1$ than the resistivity factor, and is roughly proportional to $(\delta/l)^2$. Making l 5 or 10 times greater than δ reduces the errors introduced by contact size [16]. The voltage measured between the peripheral potential

contacts should be independent of the commutation of the current contacts [10]. If this is true, it is expected that the resistances $R_{12,34}$ and $R_{23,41}$ are equal, where

$$R_{12,34} = V_{12}/I_{34}$$

and

$$R_{23,41} = V_{23}/I_{41}.$$

However, because of different contact sizes, $R_{12,34}$ is not equal $R_{23,41}$.

Due to this effect, the resistance ceases to be a scalar quantity but becomes a tensor. Alternatively, the sample specimen might become inhomogeneous, containing one or more impurity concentration gradients or a random dispersion of two materials or phases [16]. If, for a material, the ratio $R_{12,34}/R_{23,41} = R_o$ is greater than unity, the average resistivity can be determined by [16],

$$\bar{\rho} = \frac{\pi d}{\ln 2}\left(\frac{R_{12,34} + R_{23,41}}{2}\right) f(R_o) \qquad (3.2.23)$$

Van der Pauw[17] calculated the functional dependence of $f(R_o)$ on R_o and presented it graphically. He revealed that it is partly accurate with a maximum error of about 2%. A more accurate procedure is to use Newton's iterative technique. Taking ρ_o as the initial solution, then the successive approximations are obtained by [10,16],

$$\rho_{n+1} = \rho_n - \frac{\rho_n^2 (1 + \alpha + \beta)}{\pi d(\alpha R_{12,34} + \beta R_{23,41})} \qquad (3.2.24)$$

where $\alpha = -\pi d R_{12,34}/\rho_n$, $\beta = -\pi d R_{23,41}/\rho_n$ and $\rho_1 = \rho_o - f(\rho_o)/f'(\rho_o)$, $f'(\rho_0)$ denoting a derivate with respect to ρ_o.

3.2.8. Impurity concentration determination

The carrier concentration can be obtained by considering a material with multiple s-like donors with concentrations N_{Di} and energy levels E_{Di} below the conduction band and an acceptor impurity. Assuming a temperature independence of all the energy level positions and a degeneracy factor equal to 2, the Fermi energy level (E_F) position in the band gap with respect to the valence band can be estimated by solving the charge neutrality condition:

$$n + N_A^- = \sum_{i=1,2,3} N_{Di}^+ + p \qquad (3.2.25)$$

where n is the concentration of electrons in the conduction band, N_A^- is the ionized acceptor concentration, p is the concentration of holes and N_{Di} is the ionized donor concentration of donors of type D_i.

$$N_{Di}^{+} = N_{Di} \frac{1}{1 + 2\exp\left(-\frac{E_C(T) - E_{Di} - E_F(T)}{k_B T}\right)} \qquad (3.2.26)$$

and

$$n(T) = \frac{1}{4}\left(\frac{2m^* k_B T}{\pi \hbar^2}\right)^{\frac{3}{2}} e^{-\left(\frac{E_C(T) - E_F(T)}{k_B T}\right)} \qquad (3.2.27)$$

where k_B is the Boltzmann constant, T the absolute temperature of the sample, $\hbar$ the reduced Plank's constant, m^* the electron effective mass for ZnO. $E_C(T)$ is the band gap energy relative to the valence band edge. Once $E_F(T)$ is known, the conduction band carrier concentration deduced from (3.2.27) can be compared to the measured $n_H(T)$.

3.2.9. Surface conduction.

The determination of the carrier concentration from Hall measurements is slightly difficult especially at low temperatures. Bulk single crystal and thin film materials usually contain a strongly conductive layer near the surface [19]. This conductive region affects carrier concentration determination especially at low temperatures. This is because at low enough temperatures, the bulk electrons will be frozen out to their donor atoms and thus a difficulty arises in obtaining the surface donor concentration and shallow donor energy levels. At high temperatures, conduction is dominated by the bulk electrons and the carrier concentration is dependent on temperature. As the temperature is lowered, conduction becomes mixed, i.e. due to surface and bulk electrons within a certain temperature range. The carrier concentration, n is a minimum within this temperature range. At low enough temperatures, the sample indicates some degeneracy where the measured carrier concentration becomes independent of temperature. The carrier concentration measured at these low temperatures is no longer a volume concentration but a sheet concentration as was indicated by [19]. To determine a volume concentration, an electrical thickness of the sample must be assigned, d_{bulk} for the bulk electrons and d_{surf} for the surface electrons, such that the sample thickness, d can be expressed as,

$$d = d_{bulk} + d_{surf} \tag{3.2.28}$$

At high temperatures, $d_{bulk} >> d_{surf}$ and so $d_{bulk} \approx d$ and thus $n_{meas} \approx n_{bulk}$. For the near surface electrons, the true volume concentration can be obtained from,

$$n_{surf} = n_{meas} \cdot \frac{d_{bulk}}{d_{surf}} \tag{3.2.29}$$

However, the mobility is not constant at low temperatures. This makes it possible to determine the surface thickness at very low temperatures and calculate the volume concentration at these temperatures.

3.3: *I-V* measurements on Schottky Barrier Diodes (SBDs).

3.3.1: Introduction.

The performance of a Schottky diode is governed by the quality of the metal and the semiconductor contact. Contact quality gives information on how good the diode is as a rectifier. A good rectifying contact is one which should have typically low reverse leakage current, low series resistance and high barrier height. The information contained in each of the above mentioned parameters is obtained from the current-voltage measurements through the analysis of the *I-V* characteristics of the diode.

3.3.2: Metal semiconductor contacts.

3.3.2.1: Introduction.

Metal semiconductor contacts are a critical component of microelectronics. They are very important in direct current and microwave applications and also as tools in the analysis of other fundamental physical parameters [20]. The history of metal-semiconductor contacts dates back to 1874, when Braun carried out a systematic investigation of rectifying contacts. He observed the dependence of the total resistance on the polarity of the applied voltage and the detailed surface conditions. The performance of a metal-semiconductor contact is also determined by the matching between the Fermi energy levels of the metal and the semiconductor. A large mismatch in the Fermi-energies of the metal and semiconductor will result in a high resistance rectifying contact [21]. Metal-semiconductor contacts can be classified as *ohmic* and *rectifying* contacts depending on their response to an applied voltage.

3.3.2.2: Band bending.

Considering the fact that Schottky contacts are formed from a metal and semiconductor contacts, with different electronic configurations and band structures, there usually exists a phenomena known as *band bending*. This can be explained by using the concept of the Fermi-levels of the metal and the semiconductor (either n or p-type) involved, being located at different energies within the energy gap. When a metal is brought into intimate contact with a semiconductor, at thermal equilibrium, the Fermi levels of the materials must be coincident (align). If a metal is brought into thermal equilibrium with an n-type semiconductor, because of the large value of the metal work function compared to the semiconductor work function, electrons tend to flow from the semiconductor conduction band into the metal thereby lowering their energies [22]. In so doing, an excess negative charge builds up in the metal that will repel further flow of electrons from the conduction band of the semiconductor into the metal. The Fermi level of the semiconductor also falls in this region, aligning with that of the metal as higher energy electrons in the region adjacent to the metal would have moved into the metal.

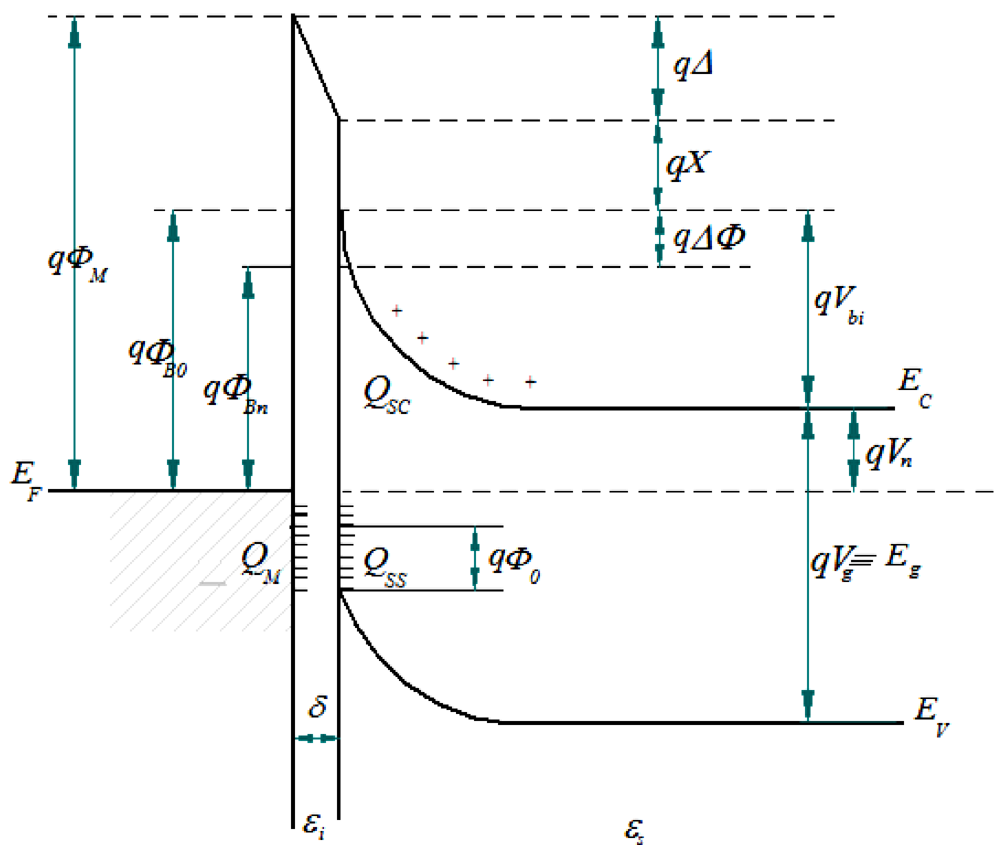

Fig. 3.5. Energy-band diagram of a metal n-type semiconductor contact with an interfacial layer of the order of atomic distance.

The generated electric potential causes the deformation of the energy bands in the semiconductor near the metal-semiconductor interface, yielding a structure shown in Fig. 3.5. As electrons move from the semiconductor into the metal, a region depleted of negative charge carriers and an excess of positive charge in the semiconductor will be created. With a p-type semiconductor, where $\Phi_S > \Phi_M$, electrons will flow from the conduction band of the metal to fill the empty valence band of the p-type semiconductor (i.e. acceptor states) created by p-type doping. This results in a curvature of the bands upwards as the semiconductor Fermi-level moves up to establish thermal equilibrium with the metal Fermi level. A region, which is depleted of holes and a potential barrier for holes to reach the interface with the metal, is established at equilibrium.

3.3.2.3: Ohmic contacts.

An ohmic contact is a metal-semiconductor contact that should ideally have a linear current-voltage relationship in both biasing directions, i.e. in the forward and reverse bias, minimal, voltage independent resistance and no tendency to rectify signals (zero or negative Schottky barrier height [21]) [4]. This contact should be such that no potential exists between the metal and the semiconductor. Ideal metal-semiconductor contacts are ohmic when the majority charge carriers provide the charge induced in the semiconductor in aligning the Fermi levels.

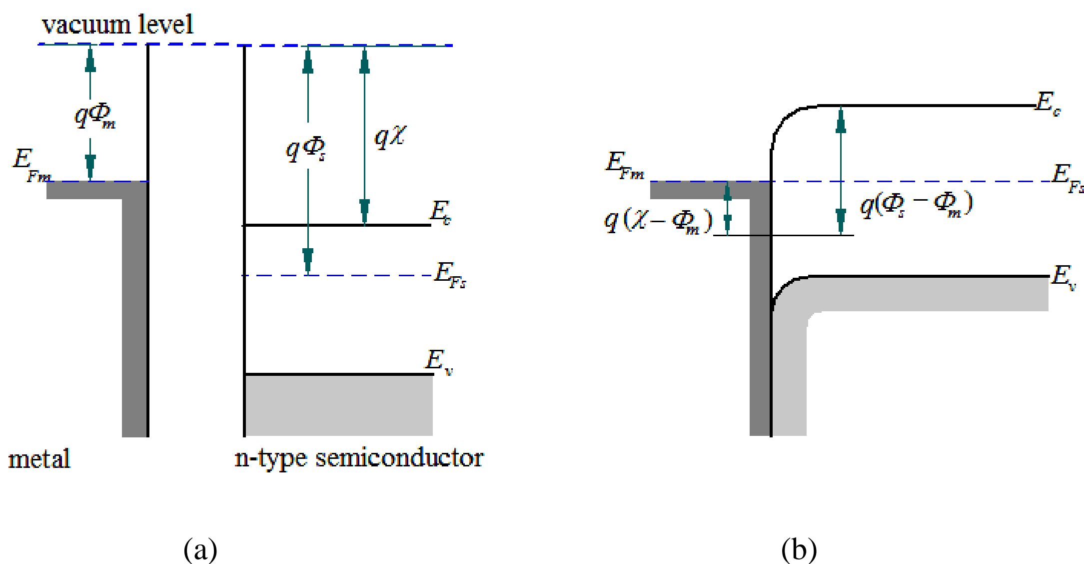

Figure 3.6. Ohmic contacts to n-type semiconductor. (a) before contact, $\Phi_M < \Phi_S$ *(b) equilibrium band diagram for the contact.*

For an n-type semiconductor, the metal work function, Φ_m must be less than that of the semiconductor, Φ_s as in Fig. 3.6a. At equilibrium, electrons are transferred from the metal to

the semiconductor thereby aligning the Fermi levels. This raises the semiconductor electron energies (lowers the electrostatic potential) relative to the metal as in Fig. 3.6b, reducing the barrier to electron flow between the metal and semiconductor, easily overcome by a small voltage. For p-type semiconductors, the metal work function should be greater than the electron affinity of the semiconductor such that at equilibrium, charge carriers are transferred from the semiconductor to the metal. The quality of the ohmic contacts is also affected by surface roughness of the semiconductor and the electronegativity of the metal [23]. Studies on M/ZnO contacts carried out by Reddy *et al.* [23] revealed the dependence of the contacts on electronegativity. Aluminium acts as a source of electrons as it has a tendency of easily releasing them because of loose bonds that exist between them due to its low electronegativity. This causes the current flowing through the junction to follow a thermionic emission mechanism (Schottky). They also observed good ohmic contacts on metals with high electronegativities (Sn and Ag). Ohmic contacts can be classified into *tunnel*, and *annealed and alloyed* contacts. Tunnel contacts are the most practical ones with a positive barrier at the metal-semiconductor interface, but also have enough doping in the semiconductor such that there is only a thin barrier separating the metal from the semiconductor. For easy tunnelling of carriers, the width of the depletion region must be of the order of 3 nm or less and the doping density should be 10^{19} cm^{-3} or higher [21]. Non-alloyed ohmic contacts with low specific contact resistance are essential for shallow junction and low voltage devices [24]. Annealed and alloyed contacts are achieved by treating the contacts at high temperature environments so that the deposited metals can alloy with the semiconductor. The selection of a metal with the right work function cannot result in the expected ohmic contact due to the pinning of the Fermi level at the interface caused by surface states. This will in turn result in a tunnel contact as a viable low resistance contact. To further reduce the resistivity and the unintentional barrier of this contact, annealing at suitably high temperatures in a forming gas is required for the metal to diffuse into the semiconductor, forming a thin highly doped region as desired for a tunnel contact [21]. The contact resistance is defined at zero bias as [20],

$$R_c \equiv \left(\frac{\partial J}{\partial V}\right)^{-1}_{V=0} \tag{3.3.1}$$

3.3.2.4: Schottky contacts.

A Schottky contact is a metal-semiconductor contact which has a tendency to rectify signals in the forward biased mode and allows negligible or no current to flow in the reverse bias. An ideal Schottky contact is formed when a difference in potential, ignoring the effects of surface and interface states, exists between the Fermi energy of the metal and the band edge where majority charge carriers reside, as shown in the flat band diagram of Fig. 3.7.

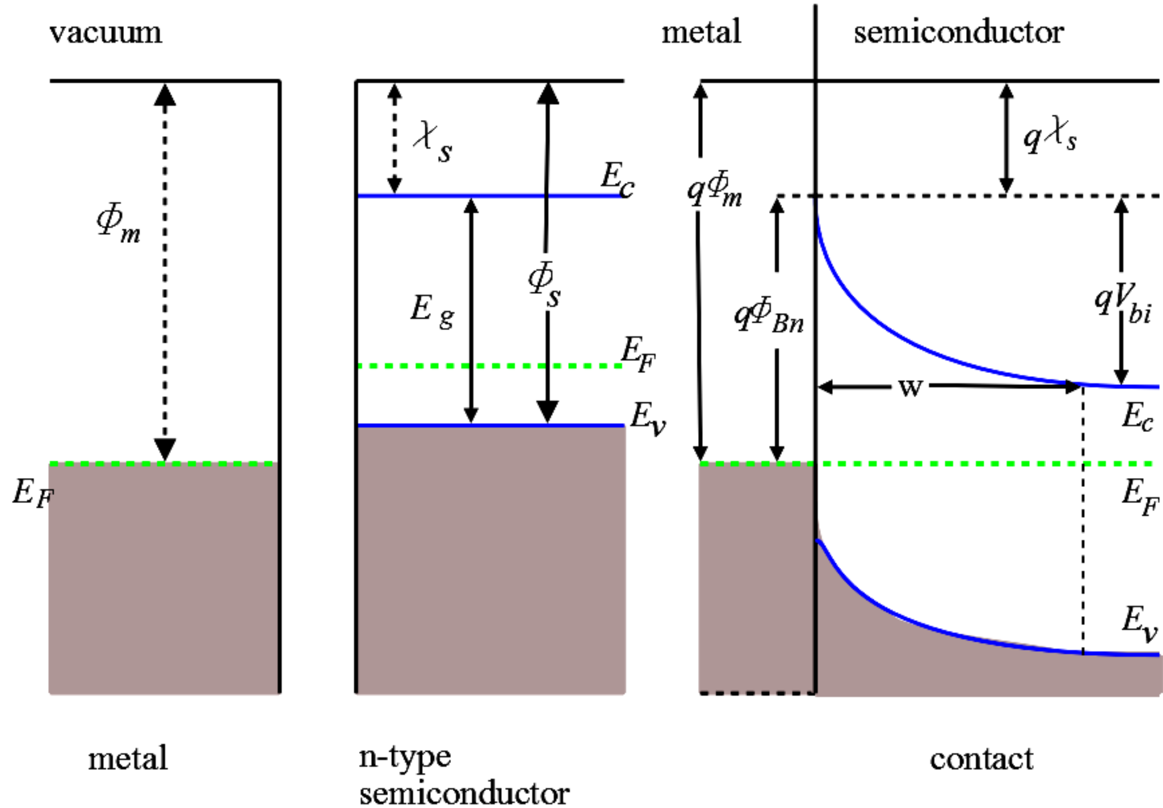

Figure. 3.7. Flatband diagram of a metal/n-type semiconductor contact at equilibrium.

This potential difference constitutes the barrier height, Φ_B of a metal-semiconductor contact, given by [20]

$$\Phi_{Bn} = \Phi_m - \chi_S \qquad (3.3.2)$$

for an n-type semiconductor, where Φ_m is the metal work function, χ_S is the electron affinity of the semiconductor. For a p-type semiconductor, the barrier height can also be written as,

$$\Phi_{Bn} = \frac{E_g}{q} + \chi_S - \Phi_m \qquad (3.3.3)$$

where E_g is the energy gap of the semiconductor, q is the electronic charge, positive for holes.

Barrier heights obtained from this method are said to be ideal, as in real contacts, chemical reactions, interfacial layers and surface states affect the size of the barrier height. The latter mentioned effects alter the barrier height, making it difficult to obtain good rectifying metal semiconductor contacts on ZnO.

3.3.2.4.1: Forward biasing.

Applying a forward biased voltage, the Fermi level moves up, pushing the conduction band of the semiconductor to a higher energy level thereby reducing the potential barrier. Electrons now have higher energies and can now cross over the barrier with little ease as the potential barrier and hence depletion width will be collapsed. A large current due to the majority charge carriers flows through the device.

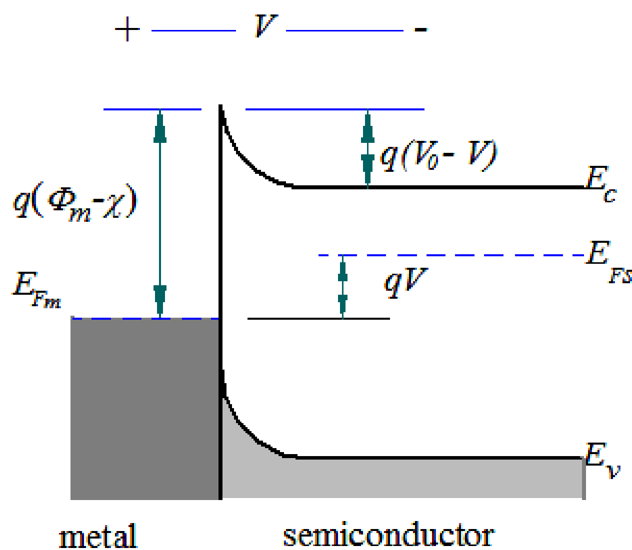

Figure 3.8 : metal-n-type semiconductor Schottky contact under forward bias.

3.3.2.4.2: Reverse biasing.

With an externally applied reverse bias voltage, the Fermi level in the semiconductor material is lowered in energy relative to the one in the metal. This results in the lowering of the energy levels of the valence and conduction bands. The potential barrier increases and charge carriers now have difficulty in crossing the barrier at the interface between the metal and the semiconductor as shown in Fig. 3.9. The depletion width also increases. Thus in the reverse biased mode, very little or negligible current flows through the device.

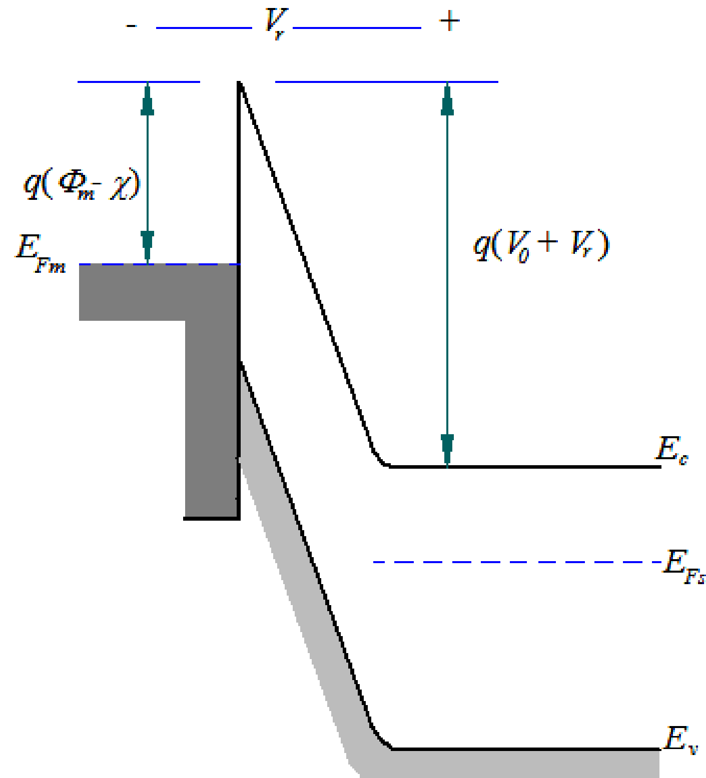

Figure 3.9 : metal-n-type semiconductor Schottky contact under reverse bias.

3.3.3.1: Surface cleanliness.

In the fabrication of metal-semiconductor contacts, the performance of the device is determined by the Schottky barrier height (SBH) which is a measure of the mismatch of the energy levels for majority carriers across the interface [25]. Since the SBH is of vital importance as it controls the electronic transport across the metal semiconductor interface, there is need to ensure that its magnitude is maximum i.e. a need to ensure that the mismatch is minimum. Under ideal conditions, i.e. in a vacuum, the SBH is given as in equation (3.3.2) and (3.3.3) [20] for a metal-n-type semiconductor contact and metal-p-type semiconductor contact, respectively. This is only achievable if the semiconductor surface is free from impurities, dangling bonds, surface states and interface states. The latter mentioned factors modify the structure of the semiconductor surface as they either increase or decrease the size of the SBH. Experiments have shown that the measured SBHs have a strong dependence on the preparation of the metal-semiconductor interface [25]. Equations (3.3.2) and (3.3.3) indicate the dependence of the SBH on the metal work function. Although it has been shown that metals with high work functions have systematically larger SBHs than those with low

work functions, the actual dependence observed is much weaker than that predicted by the Schottky-Mott theory [25], i.e.

$$S_{\Phi} \equiv \frac{\partial \Phi^{O}_{B,n}}{\partial \Phi_{M}} << 1 \qquad (3.3.4)$$

where S_{Φ} is the interface behavior parameter or the *S*-parameter of the semiconductor. The nature of the semiconductor surface is determined by the cleaning procedures used prior to Schottky contacts deposition. These in turn affect the nature of the metal semiconductor interface when a metal is deposited onto the semiconductor. The resulting interface structure is controlled by the nature of the bonds (broken or formed) during etching of samples in acids and the ones formed by depositing the metal. When a metal is deposited onto the semiconductor, because of the difference in the electronic structure of the two materials, a significant redistribution of charge is expected to take place due to the overlap of wave functions from the two different materials [25].

3.3.3.2: Surface states.

Schottky barrier heights in practical metal semiconductor contacts are affected by the processes that take place at the interface. As mentioned in the previous section, the charge redistribution is also affected by the presence of surface states also known as Tamm-Shockley states. These are electronic states often found on the surface of a semiconductor formed due to a sharp termination of solid material that ends with a surface. This surface termination introduces incomplete covalent bonds at the surface [21] leading to a change of the electronic band structure from the bulk material to the vacuum. Electron energy levels within the bandgap of the semiconductor are now created which can be either donor states or acceptor states depending on whether or not they are neutral when occupied [21]. During metal deposition, because of the incomplete covalent bonds, in trying to establish thermal equilibrium between the metal and semiconductor, some electrons from the semiconductor valence band will have to fill the vacant states in the semiconductor atoms and to maintain charge neutrality at the semiconductor surface [20], leading to the *pinning* of the Fermi-level. For a semiconductor with acceptor surface states whose density of states is given by D_s, where D_s is constant over the energy range from $q\Phi_0$ to the Fermi level, the surface state charge density is given by [20],

$$Q_{ss} = -qD_s \left(E_g - q\Phi_0 - q\Phi_{Bn} - q\Delta\Phi \right) \qquad (3.3.5)$$

where $\Delta\Phi$ is the Schottky barrier lowering, Φ_0 is the energy level at the surface, $q\Phi_{Bn}$ is the barrier height of the metal-semiconductor contact as in Fig. 3.5.

3.3.3.3: Fermi level pinning.

This is determined by, and depends on the position and concentration of the surface states in the band structure of the semiconductor. When a metal is brought into intimate contact with the semiconductor, thermal equilibrium has to be established [20] resulting in band bending. In the presence of surface states, electrons from the valence band of the semiconductor will be trapped by these vacant states. This occurs until the Fermi-level coincides with the level to which the surface states are filled [21, 25]. This is what is known as Fermi level pinning. A natural surface depletion of the semiconductor occurs and at the same time, a potential across the semiconductor is established resulting in a barrier height independent of the metal work function. The resulting SBH and built-in potential, V_s can be obtained by using the Bardeen model [26] as,

$$\Phi_B = \Phi_m - \Phi_{SO} + eV_i\,,$$

$$V_s = \frac{\Phi_m - \chi_S}{e} + V_i \qquad (3.3.6),$$

(for a model that fills the semiconductor bandgap near the interface with a distribution of electronic states with a density N_{ss} and charge neutrality position P_O), where Φ_m is the metal work function, Φ_{SO} and χ_S are the work function and the electron affinity of the semiconductor, respectively and e is the absolute value of the electronic charge. V_i is the voltage drop (potential) due to the surface states.

3.4: Temperature dependence of IV measurements on Schottky barrier diodes.

3.4.1: Introduction.

In determining the Schottky barrier height, Φ_b of metal/semiconductor contacts, general *I-V* and capacitance-voltage (*C-V*) measurements are usually employed at room temperature, which use the assumption that only thermionic emission is responsible for the flow of electrons across the potential barrier. At different temperatures, different current transport mechanisms (e.g. generation recombination and tunneling) also contribute towards the movement of electrons within the depletion region and across the barrier in Schottky contacts [27]. There is a need to consider these effects when evaluating the SBH of metal-semiconductor contacts at various temperatures. The equations usually used for the determination of the barrier height according to Schroder [1], indicate the dependence of the barrier height on the saturation current, I_s

$$\Phi_B = \frac{kT}{q} \ln \frac{AA^{**}T^2}{I_s} \tag{3.4.1}$$

where A is the diode area and A^{**} is the effective Richardson constant.

This method of computing the barrier height assumes pure thermionic emission over the barrier, such that,

$$I = I_s \left\{ \exp\left(\frac{qV}{kT}\right) - 1 \right\} \tag{3.4.2}$$

This approximation factors out the effect of the series resistance, R_s and the ideality factor, n. The value of the barrier height determined using this method is for zero bias [1]. According to Schroder [1], there usually exists an uncertainty brought about by the use of an incorrect value of A^{**}. The Richardson constant has a tendency of varying with temperature, and so there is also need to know the actual value of the constant in a range of temperatures in which the barrier height is being evaluated. Different values of the Richardson constant have been obtained by different researchers [28,29,30,31,32] using different temperature ranges. From equation (3.4.1), since A^{**} appears in the *'ln'* term, an error of two would mean the value of Φ_b will be affected by a factor of 0.7kT/q [1]. If we can include other current transport

mechanisms, to make the diode non-ideal, i.e. $n > 1$, the series resistance and the ideality factor need to be factored into equation (3.4.2) [33]:

$$I = I_s \exp\left[\frac{q\ V - IR_s}{nkT}\right]\left\{1 - \exp\frac{\left[q\ V - IR_s\ \right]}{kT}\right\} \quad (3.4.3)$$

where

$$I_s = AA^*T^2 \exp\left(\frac{-q\Phi_b}{kT}\right) \quad (3.4.4)$$

Equation (3.4.3) is commonly used in computing the values of I_s and Φ_b providing $n \leq 1.1$. As soon as the thermionic emission is no longer the only dominant mechanism or the series resistance is too large, the ideality factor n increases. By extrapolating the semi-logarithmic plot of the general I-V relationship, the saturation current is obtained as the intercept on the vertical axis acceptable when the pure thermionic emission vanishes and therefore no physical interpretation in calculating Φ_b from (3.4.4) is justified [33]. In this section, an outline on the effects of temperature on current transport mechanisms and the calculation of the barrier height and the Richardson constant on metal-semiconductor contacts are presented.

3.4.2: Current transport processes.

In metal-semiconductor contacts, unlike in p-n junctions, current flow is due to majority carriers that can be either electrons or holes passing through the potential barrier [20]. There are four main mechanisms by which carrier transport can occur in Schottky barriers in the forward biased direction [20, 34]. These are thermionic emission over the potential barrier, carrier tunneling through the potential barrier, carrier recombination and/or generation in the depletion region and carrier recombination in the neutral region, of the semiconductor, which is equivalent to minority-carrier injection.

3.4.2.1: Thermionic emission current.

This type of current flows through the metal-semiconductor device operated at moderate temperatures, e.g. room temperature [20] and is based on the theory derived by Bethe using the assumptions that the barrier height $q\Phi_b$ is much larger than kT, thermal equilibrium is

established at the plane that determines emission, and the existence of a net current does not disturb thermal equilibrium so that one can superimpose two current fluxes. This theory assumes that when a forward potential, V is applied, electrons with energy larger than the top of the barrier will cross the barrier provided they move towards the barrier [21]. The actual shape of the barrier profile is immaterial [20] and therefore can be ignored so that current flow solely depends on barrier height. The current density can now be expressed as:

$$J_{s \to m} = \int_{E_F + q\Phi_B}^{\infty} q v_x dn \qquad (3.4.5)$$

where $E_F + q\Phi_b$ is the minimum energy required for thermionic emission into the metal, and v_x is the carrier velocity in the direction of transport. In an incremental energy range, the electron density is given by,

$$dn = N(E)F(E)dE$$

$$= \frac{4\pi(2m^*)^{3/2}}{h^3}\sqrt{E - E_c}\exp[-(E - E_c + qV_n)/kT]dE \qquad (3.4.6)$$

where $N(E)$ and $F(E)$ are the density of states and the distribution function, respectively, m^* is the effective mass of the semiconductor, and qV_n is $(E_C - E_F)$. E is the energy of the electrons. Postulating that all the energy associated with the charge carriers in the conduction band is kinetic energy, then

$$E - E_C = \frac{1}{2}m^* v^2$$

$$dE = m^* v dv$$

$$\sqrt{E - E_C} = v\sqrt{m^*/2} \qquad (3.4.7)$$

Equation (3.4.6) can be written as

$$dn = 2\left(\frac{m^*}{h}\right)^3 \exp\left(-\frac{qV_n}{kT}\right)\exp\left(-\frac{m^* v^2}{2kT}\right) 4\pi v^2 dv \qquad (3.4.8)$$

This equation gives the number of electrons per unit volume that have speeds between v and $v + dv$ distributed over all directions [20]. Resolving the speed into components with the x-axis parallel to the direction of transport, we have

$$v^2 = v_x^2 + v_y^2 + v_z^2 \tag{3.4.9}$$

Using the transformation $4\pi v^2 dv = dv_x dv_y dv_z$, we obtain from equations(3.4.5), (3.4.8) and (3.4.9)

$$J_{S\to M} = \left(\frac{4\pi q m^* k^2}{h^3}\right) T^2 \exp\left(-\frac{qV_n}{kT}\right) \exp\left(-\frac{m^* v_{ox}^2}{2kT}\right) \tag{3.4.10}$$

The velocity v_{ox} is the minimum velocity required in the x-direction to surmount the barrier and is given by

$$\frac{1}{2} m^* v_{ox}^2 = q\left(V_{bi} - V\right) \tag{3.4.11}$$

where V_{bi} is the built in potential at zero bias. Substituting (3.4.11) into (3.4.10) yields

$$\begin{aligned} J_{S\to M} &= \left(\frac{4\pi q m^* k^2}{h^3}\right) T^2 \exp\left(-\frac{q\left(V_n + V_{bi}\right)}{2kT}\right) \exp\left(\frac{qV}{kT}\right) \\ &= A^* T^2 \exp\left(-\frac{q\Phi_B}{kT}\right) \exp\left(\frac{qV}{kT}\right) \end{aligned} \tag{3.4.12}$$

where Φ_B is the barrier height which is equal to the sum of V_n and V_{bi} and A^* is the effective Richardson constant for thermionic emission, neglecting the effects of optical phonon scattering and quantum mechanical reflection, and is given by

$$A^* = \frac{4\pi q m^* k^2}{h^3} \tag{3.4.13}$$

Since the barrier height for electrons moving from the metal into the semiconductor remains the same, the current flowing into the semiconductor is thus unaffected by the applied voltage [20]. It must therefore be equal to the current flowing from the semiconductor into the metal when thermal equilibrium prevails (i.e. when $V = 0$). The corresponding current density is thus,

$$J_{M\to S} = -A^* T^2 \exp\left(-\frac{q\Phi_B}{kT}\right) \tag{3.4.14}$$

The total current density is given by,

$$J_n = J_{S\to M} + J_{M\to S}$$

$$\Rightarrow J_n = \left[A^*T^2 \exp\left(-\frac{q\Phi_B}{kT}\right)\right]\left[\exp\left(\frac{qV}{kT}\right)-1\right] \tag{3.4.15}$$

$$J_n = J_{ST}\left[\exp\left(\frac{qV}{kT}\right)-1\right] \tag{3.4.16}$$

where J_{ST} is the saturation current density of thermionic emission given by,

$$J_{ST} = A^*T^2 \exp\left(-\frac{q\Phi_B}{kT}\right) \tag{3.4.17}$$

Equation (3.4.16) gives the current density of an ideal diode. To make the diode non-ideal, the series resistance, R_s and the ideality factor, n need to be factored into equation(3.4.16). The resulting expression becomes,

$$J_n = J_{ST} \exp\left[\frac{q\ V - IR_s}{nkT}\right]\left\{1-\exp\left[-\frac{q\ V - IR_s}{kT}\right]\right\} \tag{3.4.18}$$

The ideality factor is calculated as the gradient of the slope of the linear region of the semi logarithmic I-V plot and is given by [20, 29],

$$n = \frac{q}{kT}\left(\frac{dV}{d\ \ln I}\right) \tag{3.4.19}$$

The series resistance is obtained from the deviation of the semi logarithmic I-V plot from linearity at high currents [1] as,

$$R_s = \frac{\Delta V}{I} \tag{3.4.20}$$

3.4.2.2: Generation recombination current.

This current is due to the generation and recombination of carriers within the space charge region, mainly at low temperatures [35]. Recombination in the space charge region normally takes place via localized states [35]. The most effective centres are those with energies lying near the centre of the forbidden gap. Recombination occurs in two main processes, i.e. direct and indirect recombination [4]. In direct recombination processes, an electron can fall from the conduction band and recombines directly with a hole in the valence band. This can also

be referred to as band to band recombination. This process is usually common as radiative transitions in direct bandgap semiconductors. Energy conservation for this process is ensured by the fact that electrons and holes recombining are located close to the band edges of the semiconductor. In indirect recombination, an electron can fall into a trap where it can recombine with a hole afterwards. This is also known as trap-assisted recombination [21]. Since generation/recombination processes require the conservation of energy and momentum, the event requires a third partner which allows the conservation of momentum [36]. This third partner is a lattice defect, most commonly an impurity atom with an energy state deep in the bandgap i.e. not close to the band edges. As electrons are undergoing transitions from the conduction band to the valence band, they fall into the trap until the trap gets filled up such that it does not accept electrons any more. Once this occurs, the electron occupying the trap can in a second step fall into the valence band, thereby completing the recombination process. Recombination is now determined by the deep states and is no longer an intrinsic or doping dependent property. The theory of the current due to this type of recombination in Schottky diodes is similar to that of an ordinary p-n junction [35], and the current density at low forward bias is given by,

$$J_r = J_{r0} \exp\left(\frac{qV}{2kT}\right)\left\{1 - \exp\left(-\frac{qV}{kT}\right)\right\} \qquad (3.4.21)$$

where $J_{r0} = qn_i w/2\tau_r$, n_i is the intrinsic electron concentration, proportional to $\exp(-qE_g/2kT)$, w is the depletion width and τ_r is the lifetime within the depletion width. Equation (3.4.21) is derived by assuming that the energy levels of the trap centres coincide with the intrinsic level, E_i, the capture cross sections for electrons and holes are equal and that the centres are distributed in a spatially uniform manner [35].

3.4.2.3: Quantum mechanical tunneling.

Basically, in heavily doped semiconductors, and low temperature operation, tunneling current is usually the dominant transport mechanism [20]. At low temperatures, the Fermi level of the semiconductor moves up thereby reducing the barrier height. Considering the wave nature of electrons, the barrier becomes very thin and compatible with the wavelength of these electrons, i.e. their energies will be large enough to allow tunneling from the semiconductor into the metal as their energies will be too low for them to cross over the barrier. Tunneling is

also promoted by the existence of interface states on the metal/semiconductor contacts [37]. These interface states lead to the existence of a Gaussian distribution of barrier heights, i.e. low and high barriers embedded on a uniform barrier [27]. As the current flows through such a contact, charge carriers will follow a path which is easier for them to cross the barrier, as a result, they will tunnel through the low barrier areas resulting in a tunneling current. According to Rhoderick [35], tunneling of carriers in heavily doped (degenerate) semiconductors at low temperatures modifies the usual thermionic emission process into field and thermionic field emission. If current flow in the forward bias is a result of electrons having energies almost equal to the Fermi energy level tunneling through the barrier, the process becomes field emission. Considering the high doping densities of the semiconductor, the barrier is sufficiently narrow at or near the bottom of the conduction band for electrons to tunnel directly [1]. Raising the temperature but not high enough to give electrons enough energy to go over the barrier, excites carriers to higher energies, increasing the tunneling probability very rapidly and charge carriers will 'see' a thinner and sufficiently narrow reduced barrier for easier tunneling [1, 35]. However, the number of excited electrons decreases very rapidly with increasing energy, and the contribution to the current by carriers with energy above the bottom of the conduction becomes a maximum. This mechanism is referred to as thermionic field emission. In the case where the tunneling current dominates the current flow, the transmission coefficient is given by [20],

$$T\ \eta \ \sim \exp\left(-\frac{q\Phi_{Bn}}{E_{00}}\right) \tag{3.4.22}$$

where E_{00} is the characteristic energy level given by [1],

$$E_{00} = \frac{q\hbar}{2}\sqrt{\frac{N_D}{\varepsilon_s m^*}} \tag{3.4.23}$$

The tunneling current density is given by [20],

$$J_t = \exp\left(-\frac{q\phi_{Bn}}{E_{00}}\right) \tag{3.4.24}$$

3.4.3: The Richardson constant

The determination of the barrier height in metal semiconductor contacts, assuming pure thermionic emission and no series resistance is basically dependent on the saturation current, and the Richardson constant, A^* as shown in equation (3.4.4). There usually exists uncertainty due to the use of an incorrect value for A^* [1]. From equation (3.4.13), the Richardson constant depends on the electron effective mass. In turn, the electron effective mass is dependent on temperature as it is influenced by the temperature variation of the energy gap [38]. Thus the Richardson constant has a tendency of varying with temperature, and so there is a need to know the actual value of the constant in a range of temperatures in which the barrier height is being evaluated [27]. Different values of the Richardson constant have been obtained by different researchers [28, 29, 32] using different temperature ranges.

The Richardson constant can be obtained experimentally from *I-V* measurements by linearising equation (3.4.4). This linear relationship yields an equation of the form,

$$\ln\left(\frac{I_s}{T^2}\right) = \ln\ AA^* \ - \frac{q\Phi_b}{kT} \tag{3.4.25}$$

where I_s is the saturation current, obtained as the intercept on the vertical axis of the semi-logarithmic *I-V* plot, T is the temperature in Kelvin, A is the cross-sectional area of the Schottky contact, Φ_b is the barrier height and A^* is the Richardson constant. The numerical value of A^* can be obtained from a linear plot of $\ln\ I_s/T^2$ against $1000/T$ as the intercept to the $\ln\ I_s/T^2$ axis, i.e.

$$A^* = \frac{\exp(c)}{A}\left[AK^{-2}cm^{-2}\right] \tag{3.4.26}$$

where c is a constant (y-intercept). In the case that A^* is not determined experimentally, published values are used. However, this assumption is not good enough as A^* depends on contact quality [27], which involves the surface cleaning procedure during contact preparation, and sample annealing temperature [1]. A^* even appears to depend on the metal thickness and metal deposition method [39]. Rhoderick [35] also suggested the dependence of A^* on an insulator layer which can be an oxide layer formed between the metal and the semiconductor during contact fabrication. The use of an incorrect value of A^* can adversely affect the value of the Schottky barrier height, Φ_b. In the determination of the Richardson constant, the latter mentioned effects influence the measured values of the saturation current

as the barrier will be modified, leading to an incorrect value of A^*. The deviation of A^* from the correct value due to the mentioned effects can be said to be an effect of contact barrier inhomogeneity [29].

3.4.3.1: Barrier Height inhomogeneities

The barrier height of a metal-semiconductor contact can be easily modified by the nature of the contact. This modification leads to what is known as barrier inhomogeneities. This has been explained by some researchers [42, 43] as a situation in which the contact consists of low and high barrier areas at the interface mainly due to the formation of different insulative, oxide layer thicknesses between the metal and the semiconductor [27]. As a result of these potential fluctuations at the interface, the current flowing through the diode will flow preferentially through the lower barriers in the potential distribution [40]. To obtain a corrected value of the Richardson constant, barrier height inhomogeneities correction needs to be effected as was suggested by [29, 40, 41]. Usually, the barrier height obtained from equation (3.4.4) is called the apparent barrier height, which depends on the electric field across the Schottky contact, and consequently on the applied bias [29]. However the barrier height obtained under flat-band conditions is considered to be a real fundamental quantity. As opposed to the case of the zero-bias barrier height, the electrical field in the semiconductor is zero under the flat-band conditions. This eliminates the effect of image force lowering that would affect the *I-V* characteristics and removes the influence of lateral inhomogeneity [29]. In addressing the observed abnormal deviation from classical thermionic emission theory, we need to consider a system of discrete regions of low barrier imbedded in a higher background uniform barrier [42,43]. These behaviours can be explained by assuming that the distribution of the barrier heights is a Gaussian distribution of SBH with a mean value of $\bar{\Phi}$ and standard deviation σ_s which can be given by [44, 45],

$$P\left(\Phi_b\right) = \frac{1}{\sigma_s\sqrt{2\pi}}\exp\left(-\frac{\left(\Phi_b - \bar{\Phi}_b\right)^2}{2\sigma_s^2}\right) \qquad (3.4.27)$$

where $1/\sigma_s\sqrt{2\pi}$ is the normalization constant of the Gaussian barrier height distribution. The total *I (V)* across a diode containing barrier inhomogeneities can be expressed as [29]

$$I(V) = \int_{-\infty}^{+\infty} I(\Phi_b, V) P(\Phi_b) d\Phi_b \qquad (3.4.28)$$

where $I(\Phi_b,V)$ is the current at a bias V for a barrier height based on the ideal thermionic emission-diffusion (TED) theory and $P(\Phi_b)$ is the normalized distribution function giving the probability of accuracy for barrier height. Substituting equation (3.4.18) for $I(\Phi_b,V)$ and equation (3.4.27) for $P(\Phi_b)$ in equation (3.4.28), we obtain the current, $I(V)$ through the Schottky barrier at a forward bias V but with a modified barrier as [29]

$$I(V) = I_s \exp\left(\frac{qV}{n_{ap}kT}\right) \times \left[1 - \exp\left(-\frac{qV}{kT}\right)\right] \qquad (3.4.29)$$

with

$$I_s = AA^{**}T^2 \exp\left(-\frac{q\Phi_{ap}}{kT}\right) \qquad (3.4.30)$$

where n_{ap} and Φ_{ap} are the apparent ideality factor and apparent barrier height at zero bias, respectively, given by [46]

$$\Phi_{ap} = \bar{\Phi}_{b\ (T=0)} - \frac{q\sigma_{so}^2}{2kT} \qquad (3.4.31)$$

and

$$\left(\frac{1}{n_{ap}} - 1\right) = \rho_2 - \frac{q\rho_3}{2kT} \qquad (3.4.32)$$

We need to assume that the mean Schottky barrier height $\bar{\Phi}_b$ and σ_s are linearly bias-dependent on Gaussian parameters, such that $\bar{\Phi}_b = \bar{\Phi}_{b0} + \rho_2 V$ and standard deviation $\sigma_s = \sigma_{so} + \rho_3 V$, where $\bar{\Phi}_{b0}$ is the barrier height at temperature $T = 0\ K$, ρ_2 and ρ_3 are voltage coefficients which may depend on temperature, quantifying the voltage deformation of the barrier height distribution [46]. The temperature dependence of σ_s is small and therefore can be neglected [47]. The decrease of zero-bias barrier height is caused by the existence of the Gaussian distribution and the extent of its influence is determined by the standard deviation itself [29, 40]. The existence of the barrier inhomogeneities affects the current transport of electrons across the Schottky barrier. Since at low temperatures, charge carriers have very low energies to surpass the energy barrier, tunneling of electrons is the dominant process.

Due to the fact that the barrier is non homogeneous, further tunneling through the low barrier areas leads to the deviation of the barrier height from the value that could be obtained for a uniformly distributed barrier at the metal-semiconductor interface [27]. It is often noted that the Gaussian distribution effect is very common at low temperatures [40] since tunnelling is very common. A fit for the variation of the apparent ideality factor with temperature, which obeys equation (3.4.32), must be linear and the voltage coefficients, ρ_2 and ρ_3 can be obtained as the intercept and gradient, respectively. The linear behavior of the plot indicates the voltage deformation of the Gaussian distribution of the SBD [29]. Fitting of experimental data using equations (3.4.4) or (3.4.30) gives the value of the apparent barrier height, which should obey equation (3.4.31). The extent of the barrier inhomogeneities can be measured by the magnitude of σ_{so} as from the standard deviation, σ_s. The lower the value of σ_{so}, the more homogeneous the barrier height is and the better the diode rectifying performance.

3.4.3.2: The modified Richardson constant

After performing the barrier inhomogeneities correction, the Richardson constant will be modified to get a more corrected value, A^{**}. A modified plot is obtained by modifying equation (3.4.25). This is achieved by combining equations (3.4.30) and (3.4.31) such that,

$$I_s = AA^{**}T^2 \exp\left[-\frac{q\bar{\Phi}_{ap}}{kT} + \frac{q^2\sigma_{so}^2}{2k^2T^2}\right] \qquad (3.4.33)$$

and

$$\ln\left(\frac{I_s}{T^2}\right) - \left(\frac{q^2\sigma_{so}^2}{2k^2T^2}\right) = \ln\ AA^{**}\ - \frac{q\bar{\Phi}_{ap}}{kT} \qquad (3.4.34)$$

where A^{**} is the modified Richardson constant. A plot of the modified $\ln\ I_s/T^2\ -\ q^2\sigma_{so}^2/2k^2T^2$ versus $1000/T$ yields a straight line with the slope giving the mean barrier height and the intercept giving the modified Richardson constant.

3.5: CV measurements on SBD.

3.5.1: Introduction.

The barrier height of a metal-semiconductor contact can be determined by the capacitance measurement [20]. The capacitance voltage technique relies on the fact that the width of a reverse biased space charge region of a semiconductor junction device depends on the applied voltage [1]. If a small ac voltage is superimposed upon a dc bias, charges of one sign are induced on the metal and charges of the opposite sign in the semiconductor. This creates a region, which is depleted of charge carriers called the *depletion* region. Since we have charge carriers on either side of the depletion region, the junction forms a parallel plate capacitor with the depletion region acting as a dielectric. A small signal capacitance is generated under reverse biasing conditions.

3.5.2: The depletion width approximation.

The knowledge of impurity distribution in a semiconductor is essential for designing semiconductor devices, especially for obtaining fundamental relations between different device parameters that dictate device characteristics [48]. This is also important in improving semiconductor device operation. There is need for a technique that can be used to determine the correct profile. The most commonly used is the *C-V* profiling technique that makes use of the differential capacitance. The analysis of the technique is usually done using the depletion approximation, in which the semiconductor is assumed to be divided into two distinct regions, a layer that is entirely depleted of carriers (directly below the metal) and an interior region of perfect charge neutrality, and in which no electric field exists. The charge density $\rho(x)$ in the depletion region where there are no electrons in the conduction band is given by qN_D. If the depletion width is w, the charge density in the semiconductor can be written as [4, 20],

$$\rho(x) = \begin{cases} qN_D & if\ x \leq w \\ 0 & if\ x > w \end{cases} \qquad (3.5.1)$$

where N_D is the donor concentration.

3.5.3: The built-in potential.

The presence of an electric field across the depletion region results in a potential difference

across the metal-semiconductor junction. The shape of the band edge profiles can be calculated by solving Poisson's equation under certain boundary conditions. The first condition being obtained from the barrier height while the second is that there is no electric field in the bulk of the semiconductor. Choosing $x = 0$ at the interface, the boundary conditions can be written as $V(0) = V_d$ and $E(\infty) = 0$ for the solution of Poisson's equation in the semiconductor, which can be written in the one dimensional case as

$$\frac{d^2V}{dx^2} = \frac{1}{\varepsilon_s}\rho\ x \qquad (3.5.2)$$

where $\rho(x)$ is the total charge density in the semiconductor at a depth x and ε_s is the permittivity of the semiconductor. Generally, contributions from the valence band, conduction band, ionized donors and acceptors and deep levels in the semiconductor should be taken into account. This, however, leads to a more complicated equation that can only be solved numerically. Simplification of the equation can be made by use of the depletion approximation discussed in the previous section. Integrating equation (3.5.2) twice and applying the boundary conditions yields the depletion region width as [4],

$$w = \sqrt{\frac{2\varepsilon_s V_d}{qN_D}} \qquad (3.5.3)$$

while the electric field and built-in potential in the depletion region are given by

$$E(x) = -\frac{qN_D(w-x)}{\varepsilon_s} \qquad (3.5.4)$$

and

$$V(x) = -\frac{qN_D}{2\varepsilon_s}(w-x)^2 \qquad (3.5.5)$$

3.5.4: The depletion capacitance.

Consider a metal/n-type Schottky barrier diode. The semiconductor is n-type doped with doping density N_D. If a dc bias produces a space charge region of width, w, then the differential or small signal capacitance is given by,

$$C = \frac{dQ_m}{dV} = -\frac{dQ_s}{dV} \qquad (3.5.6)$$

where Q_m and Q_s are the metal and semiconductor charges, respectively. The negative sign accounts for the negative charge in the semiconductor space-charge region (ionized

acceptors) for positive voltage on the metal for reverse bias. A small-amplitude ac voltage of frequency typically 10 kHz to 1 MHz [1] is superimposed onto the dc voltage to determine the capacitance. Suppose an ac voltage is increased from zero to small positive voltage amplitude adding a charge increment dQ_m to the metal contact. For overall charge neutrality, the charge increment dQ_m must be balanced by an equal semiconductor charge increment dQ_s. The semiconductor charge is given by,

$$Q_s = qA\int_0^w (p - n + N_D^+ - N_A^-)dx \approx -qA\int_0^w N_D dx \tag{3.5.7}$$

where the approximation gives $N_A = 0$ and $p \approx n \approx 0$ in the depletion approximation [1], assuming all donors are ionized. A is the electrically active Schottky contact area, p is the hole concentration and n is the electron concentration.

It is important to note that for acceptors and donors with energy levels deep within the bandgap, the true doping density profile may not be measured.

The charge increment is as a result of the slight increase in the space-charge region width. Combining equation (3.5.6) and (3.5.7) gives the depletion capacitance as

$$C = -\frac{dQ_s}{dV} = qA\frac{d}{dV}\int_0^w N_D dx = qAN_D(w)\frac{dw}{dV} \tag{3.5.8}$$

This expression has been obtained by assuming a constant donor concentration, i.e. no variation in N_D over the distance dw. The capacitance of a reverse biased junction, if considered as a parallel plate capacitor is given by

$$C = \frac{\kappa_s \varepsilon_0 A}{w} \tag{3.5.9}$$

where κ_s is the semiconductor dielectric constant.

Differentiating equation (3.5.9) with respect to V and substituting for dw/dV in equation (3.5.8) yields,

$$N_A(w) = -\frac{C^3}{q\kappa_s \varepsilon_0 A^2\, dC/dV} = \frac{2}{q\kappa_s \varepsilon_0 A^2\, d(1/C^2)/dV} \tag{3.5.10}$$

using the identity $d(1/C^2)/dV = -(2/C^3)\,dC/dV$. Equations (3.5.9) and (3.5.10) are key for doping profiling [1]. A plot of $1/C^2$ *versus* V yields a straight line where the doping density can be calculated from the gradient. The intercept on the *V*-axis gives the built-in potential. The depth at which the doping is evaluated is obtained from equation (3.5.9). The ambiguity of the space charge region width for a Schottky barrier diode is eliminated by the fact that it spreads into the substrate. In the metal, space-charge region spreading is totally negligible [1].

3.5.5: The image charge and the image force

From the Schottky effect, i.e., under an applied electric field, an image-force induced lowering of the potential energy for charge carrier emission will be created. We need to consider a metal-vacuum system. We define the minimum energy required to remove an electron from the Fermi-level into vacuum as the work function of the metal, $q\Phi_M$, whose value is generally sensitive to surface contamination [20]. Suppose an electron is at a distance x from the metal surface, a positive charge will be induced on the metal surface. There exists a force of attraction between the induced positive charge on the surface of the semiconductor and the negative charge in the metal which is equivalent to the force that would exist between an electron at x and a positive charge at $-x$. The induced positive charge is called the image charge and the attractive force is called the image force, given by,

$$F = \frac{-q^2}{4\pi\varepsilon_0 (2x)^2} = \frac{-q^2}{16\pi\varepsilon_0 x^2} \tag{3.5.11}$$

where ε_0 is the permittivity of free space. The work done by an electron by transferring it from infinity to a point x is given by,

$$PE(x) = \int_{\infty}^{x} F dx = \frac{q^2}{16\pi\varepsilon_0 x} \tag{3.5.12}$$

This energy in equation(3.5.12) corresponds to the potential energy of an electron at a distance x from the metal surface.

Under an applied external electric field, the total potential energy as a function of distance measured from the surface of the metal is given by,

$$PE(x) = \frac{q^2}{16\pi\varepsilon_0 x} + q\xi x \qquad (3.5.13)$$

where ξ is the electric field strength. The image force lowering also called the Schottky barrier lowering, $\Delta\phi$ and the location of the lowering x_m are given by the condition $dPE(x)/dx = 0$ or

$$x_m = \sqrt{\frac{q}{16\pi\varepsilon_o\xi}} \qquad (3.5.14)$$

$$\Delta\phi = \sqrt{\frac{q\xi}{4\pi\varepsilon_0}} = 2\xi x_m \qquad (3.5.15)$$

The maximum potential energy occurs at a position x_m where the resultant electric field vanishes; where the field due to the image force is equal and opposite to the field in the depletion region. Applying the Schottky effect to metal-semiconductor contacts and performing the same analysis, assuming that there is no interfacial layer between the metal and the semiconductor, it follows that the induced or image charge will be located at a distance x_m in the semiconductor. Replacing the electric field by the maximum field at the interface, and the permittivity of free space by the appropriate permittivity characterizing the semiconductor medium, ε_s , the Schottky barrier lowering is given by,

$$\Delta\phi = \sqrt{\frac{q\xi}{4\pi\varepsilon_s}} \qquad (3.5.16)$$

The value ε_s may be different from the semiconductor static permittivity, i.e. if during the emission process, the electron transit time from the metal semiconductor interface to the barrier maximum, x_m is shorter than the dielectric relaxation time, the semiconductor medium does not have enough time to be polarized and smaller permittivity than the static value is expected [20, 35]. Since the barrier lowering is dependent on the applied electric field, different values are expected under different biasing conditions of the metal-semiconductor contacts. The effect of the barrier lowering on the band diagram of metal-n-type semiconductor material is shown in Fig. 3.10. Though the barrier lowerings shown in Fig. 3.10 are small, they have profound effect on the current transport processes in metal-semiconductor systems [20].

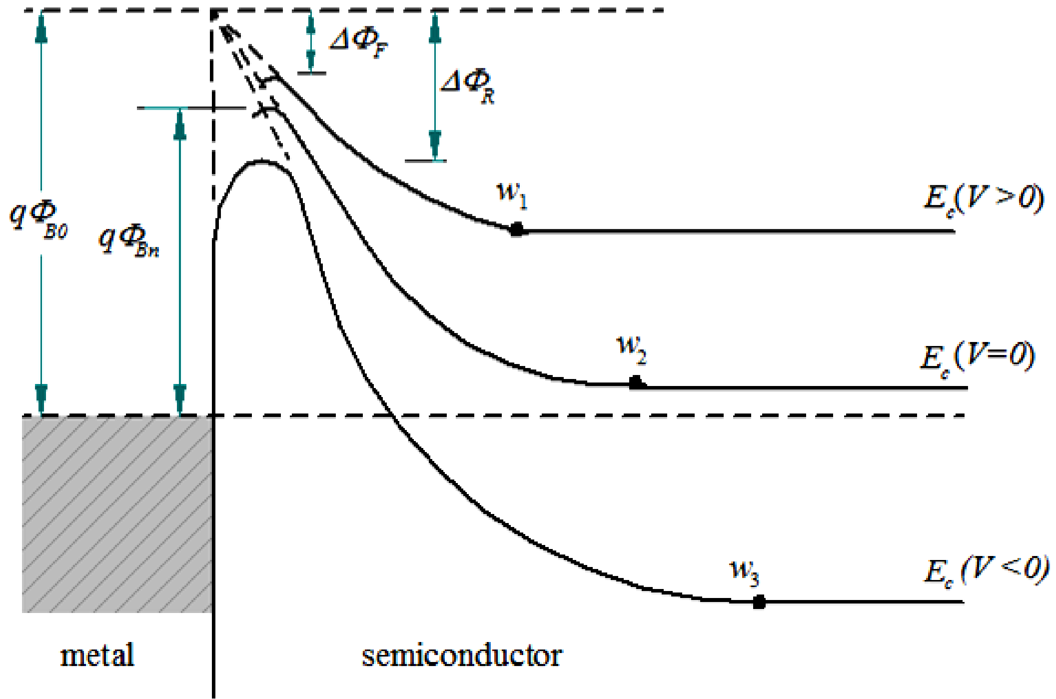

Fig. 3.10: Energy band diagram for a metal-semiconductor contact incorporating the Schottky effect under different biasing conditions. The intrinsic barrier height is $q\Phi_{B0}$. *The barrier height at thermal equilibrium is* $q\Phi_{Bn}$. *The barrier lowerings under forward and reverse bias are* $\Delta\Phi_F$ *and* $\Delta\Phi_R$, *respectively.*

3.5.6: Barrier height determination.

The Schottky barrier height of a metal-semiconductor contact can be conveniently determined by the capacitance-voltage measurement technique. This technique uses the concept of the induced or image charge in the metal and semiconductor [20]. In adopting this type of method for barrier height determination, one should assume the diode to be nearly ideal such that the doping concentration remains uniform in the semiconductor [35]. This method cannot be applied in a situation where the semiconductor is degenerate, doping is not constant, such as during ion implantation and component diffusion as the $1/C^2$ *versus* V plot deviates from linearity. The built in voltage, V_{bi} is obtained directly as the intercept on the voltage axis.

The barrier height can now be calculated as,

$$\Phi_{Bn} = V_{bi} + V_n + \frac{kT}{q} - \Delta\Phi \qquad (3.5.17)$$

where V_i is the voltage intercept interpreted as the built in voltage, V_n is the depth of the Fermi level below the conduction band which can be computed if the doping concentration is known. From the slope, the doping concentration is obtained using equation (3.5.10). $\Delta\Phi$ is the Schottky barrier lowering. The depth of the Fermi level below the conduction band is given by,

$$V_n = \frac{E_c - E_F}{q} = \frac{kT}{q}\ln\left(\frac{N_C}{N_D}\right) \tag{3.5.18}$$

where N_C is the density of states in the conduction band and is given by [4],

$$N_c = 2\left(\frac{2\pi m_n^* kT}{h^2}\right)^{3/2} \tag{3.5.19}$$

where m_n^* is the electron effective mass, k is the Boltzmann constant, T is the Kelvin temperature and h is the Plank's constant.

3.5.7: Frequency dependence of the Schottky barrier height.

As mentioned in the previous section of this chapter, barrier height determination in metal-semiconductor contacts can be influenced by the barrier capacitance. In metal-semiconductor systems with traps (and indeed donors and acceptors), the capacitance voltage relationship is altered as the capacitance becomes frequency dependent. In this scenario, it takes a lot of time for traps to capture or release charge. Given a situation where the frequency of the applied ripple voltage is too high, traps cannot charge and discharge in response [49]. This results in a decrease in the capacitance. The higher the frequency, the lower the average charge density. Keeping all the other parameters constant in equation(3.5.10), the slope of $1/C^2$ *versus* V plot becomes greater. Since the barrier capacitance used in plotting the $1/C^2$ *versus* V plot is dependent on frequency, the barrier height becomes dependent on the frequency of the applied ripple voltage.

References

[1] D. K Schroder, Semiconductor material and device characterization, 2nd Edn. Wiley, New York (1998).

[2] M. S. Tyagi, Introduction to semiconductor materials and devices, J. Wiley and Sons, (1991).

[3] D. J. Griffiths, Introduction to electrodynamics 3rd Edn, Prentice Hall. Inc, (1999).

[4] B. G. Streetman, Solid State Electronic Devices, 5th Ed, Prentice Hall, New Jersey (2000).

[5] D. C. Look, Methods in Materials Research 5a.2.1-5a.2.8 (Wiley, New York, 2000), 15 (1988).

[6] P. Blood, J. W. Orton, The Electrical characterization of Semiconductors, Rep. Prog. Phys., vol. 41, (1978).

[7] R. D. Giaque, Trace element detection with semiconductor detector X-ray spectrometers, Anal. Chem. 45, 671 (1973).

[8]L. J. van der Pauw, A method for measuring specific resistivity and Hall effect of discs of arbitrary shape.

[9] K. Seeger. Semiconductor Physics, Springer series in Solid State Sciences 40. Springer Verlag (1982).

[10] S. A.Goodman, The characterization of GaAs and AlGaAs by the Hall effect, MSc Thesis, (1989).

[11] E. M. Pell, The Hall effect in single crystals of Ba_2O, Phys. Rev. Vol. 87, 3, (1952)

[12] O. Lindberg, Proc of the IRE, 40, 1414, (1952)

[13] http://www.lakeshore.com/

[14] W. R. Runyani, Semiconductor measurements and instrumentation (McGraw-Hill 1975).

[15] L. J. van der Pauw, Philips Res. Rep., 13, (1958).

[16] H. H. Weider, Thin Solid films, 31, 123, (1976).

[17] L. J. van der Pauw, Philips Tech. Rev., 20, 220 (1958).

[18] H. J. van Daal, Philips. Res. Rep.(suppl.), No. 3, 8 (1965).

[19] D. C. Look, B. Claflin, and H. E. Smith, Appl. Phys. Lett 92, 122108 (2008)

[20] S. M. Sze Physics of semiconductor devices, 2nd Edn. Wiley, New York (1981).

[21] http://ece-www.colorado.edu/□ bart/book/surfstat.htm.

[22] http://www.cam.ac.uk/ DoITPoMs TLP-Introduction to semiconductors.

[23] N. K. Reddy, Q Ahsanulhaq, J. H. Kim, M. Devika, and Y. B. Hahn, Nanotechnology 18, 445710 (6pp) (2007).

[24] H. Sheng, S. Muthukumar, N. W. Emanetoglu, Y. Lu. Appl. Phys. Lett.. 80, 2132 (2005).

[25] R. T. Tung. Phys. Rev. B. 45, 13509 (1992).

[26] C. Malagu, M. C. Carotta, H. Fissan, V. Guidi, M. K. Kennedy, F. E. Kruis, G. Martinelli, T. G. G. Maffeis, G. T. Owen, S. P. Wilks, Sensors and Actuators B 100, 283 (2004).

[27] W. Mtangi, F.D. Auret, C. Nyamhere, P. J. Janse van Rensburg, M. Diale, A. Chawanda, Phys. B., 404, 1092 (2009).

[28] E. Gu, S. Tuzemen, B. Kilic and C. Coskun, J. Phys.: Condens. Matter 19 196206 (2007).

[29] I. Dokme, Ş. Altindal and M. M. Bulbul Appl. Surf. Sci. 252, 7749 (2006).

[30] H. Sheng, S. Muthukumar, N. W.Emanetoglu, Y. Lu,. Appl. Phys. Lett.. 80, 2132 (2005).

[31] K. Ip, Y. W. Heo, K. H. Baik, D. P. Norton, S. J. Pearton, S. Kim, J. R. LaRoche and F. Ren Appl. Phys. Lett. 84, 5133 (2004).

[32] H. von Wenckenstern, G. Biene, R. A. Rahman, E. M. Kaidashev, H. Hochmuth, M. Lorenz, and M. Grundmann, Appl. Phys. Lett. 88 2835 (2006).

[33] D. Donoval, M. Barus and M. Zdimal, Solid state electronics 34, 1365 (1991).

[34] K. Shenai and R. W. Dutton, IEEE Transcations on Electron Devices Vol 35, No. 4, April (1988).

[35] E. H. Rhoderick. Metal-Semiconductor contacts, Claredon Press. Oxford. 1988.

[36] http://www.tf.uni-kiel.de/matwis/amat/semi_en/kap_2/r2_3_3.html

[37] L. Lerach, H. Alberach Surface Science 78, 531 (1978).

[38] C. Constantinescu, S. Nan., Physica status solidi, vol 18, 277-282, Feb (2006).

[39] N. Tomaya, J. Appl. Phys. 63, 2720-2724, April (1988).

[40] Ş. Karadeniz, M. Şahin, N. Touğluoğlu and H Şafak, Semicond. Sci. Technol. 19, 91098 (2004).

[41] S. Zhu, R L. Van Meirhaege, C. Detavernier, F. Cardon, G. P. Ru, X. P. Qu, B. Z. Li, Solid State Electron. 44, 663 (2000).

[42] Ş. Altindal, S. Karadeniz, N. Touğluoğlu, A. Tataroglu, Solid-State Electron. 47,

1847 (2003).

[43] R. F. Schmitsdorf, T. U. Kampen, W. Mőnch, Surf. Sci. 324, 249 (1995).

[44] J. H. Werner, H. H. Güttler, Appl. Phys.69 1522 (1991).

[45] Y. P. Song, R L. Meirhaeghe, W. H. Laflere, F. Cardon, Solid State Electron. 29 663 (1986).

[46] A. Gümüş, A. Türüt, N. Yalçin, J. Appl. Phys. 91 245 (2002).

[47] M. K. Hudait, S. P. Venkateswarlu, S. B. Krupanidhi, Solid State Electron. 45, 133 (2001).

[48] M. Nishida, IEEE Transactions on electronic devices, Vol. Ed-26, No. 7, July (1979)

[49] H. K. Henisch. Semiconductor contacts, An approach to ideas and models, Claredon Press, Oxford, (1984)

CHAPTER 4: Experimental Techniques.

4.1: Temperature dependent Hall measurements

Undoped n-type ZnO square samples of orientation 0001 were degreased first in acetone and then methanol in the ultrasonic bath for five minutes. The samples were then blown dry using nitrogen. Triangular indium ohmic contacts were then soldered onto the four corners of the samples as shown in Fig. 4.1 at low soldering temperatures to avoid annealing of the samples before the measurements were performed,

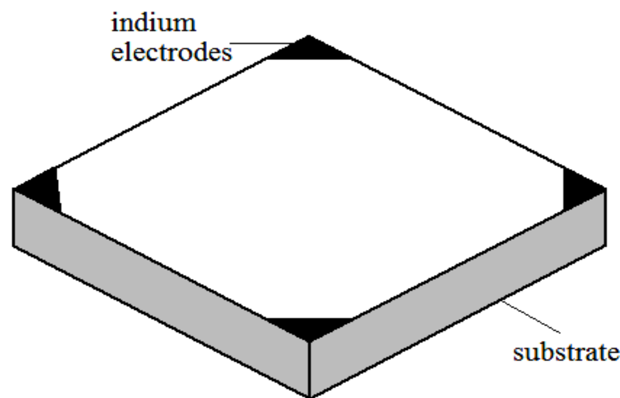

Fig. 4. 1. ZnO sample used in the TDH measurements with triangular ohmic contacts.

After the soldering of the contacts, the samples were finally mounted onto the sample holder which allows for the electrical contact with various devices. This holder was then attached to the shaft of a cryostat powered by a He cycle compressor to achieve the low temperatures used in the temperature dependent Hall (TDH) measurements. A Gold/ Chrome (0.07%) thermocouple was fitted to the tip of the cryostat shaft and was in turn connected to a Lakeshore 332 temperature controller to monitor the temperature. A silicon diode was then clipped onto the sample holder as it provides a more accurate temperature sensing near the sample compared to the thermocouple, and this was also connected to the Lakeshore 332 temperature controller. Temperature stabilization at any setpoint was necessitated by means of a heating element that was connected at the tip of the shaft which was powered by the temperature controller. The sample holder was isolated from the moisture produced in the cryostat by covering it with an inner shroud. The outer shroud was also used to isolate the

cryostat from the atmosphere. The measurements were performed under vacuum provided by the Varian forepump. A Leybold-Heraeus Thermovac TM 230 was then connected to the outer shroud to monitor the vacuum during the measuring process. Two magnet poles were then placed on either side of the sample to provide a probing magnetic field strength of 0.6 T. An HP 6030A system power supply was used as a current source to the magnet, supplying a current of approximately 7.29 A, as the voltage was controlled at about 70 V. An inverting switch was also incorporated into the system so as to invert the magnetic field as the current source could only supply a positive voltage. An HP 3245A universal current source was also used to supply the current to the sample. Contact configuration together with voltage measurement across the sample was achieved by making use of the Agilent 34970A data acquisition unit. Control of all the other instruments except the magnet switch was done via GPIB interfacing. TDH measurements in the temperature range 30-330 K were then performed through the GPIB using an automated program written in LabView™ [1]. Fig 4.1 gives a schematic diagram of the Hall measurement set up system.

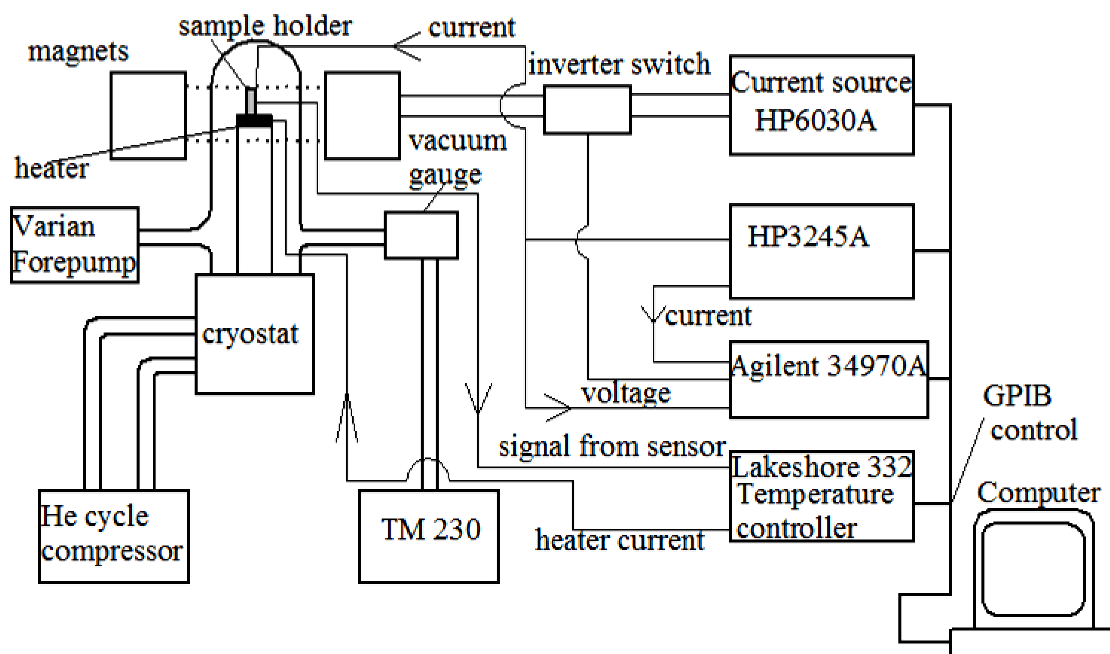

Fig. 4. 2. Temperature Dependent Hall measurement set up system.

Annealing of the samples was done in an oven with a flowing Argon atmosphere ambient at temperatures ranging from 200 °C- 800 °C for 30 minutes at any given temperature. After every anneal TDH measurements were carried out in the 30-330 K temperature range. The Hall coefficient was obtained directly from experiment by making use of equation (3.2.13). The carrier concentration and mobility were then calculated from this value. From the mobility-

temperature plots, the scattering mechanisms can be deduced. The data was then analysed by fitting a model written in Matlab to the experimental data.

4.2: *IV*, *CV* measurements

4.2.1. Sample preparation

Undoped n-type ZnO from Cermet Inc, U.S were used. The samples were degreased first in acetone, methanol and treated in peroxide (Chemically Pure, 30% concentrated) at 100°C for three minutes, prior to Schottky contact deposition. After treatment with H_2O_2, the samples were then blown dry with N_2 gas, immediately followed by contact fabrication.

4.2.2. Contact fabrication

Ohmic contacts of composition Ti/Al/Pt/Au with thicknesses 20/80/40/80 nm were electron beam deposited on the backside of the samples under a vacuum with a pressure below 1×10^{-6} Torr.

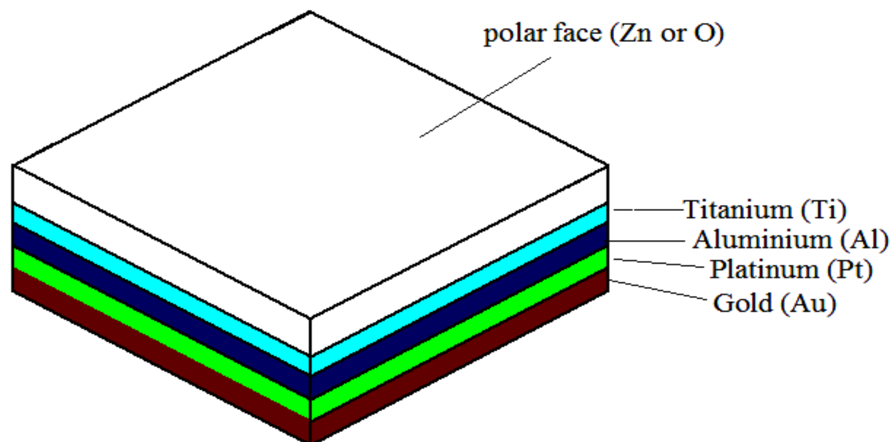

Fig. 4. 3. Ohmic contact with composition Ti/Al/Pt/Au and thicknesses 20/80/40/80 nm.

The samples were then annealed in an Argon flowing atmosphere ambient at a temperature of 200°C to obtain an annealed and alloyed contact with low resistance.

Pd Schottky contacts having a diameter of 0.6 mm and a thickness of 1000 Å were resistively deposited under a vacuum of approximately $8\text{x}10^{-6}$ Torr on the polar faces of the samples.

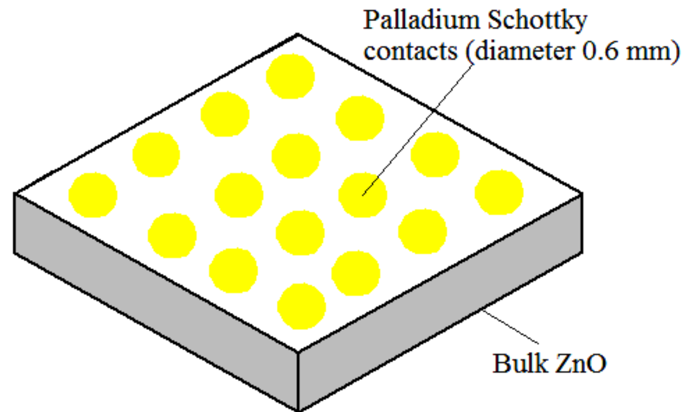

Fig. 4. 4. Palladium Schottky contacts of thickness 100 nm fabricated using the resistive evaporation method.

Electrical characterization through *I-V* and *C-V* measurements was conducted at room temperature in the dark by making use of an automated program written in Labview^{TM}. Fig 4.5 shows a schematic diagram of the *I-V*, *C-V* station used during the electrical characterization of the samples.

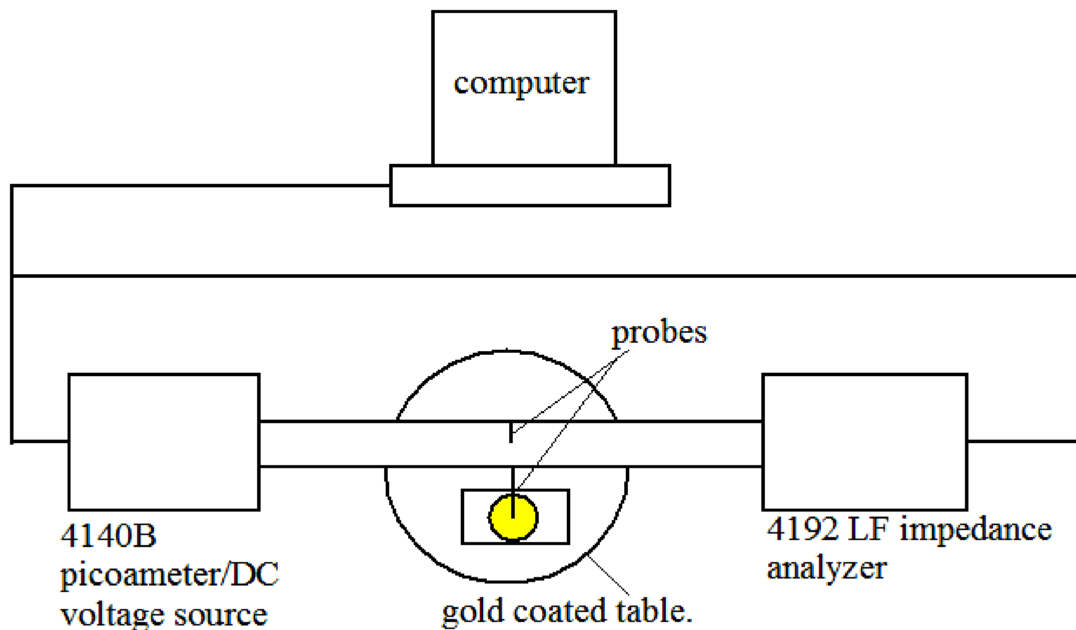

Fig. 4. 5. I-V, C-V station for determining the diode characteristics.

4.3: Temperature dependent *IV* measurements

The samples used were prepared in a similar way described in section 4.2.2. Bonding of thin gold wires was carried out on the Pd Schottky contacts using silver paint. The silver paint was also used on the O-polar face to provide for the ohmic contacts, and the samples were attached to gold plated ceramic plates. Temperature dependent *I-V* measurements were carried out in a He cryostat in the 20 K-300 K range by making use of an automated program

written in Labview™. From the linear plot of the current versus voltage, the values of the ideality factor, series resistance, reverse saturation current, generation recombination current and barrier height were extracted. The current transport mechanisms were also deduced from the nature of the curves.

4.4: Temperature dependent *CV* measurements

Sample preparation was done as outlined in section 4.2. Capacitance voltage measurements were then performed at a frequency of 1 MHz in the reverse bias mode in the -1 – 0 V voltage range. These measurements were also performed at varying temperatures. The samples were loaded in the He cryostat. Measurements were then carried out by using an automated program written in LabView™ in the temperature range $20-300$ K. The barrier height values were obtained from the linear plot of the $1/C^2$ *versus* V. The carrier concentration was also obtained from the depth profiling plot of carrier concentration versus depth (microns) from the surface of the sample.

References

[1] G. H. Kassier, The characterization of bulk as-grown and annealed ZnO by the Hall effect, MSc Thesis 2006

Chapter 5: Results and Discussions

5.1: Hall effect measurements on ZnO

5.1.1: Temperature dependent Hall (TDH) measurements on ZnO.

TDH measurements are essential to semiconductor electrical characterization. They give information about the donor concentrations and energy levels they occupy within the energy gap of a semiconductor. Information about acceptor concentrations can also be obtained from these particular measurements. Carrier mobility together with the scattering mechanisms occurring within the material can also be obtained from TDH measurements. This section gives a discussion of the results obtained on the melt grown ZnO samples.

5.1.1.1: Carrier concentration-temperature analysis.

Fig. 5.1.1 shows the variation in carrier concentration with temperature for the as-received melt grown samples obtained from Cermet as determined from TDH measurements between 20 – 330 K.

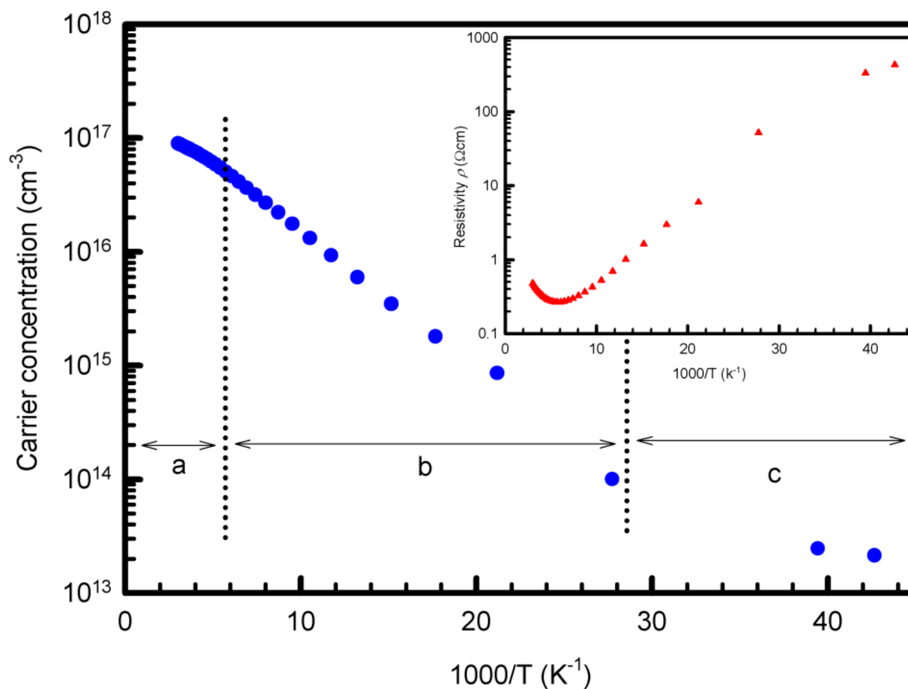

Fig. 5.1. 1: Semilogarithmic carrier concentration versus reciprocal temperature for the as-received ZnO sample in the 20 – 330 K temperature range. Insert shows the variation of bulk resistivity with temperature.

It can be clearly observed that the variation in carrier concentration with temperature can be subdivided into three distinct regions, a, b and c. The region marked a is the high temperature region which shows a strong dependence of carrier concentration on temperature, b is the intermediate temperature region which also indicates the dependence of carrier concentration on temperature, while c gives the low temperature region, in which the carrier concentration is less dependent on temperature change (degenerate region). The dependence of carrier concentration on temperature in the three distinct regions can be attributed to the type of carriers, i.e. either bulk or surface, that contribute to current flow within each particular region. The problem of the existence of more than one conducting region in semiconductors has been reported by some researchers [1,2]. In a case where two conducting layers exist in a semiconductor wafer, the total thickness of the semiconductor material will be given by the surface thickness, d_{surf} and bulk thickness d_{bulk} , $d = d_{bulk} + d_{surf}$, with the measured carrier concentrations denoted by n_{surf} and n_{bulk}.

At high temperatures, it is expected that all the donors will be ionized and current flow is due to bulk electrons, n_{bulk}, which is a volume concentration in cm^{-3}. However, there is a limitation in precisely obtaining the bulk thickness as Hall effect measurements are sensitive to surface concentrations and not volume concentrations [1]. We can assume that the surface thickness, d_{surf} is very small compared to the bulk thickness as was observed and modelled by Look et al [3], i.e. $d_{surf} << d_{bulk}$ and d_{bulk} will be approximately equal to the sample thickness, d. In this case, the bulk donor, $N_{D,bulk}$ and the acceptor $N_{A,bulk}$ volume concentrations can be obtained accurately. Also the donor energy levels $E_{D,bulk}$ can be accurately determined.

In region b, conduction is mixed, i.e. both the surface and bulk electrons contribute to current flow. In region c, conduction is dominated by the surface electrons. This is due to the fact that at low temperatures, the bulk electrons will be frozen out to their donor atoms since ionization will be less. This is also evidenced by an increase in bulk resistivity at low temperatures as in the insert of Fig. 5.1.1. The concentration obtained in this case is a sheet concentration in cm^{-2} as the thickness of the surface, d_{surf} is not known. This makes it difficult to obtain the surface donor and acceptor volume concentrations and the associated energy levels [3].

In this particular analysis, the experimental data was modelled for the carrier concentration obtained in regions (a) and (b) using a Matlab coded program. The modelling was performed by assuming that we have two s-like donors whose energy levels are temperature independent

and one fully ionized acceptor, the position of the Fermi level relative to the valence band can be estimated by solving the charge balance equation,

$$n + N_A^- = \sum_{i=1}^{k} N_D^+ + p \tag{5.1.1}$$

with

$$N_D^+ = \frac{N_{Di}}{\frac{g_{Di} n T^{-3/2}}{N_C} \exp\left(\frac{\Delta E_{Di}}{k_B T}\right) + 1} \tag{5.1.2}$$

where N_c is the effective density of states in the conduction band for ZnO, n, is the concentration of electrons in the conduction band, p is the concentration of holes which is very negligible compared to that of electrons for n-type material and can be considered to be approximately equal to zero, ΔE_{Di} is the energy level of the donor within the energy gap or position of the donor relative to the conduction band edge (also called the activation energy of the donor), g_{Di} is the degeneracy factor equal to 2, k_B is the Boltzmann constant and T is the absolute temperature in Kelvin. It follows that,

$$n + N_A^- = \sum_{i=1}^{k} \left[\frac{N_{Di}}{\frac{g_{Di} n T^{-3/2}}{N_C} \exp\left(\frac{\Delta E_{Di}}{k_B T}\right) + 1} \right] \tag{5.1.3}$$

where n is the number of electrons in the conduction band, given by,

$$n(T) = \frac{1}{4}\left(\frac{2m^* k_B T}{\pi \hbar^2}\right)^{3/2} \exp\left[-\left(\frac{E_G(T) - E_F(T)}{k_B T}\right)\right] \tag{5.1.4}$$

where $E_G(T)$ is the band gap energy relative to the top of the valence band. Its temperature variation has been obtained from Jagadish *et al.* [5], m^* is the electron effective mass of ZnO which is considered to be isotropic and is corrected for the polar coupling with the lattice. Once the value of $E_F(T)$ is known the conduction band carrier concentration deduced from equation 5.1.4 can be compared to the measured carrier concentration, n_H and the neutral donor and ionized donor concentrations can be deduced [4]. Fig. 5.1.2 shows the variation of carrier concentration with temperature for the modelled data. By assuming two s-like donors and one acceptor, the model fits perfectly well to the experimental data. Values of the donor

and acceptor concentrations deduced from the fit to the data in Fig. 5.1.2 are shown in Table 5.1.1.

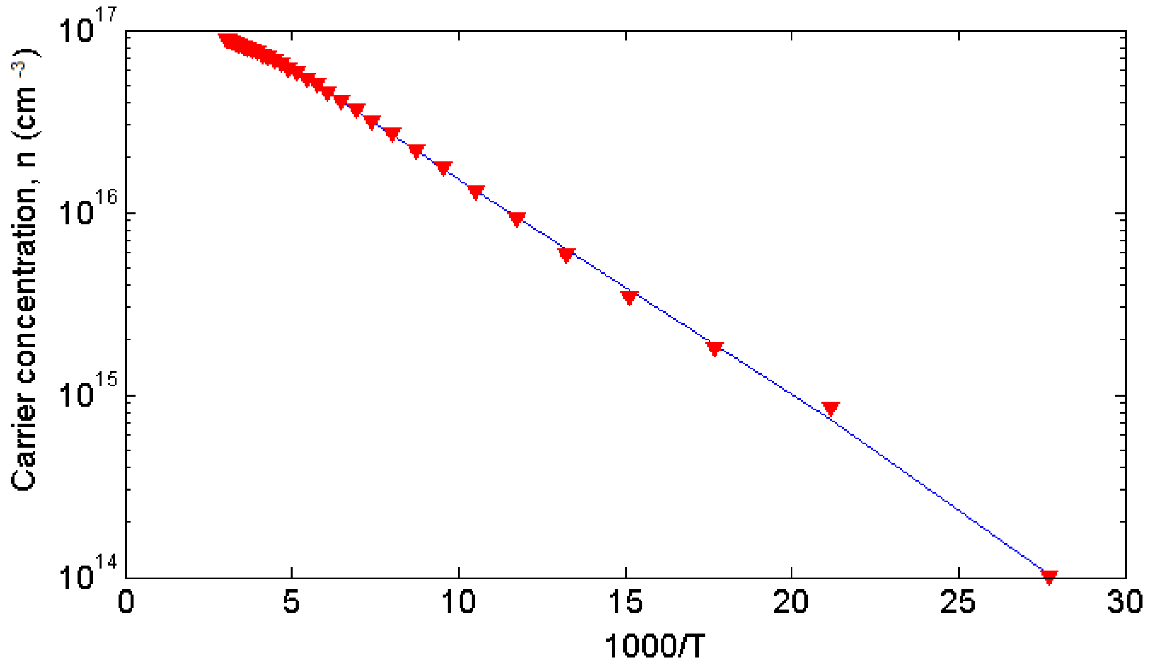

Fig. 5.1.2: Carrier concentration versus reciprocal temperature. Triangles show the measured carrier concentration, $n_{H,meas}$ with the bold line showing the fit to the experimental data.

Table 5.1.1: Values of the donor concentrations, activation energies and acceptor concentration for the as-received melt grown ZnO samples. Carrier concentrations are given in $10^{16}cm^{-3}$ and energy levels in meV.

$N_{D1}(10^{16}cm^{-3})$	E_{D1}(meV)	$N_{D2}(10^{16}cm^{-3})$	E_{D2}(meV)	$N_A\,(10^{16}cm^{-3})$
4.8 ± 0.3	37.8 ± 0.3	5. 7 ± 0.3	54.5 ± 0.9	0.013 ± 0.001

The two shallow donor energy levels in Table 5.1.1 are not far off from the reported levels in the 33 - 35 and 49 – 53 meV ranges [5,6] which have been attributed to native defects in ZnO, possibly Zn_i complexes and H-related complexes. Comparing E_{D1} to these values, E_{D1} can be said to be H-related. The value of E_{D2} is also in close agreement to a level 60 – 63 meV that was also observed by Look *et al.* [6] from photoluminescence measurements. We can also assign E_{D2} to an aluminium (Al) related defect. The acceptor concentration is

very low compared to the total donor concentration, ($N_{D1} + N_{D2}$) and so the sample is not fully compensated.

5.1.1.2: Mobility-temperature analysis.

Fig 5.1.3 shows the variation in the mobility with temperature within the 20 – 330 K.

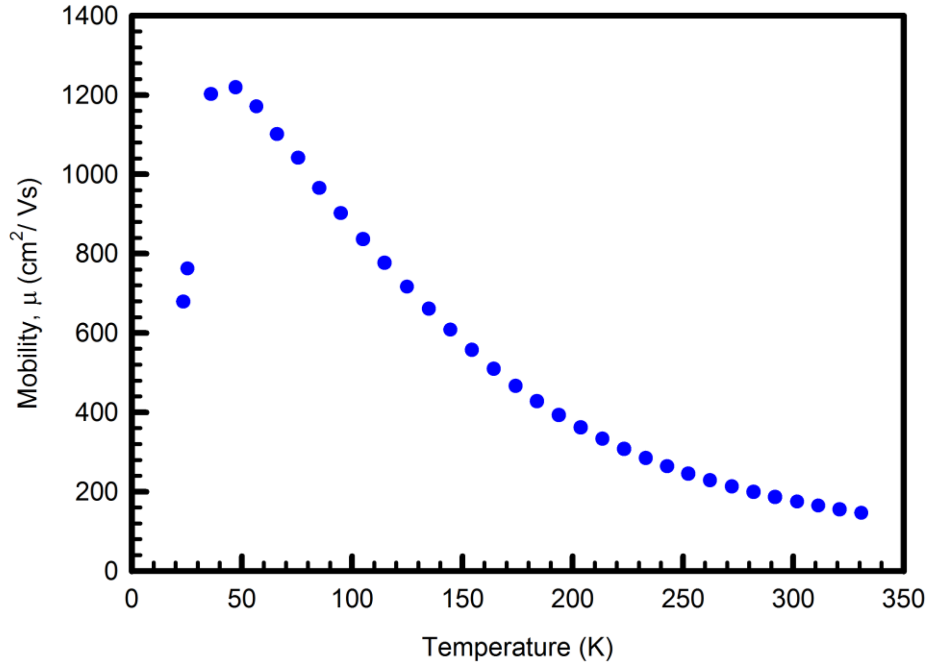

Fig. 5.1.3: Mobility-temperature variation for the as-received melt grown ZnO samples. Measurements performed in the 20 – 330 K temperature range.

The mobility shows temperature dependence within the 20 – 330 K temperature range. A peak mobility of about 1200 cm^2/Vs was observed at about 50 K. Below this temperature, the ionized and neutral impurities scatter the carriers causing a decrease in carrier mobility. Above 50 K, the mobility decreases due to the effects of lattice scattering. A mobility of close to 200 cm^2/Vs was measured at room temperature.

The mobility can be modelled by making use of the Brooks-Herring ionized impurity scattering as was suggested by [3,7]. In the relaxation time approximation (RTA) calculation of $\mu(T)$ the current is assumed to flow orthogonal to the c axis according to the experimental geometry where the neutral and ionized impurities, dislocations, acoustic deformation, piezoelectric and polar optical potentials are considered as possible scattering centers. The RTA approach [5] is based on the assumption that each scattering process (j) affecting the carrier mobility is uncorrelated and can be described by a relaxation time $\tau_j(E)$ that may depend on the carrier energy, E. Therefore, in this approximation, the total relaxation time for

a carrier with energy E ($\tau_{tot}(E)$) is equal to $\left(\sum_j 1/\tau_j(E)\right)^{-1}$ (Matthiesen's rule). Once $\tau_{tot}(E)$ is known, the Hall scattering factor, r_H can be evaluated since:[5]

$$r_H = \frac{<\tau_{tot}^2>}{<\tau_{tot}>^2} = \frac{\int_0^{+\infty} \tau_{tot}^2(E)E^{3/2}e^{-\frac{E}{k_BT}}dE}{\left(\int_0^{+\infty} \tau_{tot}(E)E^{3/2}e^{-\frac{E}{k_BT}}dE\right)^2} \quad (5.1.5)$$

For the neutral impurity scattering, the relaxation time τ_n is evaluated according to,

$$\tau_n = \frac{m^* e^2}{80\pi\hbar^3\varepsilon_0\varepsilon_{r\perp}N_D^0} \quad (5.1.6)$$

where e is the electron charge and ε_0 and $\varepsilon_{r\perp}$ are the free space static permittivity and the relative permittivity for ZnO orthogonal to the c axis, respectively. For the ionized impurity scattering, τ_{ion} is given by,

$$\tau_{ion}(E) = \frac{16\pi\sqrt{m^*}(\varepsilon_0\varepsilon_{r\perp})^2 E^{3/2}}{(N_D^+ + N_A)e^4\left[\ln\ 1+\eta\ + \frac{\eta}{1+\eta}\right]} \quad (5.1.7)$$

with

$$\eta = \frac{2m^*E}{\hbar^2\left[\pi\ \ N_D^+ - N_A\ \right]^{2/3}} \quad (5.1.8)$$

The Table below shows the constants used in the TDH measurements analysis.

Table 5.1.2: ZnO constants used in the modelling of the TDH measurements data.

Polaron effective mass, m^*/m	0.318	Polar phonon Debye temperature, T_{po}(K)	837
Effective mass energy gap, E_g(eV)	3.43	Longitudinal elastic constant c_l (10^{10}Nm^{-2})	20.47
Low-frequency dielectric constant $\varepsilon_0/\varepsilon$	8.12	Deformation potential E_l (eV)	3.8
High-frequency dielectric constant $\varepsilon_\infty/\varepsilon$	3.72	Piezoelectric coupling constant $P\perp/P\parallel$	0.21/0.36

By taking into account the scattering due to deformation potential and piezoelectric acoustic phonons, polar optic phonons, and ionized impurities in ZnO and using N_A as a fitting parameter, the mobility was fitted as in Fig. 5.1.4.

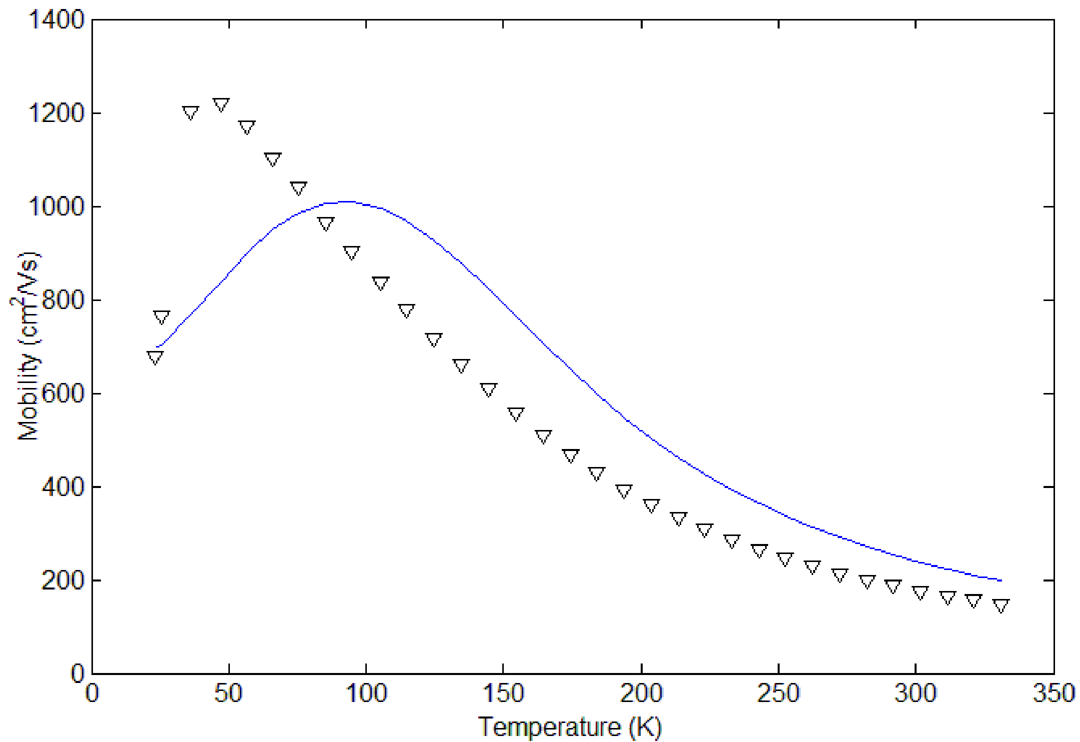

Fig. 5.1.4: Mobility versus temperature of as-received ZnO samples. Triangles show the measured carrier mobility, $\mu_{H,meas}$ with the bold line showing the fit to the experimental data.

As depicted in Fig. 5.1.4, the model does not fit perfectly well to the experimental data. More work has to be done to modify the fit so that it agrees with the experiment. The deformation potential was also used as a fitting parameter but it didn't improve the fit to the data. Fitting of the melt grown ZnO data proves to be difficult as similar problems seem to have been encountered by other researchers [11].

5.1.1.3: Annealing studies of ZnO.

5.1.1.3.1: Introduction.

Annealing of ZnO grown by different techniques have been studied by several researchers [1, 8, 9]. Look *et al.* [1,9] studied the effects of annealing hydrothermally grown ZnO samples in forming gas and nitrogen, while Kassier *et al.* [8] also studied the effects of annealing hydrothermal samples in argon ambient. Kassier *et al.* [10] also studied the effects of annealing hydrogen implanted melt grown samples in an argon environment. The motivation is mainly to study the effects of high temperature annealing on surface conduction in ZnO as it helps get valuable and important information in device fabrication. We have also performed annealing studies on as-received melt grown ZnO samples after treating them with hydrogen peroxide. This chapter gives an overview of our findings.

5.1.1.3.2: Carrier concentration-temperature analysis.

Fig. 5.1.5 shows the variation in carrier concentration with temperature for the samples annealed in the 200°C to 800°C range in an argon atmosphere with no contacts.

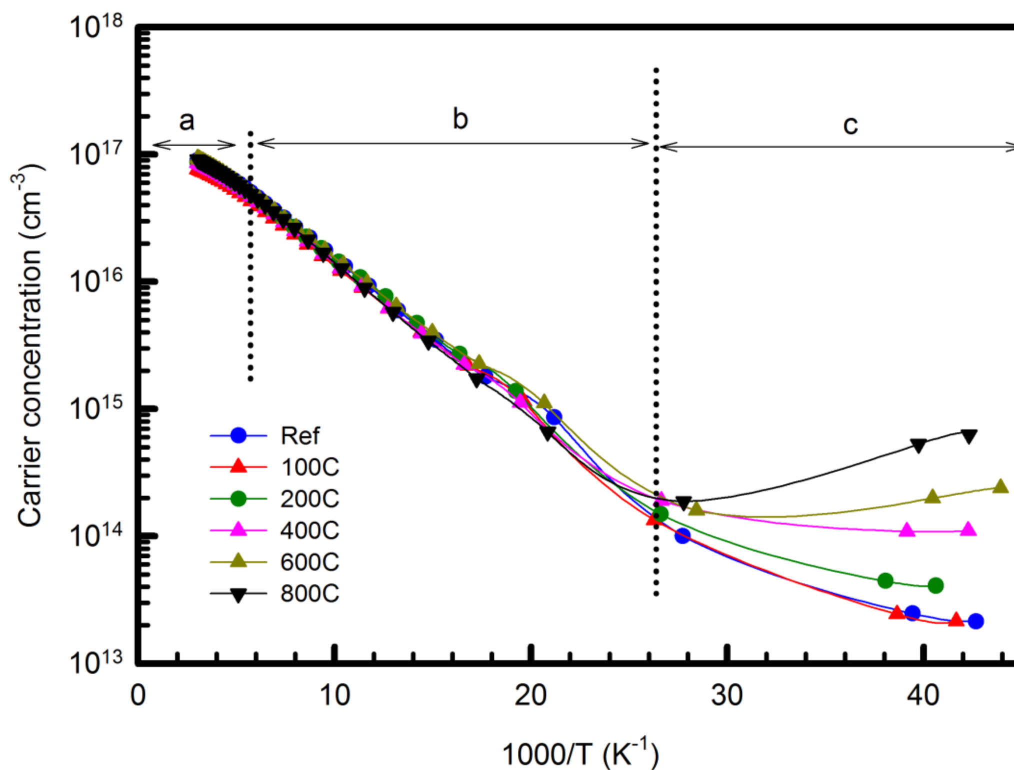

Fig. 5.1.5 : Carrier concentration versus the reciprocal temperature for the as received melt grown ZnO sample annealed in an Ar ambient at different temperatures.

The data as in Fig 5.1.5 can be divided into three distinct regions where conduction can either be due bulk electrons (a), a combination of bulk and surface electrons (b) and conduction due to surface electrons (c). Results obtained from the annealing studies of the hydrogen peroxide treated ZnO samples from Cermet indicate an increase in surface conduction with increasing temperature since the carrier concentration increases with decreasing temperature. Fig. 5.1.5 shows the results obtained with the bold connecting lines showing the theoretical fits to the experimental data. It should be noted that the data has been fitted to two donors and a single acceptor for all the annealing temperatures.

Table 5.1.3 Values of the bulk donor and bulk acceptor volume concentrations for the H_2O_2 treated annealed melt grown samples.

Annealing Temperature(°C)	N_{D1} (x 10^{16}cm^{-3})	E_{D1} (meV)	N_{D2} (x 10^{16}cm^{-3})	E_{D2} (meV)	N_A (x 10^{14}cm^{-3})
Ref(No anneal)	5.3 ± 0.3	39.4 ± 0.3	3.7 ± 0.3	65.8 ± 0.9	1.2 ± 0.1
200°C	6.5 ± 0.3	19.9 ± 0.3	7.4 ± 0.3	50.6 ± 0.9	3.9 ± 0.1
400°C	5.2 ± 0.3	17.8 ± 0.3	8.6 ± 0.3	47.6 ± 0.9	3.9 ± 0.1
600°C	8.7 ± 0.3	50.4 ± 0.3	2.1 ± 0.3	33.5± 0.9	0.9 ± 0.1
800°C	9.7 ± 0.3	47.7 ± 0.3	6.5 ± 0.3	31.8 ± 0.9	2.0 ± 0.1

From Table 5.1.3, E_{D1} becomes shallower after annealing the samples at 400°C. The 17.8 meV observed after annealing at 200 °C and 19.9 meV observed after annealing at 400 °C could possibly be a Group I related element. This is in comparison with the 21 meV donor that was observed by Kassier *et al.* [8] in hydrothermally grown ZnO after annealing the samples at 930°C. Since in melt grown samples there are low concentrations of Li, the two levels could possibly be Na or K related, occupying the Zn sites. After annealing at 600°C the observed donor with energy level, 31 – 33 meV can be said to be Zn_i related. The temperature dependent Hall-effect data for the annealed samples in Fig. 5.1.5 indicate the dominance of surface conduction in the 20 – 40 K temperature range (region c). At low temperatures, region c, the shallow donors, N_{Dsurf}, and acceptors, N_{Asurf} can be deduced by first determining the value of the surface thickness, d_{surf}. An analysis in obtaining the surface donor and acceptor concentrations has been suggested and performed by Look *et al.* [1] on hydrothermally grown ZnO samples. The surface donor and acceptor concentrations can be approximately determined from the following equations [1]:

$$N_{D,surf} = \frac{1}{2}\left(\frac{7.647\times10^{17}T^{3/2}}{\mu_{H,meas}(T)\left\{ \ln\left[1+y(d_{surf})\right] - \frac{y(d_{surf})}{1+y(d_{surf})} \right\}} + n_{meas}\frac{d_{total}}{d_{surf}} \right) \quad (5.1.9)$$

$$N_{A,surf} = \frac{1}{2}\left(\frac{7.647\times10^{17}T^{3/2}}{\mu_{H,meas}(T)\left\{ \ln\left[1+y(d_{surf})\right] - \frac{y(d_{surf})}{1+y(d_{surf})} \right\}} - n_{meas}\frac{d_{total}}{d_{surf}} \right) \quad (5.1.10)$$

where

$$y(d_{surf}) = 1.392\times10^{-6}\left(n_{meas}\frac{d_{total}}{d_{surf}} \right)^{1/3} \quad (5.1.11)$$

where $\mu_{H,meas}$ and n_{meas} are the TDH measured values of mobility and carrier concentration, respectively and d_{total} is the total layer thickness given by $d_{total} = d_{bulk} + d_{surf}$. Taking the value of d_{total} to be approximately equal to 540 μm [3] for melt grown samples, the minimum possible value of the surface thickness can be obtained by setting $N_{A,surf} = 0$ and using the measured values of the carrier concentration and mobility at the lowest temperature. The surface thicknesses and surface donor concentrations obtained from this method are shown in Table 5.1.4 for the annealing temperatures 200 – 800°C.

Table 5.1.4: Values of the surface donor volume concentrations for the H_2O_2 treated and annealed melt grown samples.

Annealing Temperature (°C)	Surface thickness d_{surf} (nm)	$N_{D,surf}$ ($\times$ 10^{18} cm^{-3})
200	32	0.63
400	48	1.15
600	45	2.67
800	72	4.37

As revealed by Table 5.1.4, the minimum surface donor concentration obtained from equation (5.1.9) increases with an increase in annealing temperature.

5.1.1.3.3: Electron mobility-temperature analysis.

The variation of mobility with annealing temperature for the melt grown ZnO samples is shown in Fig. 5.1.6.

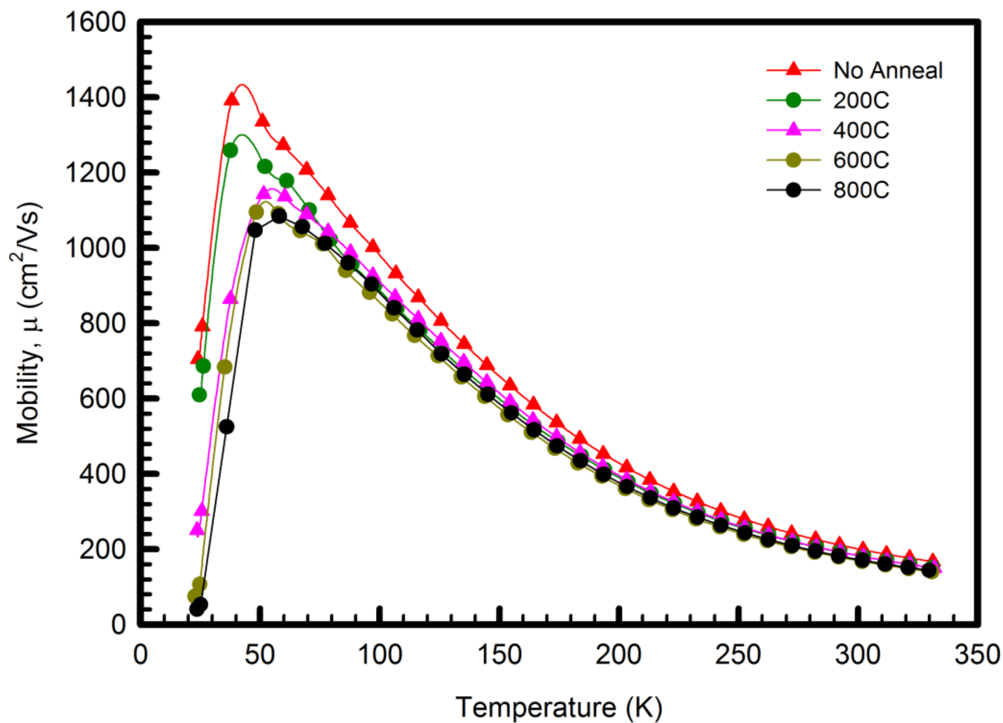

Fig. 5.1.6 : Mobility as a function of temperature for the melt grown ZnO samples annealed in an Ar ambient at different temperatures after H_2O_2 treatment.

The peak mobility decreases with an increase in annealing temperature. With no anneal, but after H_2O_2 treatment, a peak mobility of approximately 1400 cm^2/Vs was observed. After annealing at 800°C, the peak mobility dropped to about 1100 cm^2/Vs. This trend can be explained by the fact that the Hall effect technique is sensitive to what happens on the surface. As the material is annealed, some of the impurities become electrically active and contribute to the electrical conductivity of the material. This will increase the effects of neutral impurity scattering at low temperatures which in turn causes the decrease in the peak mobility at high annealing temperatures as shown in Fig. 5.1.6. It was also suggested by Kassier *et al.* [11] that annealing ZnO at high temperatures causes the aluminium dopants to migrate towards the grain boundaries, decreasing the crystal quality and hence lowering the mobility.

5.1.2: Conclusions.

Temperature dependent Hall effect measurements performed on the as-received ZnO material have revealed the existence of two shallow defects. Fitting the experimental data to a model in Matlab by assuming two s-like donors has yielded donors with energy levels (37.8 ± 0.3) meV and (54.5 ± 0.9) meV and associated concentrations of (4.8 ± 0.3) x 10^{16}cm^{-3} and (5. 7 ± 0.3) x 10^{16}cm^{-3}, respectively. The (37.8 ± 0.3) meV shallow donor has been explained as Zn_i related and possibly H-complex related, while the (54.5 ± 0.9) meV has been explained as an Al-related donor. The two shallow donor levels (19.9 meV and 17.8 meV) introduced after annealing the samples have been ascribed as being related to Group I elements occupying the Zn sites, X_{Zn}. An acceptor with concentration (1.3 ± 0.1) 10^{14}cm^{-3} has also been obtained from the fitting for the as received sample. The peak mobility for the as-received sample has been measured as 1250 cm^2/Vs. After treatment with H_2O_2, the mobility increased to a peak of approximately 1400 cm^2/Vs. The peak mobility of the samples decreases with increasing annealing temperature. This has been attributed to an increase in the number of the electrically active neutral donors, possibly Group I element related, that increase the probability of carrier scattering. Annealing studies performed on the hydrogen peroxide treated ZnO samples indicate an increase in surface conduction with increasing annealing temperature. Calculated surface donor volume concentrations for the annealed samples increases with an increase in annealing temperature. TDH results on the hydrothermally grown samples are discussed in the publication at the end of this particular section.

References

[1] D. C. Look, B. Claflin, and H. E. Smith, Appl. Phys. Lett 92, 122108 (2008)

[2] O. Schmidt, P. Kiesel, C. G. van de Walle, J. M. N. Johnson, J. Nause and G. H. Dohler, J. Journal of Appl. Phys 44, 7271 (2005)

[3] D. C. Look, Surf. Sci. 601, 5315 (2007)

[4] R. Schifano, E. V. Monakhov, L. Vines, B. G. Svensson, W. Mtangi, and F. D. Auret, J. Appl. Phys. 106, 043706 (2009).

[5] C. Jagadish and S. J. Pearton, *Zinc Oxide Bulk, Thin Films and Nanostructures* Elsevier, New York, (2006).

[6] D. C. Look, G. C. Farlow, P. Reunchan, S. Limpijumnong, S. B. Zhang, and K. Nordlund, Phys. Rev. Lett. 95, 225502 (2005).

[7] D. C. Look, H. L. Mosbacker, Y. M. Strzhemechny, and L. J. Brillson, Superlattices Microstruct. 38, 406 (2005).

[8] G. H. Kassier, M. Hayes, and F. D. Auret, J. Appl. Phys. 102, 014903 (2007).

[9] D. C. Look, Superlattices Microstruct. 42 284 (2007)

[10] G. H. Kassier, M. Hayes, F. D. Auret, M. Diale, and B. G. Svensson, phys. stat. sol. (c) 5, 569 (2008).

[11] G. H. Kassier, M. Hayes, F. D. Auret, M. Diale, and B. G. Svensson, Hall effect studies of donors and acceptors in different types of bulk ZnO modified by annealing and hydrogen implantation, SAIP 2007.

UNIVERSITEIT VAN PRETORIA
UNIVERSITY OF PRETORIA
YUNIBESITHI YA PRETORIA

Publications.

JOURNAL OF APPLIED PHYSICS **106**, 043706 (2009)

Defects in virgin hydrothermally grown *n*-type ZnO studied by temperature dependent Hall effect measurements

R. Schifano,[1,a] E. V. Monakhov,[1] L. Vines,[1] B. G. Svensson,[1] W. Mtangi,[2] and F. D. Auret[2]

[1]*Department of Physics/Center for Materials Science and Nanotechnology, University of Oslo, P.O. Box 1048 Blindern, N-0316 Oslo, Norway*
[2]*Department of Physics, University of Pretoria, Pretoria 0002, South Africa*

(Received 26 January 2009; accepted 9 June 2009; published online 25 August 2009)

Temperature dependent Hall (TDH) effect measurements have been performed on three virgin and hydrothermally grown ZnO samples with resistivities between ~5 and ~200 Ω cm at room temperature. The electrical conduction observed experimentally in the temperature range of 330–70 K can be accurately described by three donor levels with positions 41–48, 60–66, and ~300 meV below the conduction band edge (E_C) and an acceptor level in the lower part of the energy band gap (E_G). Correlation of the TDH data with results from secondary ion mass spectrometry and admittance spectroscopy on the same samples suggests a rather firm association of the intermediate donor level with complexes involving Al impurities, while the shallowest one is tentatively ascribed to H-related centers. A large fraction of the deep donor remains nonionized in the temperature range studied and contributes substantially to the neutral-impurity-scattering of the conducting electrons. A detailed analysis of the TDH data, using the relaxation time approximation, reveals, however, that ionized-impurity-scattering and optical phonon scattering are the main mechanisms limiting the electron mobility which exhibits a maximum value of ~125 cm^2/V s at ~200 K. The major reason for this modest value is the high concentration of compensating acceptors in the lower part of E_G reaching values of $\sim 3 \times 10^{17}$ cm^{-3} and where Li plays an important role. However, the Li content is not sufficient to account for all the acceptors and additional impurities, excluding group I elements, and/or intrinsic defects have to be considered. © *2009 American Institute of Physics.* [DOI: 10.1063/1.3168488]

I. INTRODUCTION

Zinc oxide (ZnO) is a promising semiconductor for the realization of solid state ultraviolet emitters in high efficiency lighting devices for general illumination and in high density optical information storage systems because of its wide direct band gap of ~3.4 eV at 300 K and its large exciton binding energy of ~60 meV.[1–3] In addition, ZnO has some substantial advantages with respect to GaN, its major competitor in the above mentioned applications: the possibility of low temperature epitaxial growth[4] and the availability of large-area single crystals.[5–7] ZnO bulk single crystals, to be used both as device material and as substrates for subsequent epitaxial growth, are mainly grown by chemical vapor transport, from melt or under hydrothermal conditions.[8,9] In the hydrothermal case the use of a mineralizer solution containing alkali metals is prone to the inclusion of impurities, especially Li, into the material.[10] On the other hand, the technique is particularly interesting from a technological point of view since the quality of the substrates is high[11] and the method is scalable.[9]

Charge carrier mobility is a vital issue for the ZnO technology, but there is no widespread consensus on the analysis of experimental data: for obtaining a good fit of the mobility data versus temperature it has become common practice to set the acoustic mode deformation potential as a fitting parameter[12,13] instead of using the experimental value[14] of 3.8 eV. Moreover, the necessity of assuming a concentration of electrically neutral impurities as high as $\sim 1.8 \times 10^{18}$ cm^{-3} in hydrothermally grown samples and $\lesssim 2 \times 10^{17}$ cm^{-3} for samples grown by chemical vapor transport or from melt has recently been pointed out.[15] In these cases an effective polar optical phonon temperature of 750 K is assumed and no identification of the neutral impurities involved is provided.

In this work temperature dependent Hall effect (TDH) measurements have been performed using hydrothermally grown samples. The results are analyzed in the relaxation time approximation (RTA) to reveal if the neutral impurity scattering can be attributed to the deep donor level commonly reported in bulk ZnO (Refs. 12 and 16–18) and located ~0.3 eV below the conduction band edge (E_C). In addition, the concentrations of the ionized compensating centers and the shallow donors, estimated by a combined analysis of the mobility data and the carrier concentration versus temperature data, are correlated with the chemical Li, Na, K, Al, Ga, and In concentrations determined by secondary mass spectrometry (SIMS).

II. EXPERIMENTAL DETAILS

Three nominally undoped hydrothermally grown *n*-type ZnO square samples A, B, and C were cut from three different 500 μm thick wafers originating from the same batch

[a]Electronic mail: ramon.schifano@smn.uio.no.

 © 2009 American Institute of Physics

Downloaded 12 Oct 2009 to 137.215.6.53. Redistribution subject to AIP license or copyright; see http://jap.aip.org/jap/copyright.jsp

UNIVERSITEIT VAN PRETORIA
UNIVERSITY OF PRETORIA
YUNIBESITHI YA PRETORIA

and purchased from SPC Goodwill. A resisitivity of 5.1 ± 0.6, 15 ± 2, and 220 ± 20 Ω cm was evaluated by four point probe measurements, for samples A, B, and C, respectively. Then the samples were cleaned in an ultrasonic bath with acetone and ethanol, rinsed in de-ionized water and blown dry with N_2. Using a van der Pauw configuration for the TDH measurements, Ti/Al/Pt/Au multilayers (each 200 Å thick) triangular Ohmic contacts were subsequently deposited at the corners of the samples on the O-face $(000\bar{1})$ followed by an annealing at 200 °C for 1 h in air. Finally, an In drop was soldered on top of the metallization as protection.

The TDH measurements were performed in the temperature range of 70–330 K with a probing magnetic field strength of 0.6 T. All the measurements were undertaken with the samples in vacuum and no exposure to light.

SIMS measurements using a Cameca IMS 7*f* microanalyzer were performed on A', B', and C' samples cut out from the same ZnO wafers as the samples A, B, and C, respectively, and similarly annealed at 200 °C for 1 h prior to the SIMS analysis. The Li, Na, and Al concentration profiles were determined using ion implanted reference samples, while relative sensitivity factors were employed for K, Ga, and In. A constant erosion rate was assumed for depth calibration and the crater depths were measured using a Dektak 8 stylus profilometer.

III. HALL EFFECT THEORY

TDH measurements of an extrinsic semiconductor can be used to determine both the Hall carrier concentration (n_H) and the Hall mobility (μ_H) in the examined sample; these estimates are related to the actual carrier concentration n and the drift mobility μ in the material by the expressions $n = n_H r_H$ and $\mu = \mu_H / r_H$ with r_H being the Hall scattering factor.[1,19] Moreover, the temperature dependence of these quantities are related to the concentration of the main shallow impurities and their corresponding energy positions as well as to the concentration of compensating centers. Hence, a comparison of the measured values with the ones obtained by using a suitable model can be used to elucidate the characteristics of the main impurities.

In the present study, the measured $n_H(T)$ temperature dependence is modeled assuming the presence of a fully ionized single charged acceptor (A) and three s-like donors (Di, $i=1,2,3$) with energy levels E_{Di} below E_C. These energies are extracted independently (see Ref. 20) by thermal admittance spectroscopy (TAS) measurements on samples A, B, and C. A degeneracy factor equal to 2 and no temperature dependence of the energy level positions are assumed for all the three donors. With these assumptions the Fermi level energy position (E_F) in the band gap with respect to the valence band edge can be estimated by solving the charge neutrality condition

$$n + N_A^- = \sum_{i=1,2,3} N_{Di}^+ + p, \tag{1}$$

with[21]

$$N_{Di}^+ = N_{Di}\frac{1}{1+2e^{-(E_G(T)-E_{Di}-E_F(T)/k_BT)}},$$

and

$$n(T) = \frac{1}{4}\left(\frac{2m^* k_B T}{\pi\hbar^2}\right)^{3/2} \times e^{-(E_G(T)-E_F(T)/k_BT)}, \tag{2}$$

where n is the concentration of electrons in the conduction band, p is the total hole concentration in the valence band, N_A^- is the ionized acceptor concentration that is providing the compensation, N_{Di} and N_{Di}^+ are the total and ionized concentration of donors of type Di, respectively, k_B, T, $\hbar$, and m^* are, respectively, the Boltzmann constant, the absolute temperature of the sample, the reduced Planck constant and the electron effective mass in ZnO. The latter is considered to be isotropic and is corrected for the polar coupling with the lattice (polaron mass). $E_G(T)$ is the band gap energy relative to the valence band edge and the variation of E_G with T is taken from Ref. 1. Once $E_F(T)$ is known, the conduction band carrier concentration, $n(T)$, deduced from Eq. (2) can be compared with the measured $n_H(T)$. In addition, the concentrations of neutral donors $N_D^0 = \Sigma_{i=1,2,3} N_{Di}^0$ and of ionized donors $N_D^+ = \Sigma_{i=1,2,3} N_{Di}^+$ versus temperature are evaluated as well.

In the RTA calculation of $\mu(T)$ the current is assumed to flow orthogonal to the c axis according to the experimental geometry where the neutral and ionized impurities, dislocations, acoustic deformation, piezolectric and polar optical potentials are considered as possible scattering centers. The RTA approach[1,19] is based on the assumption that each scattering process (j) affecting the carrier mobility is uncorrelated and can be described by a relaxation time $\tau_j(E)$ that may depend on the carrier energy E. Therefore, in this approximation, the total relaxation time for a carrier with energy E, $\tau_{\text{tot}}(E)$, is deduced from $\tau_{\text{tot}}(E) = (\Sigma_j 1/\tau_j(E))^{-1}$ (Matthiesen's rule). Once $\tau_{\text{tot}}(E)$ is known r_H can be evaluated since[1,19]

$$r_H = \frac{\langle \tau_{\text{tot}}^2 \rangle}{\langle \tau_{\text{tot}} \rangle^2} = \frac{\int_0^{+\infty} \tau_{\text{tot}}^2(E) E^{3/2} e^{-E/k_BT} dE}{\left(\int_0^{+\infty} \tau_{\text{tot}}(E) E^{3/2} e^{-E/k_BT} dE\right)^2}. \tag{3}$$

For the neutral impurity scattering the relaxation time (τ_n) is evaluated according to[22]

$$\tau_n = \frac{m^* q^2}{80\pi\hbar^3 \epsilon_0 \epsilon_{r\perp} N_D^0}, \tag{4}$$

where q is the electron charge and ϵ_0 and $\epsilon_{r\perp}$ are the free space and the ZnO static relative permittivity orthogonal to the c axis, respectively.

Because of the high compensation ratio expected, the Falicov–Cuevas,[23] instead of the more commonly used Brooks–Herring,[22] equation is chosen for describing the ionized impurity scattering (τ_{ion})

Downloaded 12 Oct 2009 to 137.215.6.53. Redistribution subject to AIP license or copyright; see http://jap.aip.org/jap/copyright.jsp

$$\tau_{\text{ion}}(E) = \frac{16\pi\sqrt{2m^*}(\epsilon_0\epsilon_{r\perp})^2 E^{3/2}}{(N_D^+ + N_A)q^4\left[\ln(1+\eta) + \frac{\eta}{1+\eta}\right]}, \quad (5)$$

with

$$\eta = \frac{2m^*E}{\hbar^2[\pi(N_D^+ - N_A)]^{2/3}}.$$

The derivation of a proper relaxation time for the dislocation scattering $\tau_{\text{dis}}(E)$ is here described in some detail since an expression for $\tau_{\text{dis}}(E)$ valid in the whole temperature range studied is not readily found in the literature and, further, the Pödör high temperature limit approximation[24] of $\tau_{\text{dis}}(E)$ has been questioned.[25] In general, for a scattering process the following equality holds between the relaxation time as a function of the wave vector **k**, $\tau(\mathbf{k})$, and as a function of energy, $\tau(E)$:[21]

$$\int\int\int d^3\mathbf{k}v_x^2\left(\frac{\partial f}{\partial E}\right)\tau(\mathbf{k}) = -\frac{2\sqrt{2m^*}}{\hbar^3}\int_0^{\pi} d\vartheta \int_0^{2\pi} d\varphi \int_0^{+\infty} E^{3/2}\sin^3\vartheta\cos^2\varphi \times\left(\frac{\partial f}{\partial E}\right)\tau(E,\vartheta,\varphi)dE, \quad (6)$$

where the electric field appears in the x direction, v_x is the electron velocity component in the x direction, and $\partial f/\partial E$ is the derivative with respect to E of the electron probability distribution f at thermal equilibrium, i.e., the Fermi–Dirac distribution. Then, once the integration over $d\vartheta$ and $d\varphi$ in Eq. (6) are performed an expression for $\tau(E)$ can be easily obtained if $\tau(\mathbf{k})$ is known. Specifically, we assume that all the dislocations are orthogonal to the current flow and employ the Pödör expression $\tau_{\text{dis}}(\mathbf{k})$ as $\tau(\mathbf{k})$ in Eq. (6) (Ref. 24)

$$\tau_{\text{dis}}(\mathbf{k}) = \frac{8(\epsilon_0\epsilon_{r\perp})^2\hbar^3}{Q^2q^2m^*\lambda N_{\text{dis}}}\left(\frac{1}{4\lambda^2}+k_\perp^2\right)^{3/2}, \quad (7)$$

where N_{dis} is the dislocations density, Q the charge of the dislocation per unit length, $k_\perp$ the electron wave vector component orthogonal to the dislocation direction, and $\lambda = \sqrt{k_BT\epsilon_0\epsilon_r/q^2n}$ the Debye length. Then the following equation for $\tau_{\text{dis}}(E)$ can be derived:

$$\tau_{\text{dis}}(E) = \frac{3(\epsilon_0\epsilon_{r\perp})^2\hbar^3}{4Q^2m^*q^2\lambda^4N_{\text{dis}}} \times \int_0^{\pi}\left(1+\frac{8m^*\lambda^2E}{\hbar^2}\sin^2\theta\right)^{3/2}\sin^3\theta d\theta, \quad (8)$$

that reduces to the Pödör approximation[24] of $\tau_{\text{dis}}(E)$ in the high temperature limit. A dislocation density equal to the typical value[9] (10^4 cm^{-2}) reported for hydrothermally grown ZnO is used in our calculations (see Table I).

The acoustic deformation potential (τ_{acu}) and the piezoelectric scattering (τ_{piez}) are, respectively, given by[22]

$$\tau_{\text{acu}}(E) = \frac{\pi\hbar^4c_l}{\sqrt{2}m^{*3/2}\epsilon_{\text{ac}}^2k_BT}E^{-1/2}, \quad (9)$$

TABLE I. ZnO constants used in the TDH measurements analysis.

$\epsilon_{r\perp}$ [a]	7.77	$\epsilon_{\infty\perp}$ [a]	3.70
m^* [e,f]	0.336	ϵ_{ac} [d] (eV)	3.8
c_l [d] (N m^{-2})	2.05×10^{11}	$K_\perp$ [d]	0.21
T_{po} [a] (K)	824	N_{dis} [b] (cm^{-2})	10^4
Q [c] (C m^{-1})	2.7×10^{-10}		

[a]From Ref. 8.
[b]From Ref. 9.
[c]From Ref. 26.
[d]From Ref. 14.
[e]From Ref. 15.
[f]From Ref. 27.

$$\tau_{\text{piez}}(E) = \frac{2^{3/2}\hbar^2\epsilon_0\epsilon_{r\perp}}{m^{*1/2}2^2K_\perp^2k_BT}E^{1/2}, \quad (10)$$

where c_l is the longitudinal elastic constant, ϵ_{ac} is the deformation potential, and $K_\perp$ is the piezolelectric coefficient orthogonal to the c axis.

Finally, the interaction of the carriers with the optical phonons is taken into account. In these collisions the energy exchange can be larger than the thermal energy of the electrons. Hence this process should be treated as inelastic, i.e., a strict momentum relaxation time is not applicable. The approximate expression[22]

$$\tau_{\text{op}}(E) = \sqrt{\frac{\hbar^2E}{k_B^3T_{\text{po}}^3}}\frac{1}{\alpha N_q} \times\left(\ln\left|\frac{a+1}{a-1}\right| + e^{T_{\text{po}}/T}\ln\left|\frac{1+b}{1-b}\right|\right)^{-1}, \quad (11)$$

is used in the following analysis, where T_{po} is the optical phonon equivalent temperature, α is the polar constant, and N_q is the mean number of optical phonons at temperature T. That is

$$\alpha = \frac{q^2\sqrt{m^*}}{4\pi\epsilon_0\hbar\sqrt{2k_BT_{\text{po}}}}\left(\frac{1}{\epsilon_{\infty\perp}}-\frac{1}{\epsilon_{r\perp}}\right),$$

$$N_q = (e^{T_{\text{po}}/T}-1)^{-1},$$

where a and b are given by

$$a = \left(1+\frac{k_BT}{E}\right)^{1/2} \quad b = \text{Re}\left[1-\frac{k_BT}{E}\right]^{1/2},$$

with $\epsilon_{\infty\perp}$ being the ZnO high frequency permittivity orthogonal to the c axis and Re is the operator that takes the real part of the quantity within square brackets. In ZnO longitudinal optical phonon replicas occur with a separation in the 71–73 meV range,[8] corresponding to an equivalent temperature of ~824 K, which is used in our evaluation, see Table I.

Once $\tau_{\text{tot}}(E)$ is determined r_H can be calculated [see Eq. (3)] and the measured $n_H(T)$ and $\mu_H(T)$ can be corrected accordingly. The contact size effect on the Hall mobility and Hall carrier concentration is also taken into account by considering the correction factors for the resisitvity and Hall voltage discussed in Ref. 28.

Using the ZnO constants given in Table I, which all are taken from the literature and following an iterative procedure three free parameters are fitted: N_{D1} N_{D3} and N_A^-. N_{D2} is

Downloaded 12 Oct 2009 to 137.215.6.53. Redistribution subject to AIP license or copyright; see http://jap.aip.org/jap/copyright.jsp

TABLE II. Al, Ga, In, Li, Na, and K concentrations in 10^{17} cm^{-3} for samples A, B, and C, as determined by SIMS.

	Al	In	Li	Na	Ga, K
A	1.3 ± 0.1	$\lesssim 0.001$	1.6 ± 0.3	$\lesssim 0.01$	$\lesssim 0.005$
B	1.5 ± 0.1	$\lesssim 0.001$	1.9 ± 0.5	$\lesssim 0.01$	$\lesssim 0.005$
C	1.3 ± 0.1	$\lesssim 0.001$	0.9 ± 0.1	$\lesssim 0.01$	$\lesssim 0.005$

taken as the Al concentration measured by SIMS, as will be justified later. As mentioned previously, the donor energy levels position E_{D1}, E_{D2} and E_{D3} are determined independently using TAS (see Ref. 20). After assuming some starting values the iteration is continued until consistent results are obtained for both $n(T)$ and $\mu(T)$.

IV. RESULTS AND DISCUSSION

The Al, Ga, In, Li, Na, and K concentrations obtained by SIMS are given in Table II. Al, Ga, and In are well known shallow dopants in ZnO and according to Ref. 29, they are all expected to be responsible for levels ~50 meV below E_C. This value agrees with that of E_{D2} observed by TAS (Ref. 20) (Table III). On the basis of their concentrations determined by SIMS (Table II), Al is the clearly dominating element by more than two orders of magnitude. Hence, D_2 is primarily ascribed to Al and N_{D2} is put equal to the chemical concentration of Al.

In Fig. 1, the carrier concentration versus temperature for the samples A, B, and C after correction for the Hall scattering factor is shown. At temperatures below those shown in Fig. 1 substantial scattering of the experimental data occurs and this is attributed to an increase in the contact resistance and/or to the fact that the samples are not fully uniform with a high compensation ratio. Furthermore, no apparent low temperature carrier concentration increase or flattening is detected, i.e., there is no experimental evidence for the presence of a highly conductive surface layer.[1,12] Therefore, the previously described analysis can be applied directly without performing any two-layer correction. In addition, for each sample a second measurement was undertaken at least 15 h after the first one without breaking the vacuum or exposing the sample to light. No significant difference between the two measurements, due to, for example, the presence of persistence surface conduction,[30] was observed.

In Fig. 2(a), the experimentally obtained mobility values, corrected for the r_H-factor, are depicted versus sample temperature. A maximum electron mobility of ~ 125 cm^2 V^{-1} s^{-1} is reached at ~ 200 K. The set of parameter values used for describing the experimental data in Figs. 1 and 2(a) with a three donor charge balanced equation and the *RTA* approach for $\mu(T)$ are summarized in Table III. For all the three samples, the same kind of donor and acceptor centers are assumed, which appears reasonable since the samples originate from the same batch. The values of E_{D1}, E_{D2}, and E_{D3} are taken from the results of TAS measurements performed independently on the samples A, B, and C, as exemplified in Fig. 3 and discussed thoroughly in Ref. 20. For sample C the deduced total concentration of shallow donors $(N_{D1}+N_{D2})$ from the TDH data is less than N_A^-, consistent with that only D_3 is observed by TAS in this sample. In principle, the TDH results for sample C can be described by assuming one shallow donor only, but then with a concentration exceeding that of Al (N_{D2}) implying the existence of at least one shallower donor than Al. A similar conclusion holds also for sample B where D_2 and D_3 are detected by TAS, but not D_1; in this sample $(N_{D1}+N_{D2})$ is slightly higher than N_A^- and D_2 appears in Fig. 3, while D_1 is fully compensated. Interestingly, for sample A D_1 appears in the TAS spectrum despite that N_{D1} is lower than N_A^-. However, the SIMS measurements unveil a lateral variation of the Li concentration in sample A, as well as samples B and C, as reflected by a relative uncertainty of $\lesssim 25\%$ for the values given in Table II, and since Li is major candidate as compensating acceptor also a lateral variation of N_A^- can be expected. Indeed, this is supported by TAS measurements using contacts with different position on the surface of sample A, as shown in Fig. 3 where position 2 does not display the presence of D_1 (and D_2) in contrast to that for position 1. Hence, the values of N_{D1}, N_{D3}, and N_A^- extracted from the TDH analysis and given in Table III should be regarded as average ones and local variations exist in the samples, especially for N_A^-. Here it should also be emphasized that the values of N_{D1}, N_{D3}, and N_A^- represent the total (chemical) concentration of the corresponding centers since not only the

TABLE III. Donor concentrations, activation energies, and N_A^- for the samples A, B, and C. Concentrations are in 10^{17} cm^{-3} and activation energies in meV. In case of N_{D3} for the samples A and B, the range of possible values obtained by varying E_{D3} within the experimental uncertainty are given.

	N_{D1}	E_{D1} [a]	N_{D2} [b]	E_{D2} [a]	N_{D3}	E_{D3} [a]	N_A^-
A	2.0 ± 0.4	30 ± 10	1.3 ± 0.1	50 ± 10	3–7	300 ± 40	3.1 ± 0.4
B	1.5 ± 0.4	30 ± 10	1.5 ± 0.1	50 ± 10	0.4–3	290 ± 30	2.9 ± 0.4
C	0.8 ± 0.4	30 ± 10	1.3 ± 0.1	50 ± 10	1.1 ± 0.3	290 ± 40	2.3 ± 0.4

[a]From Ref. 20.
[b]Based on SIMS measurements.

Downloaded 12 Oct 2009 to 137.215.6.53. Redistribution subject to AIP license or copyright; see http://jap.aip.org/jap/copyright.jsp

UNIVERSITEIT VAN PRETORIA
UNIVERSITY OF PRETORIA
YUNIBESITHI YA PRETORIA

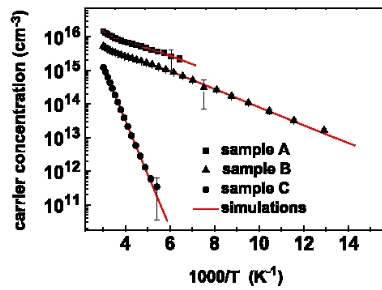

FIG. 1. (Color online) Carrier concentrations corrected for the contact size and the r_H-factor vs the reciprocal absolute temperature for samples A, B, and C. The solid curves are fit to the experimental data.

effective carrier concentration versus temperature, $n(T)$, is accounted for the modeling but also the dependence of the carrier mobility versus temperature, $\mu(T)$.

For sample A, where the shallow donors are most dominant, simulations performed with $N_{D1}=1.3\times10^{17}$ cm^{-3} and $N_{D2}=2.0\times10^{17}$ cm^{-3}, i.e., the concentrations of D_1 and D_2 are exchanged relative to those given in Table III, do not reproduce the carrier concentration versus temperature tail at low temperatures. Thus, not only the energy position of the D_2 level, but also the absolute concentration favors strongly an assignment of D_2 to Al. Here it should be pointed out that when the energy position of D_1 and D_2 are corrected for the

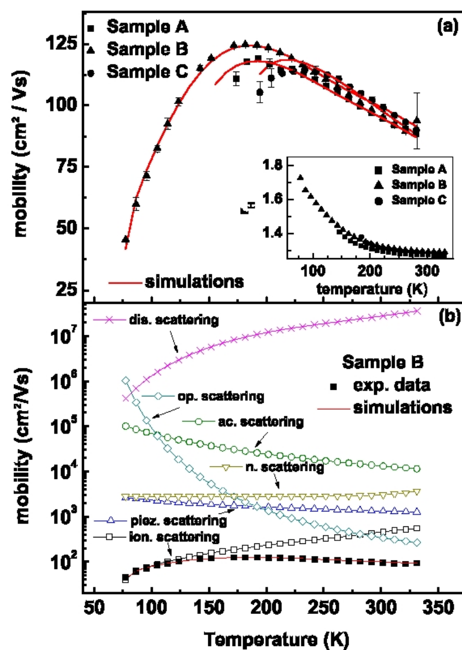

FIG. 2. (Color online) (a) The experimental data corrected for the contact size and the r_H-factor (squares) and the resulting simulations curves (solid line) obtained by considering all the scattering processes. In the inset the dependence of the r_H-factor on the temperature is reported. (b) The individual contributions from the different scattering processes to the mobility assuming independent processes, for clarity results are shown for sample B only, but similar results hold also for the samples A and C.

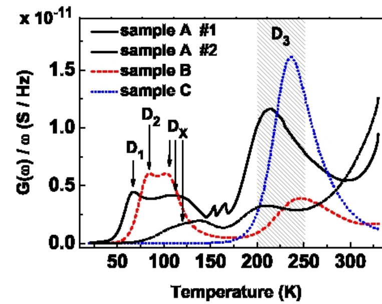

FIG. 3. (Color online) Conductance normalized by the probing angular frequency (ω) vs temperature obtained by TAS after depositing Schottky contacts on the samples A, B, and C. For sample A, results are included from two different contacts 1 and 2 in order to illustrate the sample nonuniformity. The measurements shown were taken with $\omega/2\pi=60$ KHz.

standard Coulomb screening effect,[31] i.e., $E_{Di}(N_{Di}=0)=E_{Di}+\beta N_{Di}^{1/3}$ assuming $\beta\sim2-3\times10^{-5}$ meV cm for ZnO, $E_{D1}(N_{D1}=0)$ becomes in the 41–48 meV range and $E_{D2}(N_{D2}=0)$ in the 60–66 meV range. Shallow donors with activation energies in the 33–35 meV, 49–53 meV ranges, after the Coulomb screening effect correction, are commonly reported[1,32] and attributed to native defects, possibly Zn_i complexes, and H-related complexes. A comparison of these values with E_{D1} indicates that a hydrogen-related complex is a possible candidate for the origin of D_1. In fact, recent results from Fourier transform infrared spectroscopy studies of similar samples as used in this work yield a hydrogen content in the 10^{17} cm^{-3} range[33] fully consistent with the N_{D1} value of Table III. Further it can be noted that our estimate of the D_2 donor level position is ~10 meV shallower than that expected for the Al-related donor according to previous TDH measurements.[1,32] On the other hand, photoluminescence measurement supports a shallower energy position[32] of 60–63 meV for the Al-related donor in good agreement with our assignment of D_2 to a center involving Al.

The position of the third donor level, E_{D3}, is substantially deeper than E_{D1} and E_{D2}, but the rather high values of N_{D3}, in the 10^{16} to 10^{17} cm^{-3} range consistent with the TAS results,[20] yields a relative contribution to the total carrier concentration of $\gtrsim10\%$ in the 270–280 K range (see Fig. 1). The value of E_{D3} is identical with the position of the so-called E_3 level, commonly reported in the literature[12,16,18] and considered to be of donor-type. The E_3 level has been attributed to Fe or Ni impurities[34] or to intrinsic defects such as oxygen vacancies[17] (V_O) and zinc interstitials[35] (Zn_i). Moreover, there is experimental evidence[36] of two closely spaced levels E_3/E_3' with a difference in energy of only ~3 meV but with clearly different capture cross sections. In fact, the existence of two overlapping levels E_3 and E_3' is consistent with the shift in temperature position and skewed shape of the D_3 peak in sample A compared to that in samples B and C, (Fig. 3). Here, it should also be pointed out that the TAS measurements reveal one additional (fourth) level, labeled as D_X in Fig. 3. However, no evidence is found for D_X by TDH measurements, which is possibly due to a negative-U character of D_X, as indicated by the TAS results and discussed in detail in Ref. 20.

Downloaded 12 Oct 2009 to 137.215.6.53. Redistribution subject to AIP license or copyright; see http://jap.aip.org/jap/copyright.jsp

UNIVERSITEIT VAN PRETORIA
UNIVERSITY OF PRETORIA
YUNIBESITHI YA PRETORIA

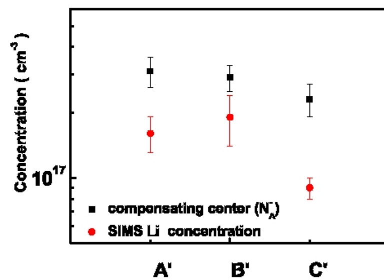

FIG. 4. (Color online) Comparison of the Li content determined by SIMS measurements and the compensating center concentration (N_A^-) estimated by modeling for the three different samples used.

As displayed in Fig. 2(a), the calculated mobility values as a function of temperature are compared with the measured ones, corrected for the r_H-factor, for all the samples used. In order to evaluate which scattering terms are limiting the mobility each scattering mechanism was considered separately, as illustrated in Fig. 2(b) for sample B. In all the three samples, both the contributions from the acoustic deformation potential and the dislocation scattering are negligible. It is also worth to point out that the Debye length used for evaluating $\tau_{\text{dis}}(E)$, as previously described, has not been corrected for bound carriers[25] that contribute, as well, to the effective screening. Hence, the mobility limited by dislocations scattering in Fig. 2(b) is an underestimation. For all the samples, significant contributions occur from both the intrinsic mechanisms of scattering due to polar optical and piezoelectric fields and the extrinsic ones due to neutral and ionized impurities. In particular, below ~200 K the ionized impurities represent the main scattering contribution yielding a gradual increase in the r_H-factor at low temperatures, as shown by the inset of Fig. 2(a). It has also to be emphasized that the r_H-factor equals ~1.3 at room temperature rather the commonly assumed value of unity. Moreover, in the temperature range studied, the contribution from neutral impurity scattering is comparable with that from the piezoelectric field scattering term when the concentration of neutral centers is in the $\sim 10^{17}$ cm^{-3} range (the neutral impurity scattering contribution shown in Fig. 2(b) corresponds to a concentration of 2.2×10^{17} cm^{-3}). The neutral centers originate mainly from to the high fraction of D_3 that remains nonionized in the temperature range of analysis. Finally, at sufficiently high temperatures when the optical phonon scattering becomes dominant, the simulated mobility starts to deviate slightly from the measured one. This deviation is due to the afore mentioned approximation of treating the optical phonon scattering in the relaxation time approach. More accurate approaches such as numerical solution of the Boltzmann transport equation, as implemented by Rode,[14] are needed for a more precise description of the mobility at and above room temperature.

In Fig. 4, the N_A^- values deduced from the simulations and reported in Table III are compared with the Li content measured by SIMS. It is well known that Li acts as a compensating center in ZnO and a clear correlation between loss of Li and a resistivity decrease[37,38] has been reported. However, even when considering the total Li content it accounts only from 25% to 65% of N_A^- extracted from the mobility simulations. Moreover, as shown in Fig. 4, the Li concentration decreases by a factor of three from sample B' to C' despite the fact that the resistivity increases from ~15 to ~220 Ω cm. Additional candidates to N_A^- are Na and K, which are expected to introduce acceptor levels[8,37] in the lower part of the band gap. However, both the Na and K content are at least two orders of magnitude lower than the Li content (cf. Table II) and hence they give negligible contribution to the compensation. Alternatively, intrinsic defects may be considered. For instance, assuming n-type samples grown under high zinc partial pressure calculations based on density-functional theory in the local-density approximation[39] suggest a formation energy (ΔE_f) of ~ −0.2 eV for the Zn vacancy in the −2 state (V_{Zn}^{-2}). For the neutral oxygen vacancy V_O^0 a ΔE_f value of ~0.02 eV is expected. Hence, from theory a concentration ratio $N(V_{\text{Zn}}^{-2})/N(V_O^0) \sim \exp[-(\Delta E_f(V_{\text{Zn}}^{-2}) - \Delta E_f(V_O^0))/kT] \approx 7$ is obtained and V_{Zn}^{-2} may play a crucial role in determining the final resisitivity of hydrothermally grown ZnO.

V. CONCLUSIONS

Hydrothermally grown and nominally undoped single crystal ZnO bulk samples of n-type have been characterized by TDH employing TAS and SIMS as complementary techniques. The experimental TDH data can be modeled within the RTA approximation and an excellent agreement is demonstrated in the temperature range studied (70–330 K) assuming three types of donors in the upper part of E_G and one acceptor in the lower part of E_G. The donor energy level position used in the modeling are taken from independent TAS measurements and are given by ~41−48, ~60−66, and ~300 meV below E_C, respectively. Through correlation between TDH and SIMS data, the intermediate donor is ascribed to Al-related centers, while the shallowest one is tentatively assigned to complexes involving hydrogen. The electron mobility exhibits a maximum of ~125 cm^2/V s at ~200 K and a detailed analysis of the scattering mechanisms reveals that this modest value is primarily limited by substantial ionized-impurity-scattering due to the compensating acceptors with concentrations in the 10^{17} cm^{-3} range. Residual Li impurities are found to be one main contributor to the acceptors, while other group I elements such as Na and K, can be excluded. However, the Li content is not sufficient to account for the total acceptor concentration and additional contributions from, for example, intrinsic acceptorlike defects have to be considered.

ACKNOWLEDGMENTS

We thank Dr. U. Grossner for the helpful discussions and suggestions during the accomplishment of this work. Partial financial support was kindly provided by the Norwegian Research Council via the Nanomat-FOET/B2 program and NFR/RCN South Africa-Norway program for Research Cooperation.

Downloaded 12 Oct 2009 to 137.215.6.53. Redistribution subject to AIP license or copyright; see http://jap.aip.org/jap/copyright.jsp

[1]C. Jagadish and S. J. Pearton, *Zinc Oxide Bulk, Thin Films and Nanostructures* (Elsevier, New York, 2006).
[2]D. C. Look, B. Claflin, Y. I. Alivov, and S. J. Park, Phys. Status Solidi A **201**, 2203 (2004).
[3]R. F. Service, Science **276**, 895 (1997).
[4]S. Yamauchi, H. Handa, A. Nagayama, and T. Hariu, Thin Solid Films **345**, 12 (1999).
[5]Please visit the web site http://www.cermetinc.com/.
[6]Please visit the web site http://www.tew.co.jp/e/.
[7]Please visit the web site http://www.spcgoodwill.com/.
[8]Ü. Özgür, Y. I. Alivov, C. Liu, A. Teke, M. A. Reshchikov, S. Doğan, V. Avrutin, S.-J. Cho, and H. Morkoç, J. Appl. Phys. **98**, 041301 (2005).
[9]E. V. Kortunova, N. G. Nikolaeva, P. P. Chvanski, V. V. Maltsev, E. A. Volkova, E. V. Koporulina, N. I. Leonyuk, and T. F. Kuech, J. Mater. Sci. **43**, 2336 (2008).
[10]L. N. Demianets, D. V. Kostomarov, I. P. Kuz'mina, and S. V. Pushko, Crystallogr. Rep. **47**, S86 (2002).
[11]M. Suscavage, M. Harris, D. Bliss, P. Yip, S.-Q. Wang, D. Schwall, L. Bouthillette, J. Bailey, M. Callahan, D. C. Look, D. C. Reynolds, R. L. Jones, and C. W. Litton, MRS Internet J. Nitride Semicond. Res. **4S1**, G3.40 (1999).
[12]G. H. Kassier, M. Hayes, F. D. Auret, M. Mamor, and K. Bouziane, J. Appl. Phys. **102**, 014903 (2007).
[13]D. Look, D. Reynolds, J. Sizelove, R. Jones, C. L. G. Cantwell, and W. Harsch, Solid State Commun. **105**, 399 (1998).
[14]D. L. Rode, *Semiconductors and Semimetals 10* (Academic, London, 1975).
[15]X. Yang, C. Xu, and N. C. Giles, Mater. Res. Soc. Symp. Proc. **1035**, L04-07 (2008).
[16]U. Grossner, S. Gabrielsen, T. M. Børseth, J. Grillenberger, A. Y. Kuznetsov, and B. G. Svensson, Appl. Phys. Lett. **85**, 2259 (2004).
[17]J. C. Simpson and J. F. Cordaro, J. Appl. Phys. **63**, 1781 (1988).
[18]F. D. Auret, S. A. Goodman, M. J. Legodi, W. E. Meyer, and D. C. Look, Appl. Phys. Lett. **80**, 1340 (2002).
[19]P. Blood and J. W. Orton, *The Electrical Characterization of Semiconductors: Majority Carriers and Electron States* (Academic, London, 1992).
[20]R. Schifano, E. V. Monakhov, B. G. Svensson, W. Mtangi, P. J. Janse van Rensburg, and F. D. Auret, Physica B (unpublished).
[21]B. Sapoval and C. Hermann, *Physics of Semiconductor* (Springer-Verlag, Berlin, 1995).
[22]K. Seeger, *Semiconductor Physics*, Springer Series in Solid State Sciences Vol. 40 (Springer, Berlin, 1997).
[23]L. M. Falicov and M. Cuevas, Phys. Rev. **164**, 1025 (1967).
[24]B. Pödör, Phys. Status Solidi **16**, K167 (1966).
[25]D. C. Look and J. R. Sizelove, Phys. Rev. Lett. **82**, 1237 (1999).
[26]V. F. Petrenko and R. W. Whitworth, Philos. Mag. A **41**, 681 (1980).
[27]N. Syrbu, I. M. Tiginyanu, V. V. Zalmai, V. V. Ursaki, and E. V. Rusu, Physica B **353**, 111 (2004).
[28]R. Chwang, B. J. Smith, and C. R. Crowell, Solid-State Electron. **17**, 1217 (1974).
[29]B. K. Meyer, H. Alves, D. M. Hofmann, W. Kriegseis, D. Forster, F. Bertram, J. Christen, A. Hoffmann, M. Straßburg, M. Dworzak, U. Haboeck, and A. V. Rodina, Phys. Status Solidi B **241**, 231 (2004).
[30]Z.-Q. Fang, B. Claflin, and D. C. Look, J. Appl. Phys. **103**, 073714 (2008).
[31]D. C. Look, J. W. Hemsky, and J. R. Sizelove, Phys. Rev. Lett. **82**, 2552 (1999).
[32]D. C. Look, G. C. Farlow, P. Reunchan, S. Limpijumnong, S. B. Zhang, and K. Nordlund, Phys. Rev. Lett. **95**, 225502 (2005).
[33]H. B. Normann, Thesis, University of Oslo, 2009.
[34]Y. Jiang, N. C. Giles, and L. E. Halliburton, J. Appl. Phys. **101**, 093706 (2007).
[35]G. Brauer, W. Anwand, W. Skorupa, J. Kuriplach, O. Melikhova, C. Moisson, H. von Wenckstern, H. Schmidt, M. Lorenz, and M. Grundmann, Phys. Rev. B **74**, 045208 (2006).
[36]H. von Wenckstern, H. Schmidt, M. Grundmann, M. W. Allen, P. Miller, R. J. Reeves, and S. M. Durbin, Appl. Phys. Lett. **91**, 022913 (2007).
[37]S. Graubner, C. Neumann, N. Volbers, B. K. Meyer, J. Bläsing, and A. Krost, Appl. Phys. Lett. **90**, 042103 (2007).
[38]B. G. Svensson, T. M. Børseth, K. M. Johansen, T. Maqsood, R. Schifano, U. Grossner, J. S. Christensen, L. Vines, P. Klason, Q. X. Zhao, M. Willander, F. Tuomisto, W. Skorupa, E. V. Monakhov, and A. Yu. Kuznetsov, Mater. Res. Soc. Symp. Proc. **1035**, L04-01 (2008).
[39]A. F. Kohan, G. Ceder, D. Morgan, and C. G. V. de Walle, Phys. Rev. B **61**, 15019 (2000).

Downloaded 12 Oct 2009 to 137.215.6.53. Redistribution subject to AIP license or copyright; see http://jap.aip.org/jap/copyright.jsp

5.2: IV measurements on ZnO Schottky Barrier Diodes.

Current-voltage measurements have been performed using the metal Schottky contacts deposited on the Zn- and O-polar faces of bulk ZnO crystals. This section gives an outline of the parameters extracted from the results obtained.

5.2.1: General IV characteristics of M/ZnO Schottky diodes.

Fig. 5.2.1 and Fig. 5.2.2 show the general IV characteristics of the Pd and Au Schottky contacts deposited on the Zn-polar face of ZnO.

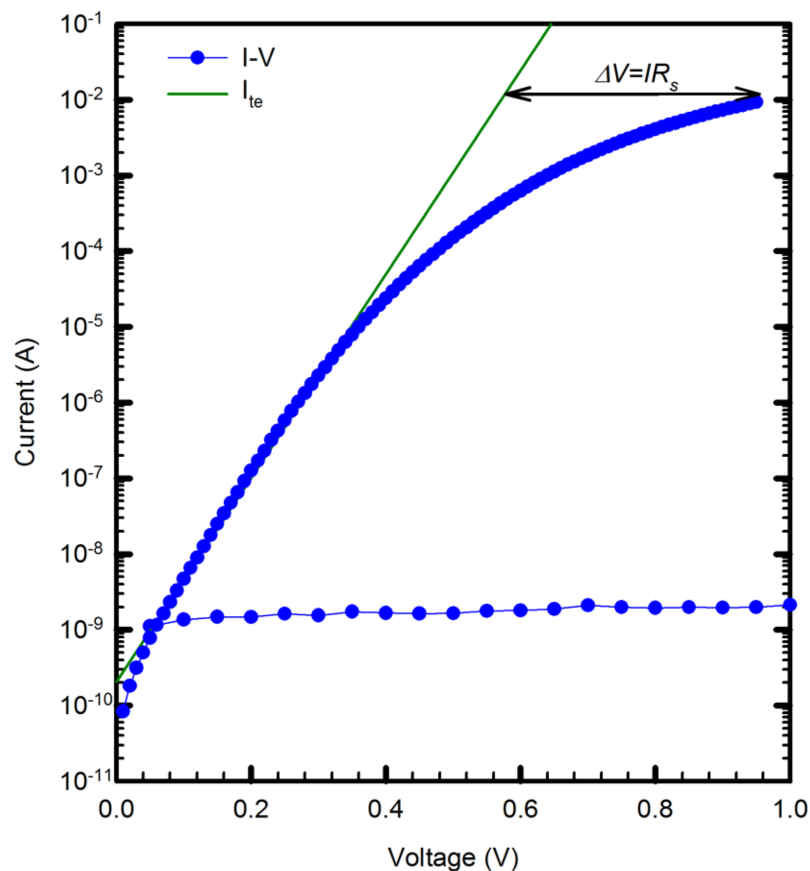

Fig. 5.2.1: General I-V characteristics of the as-deposited Pd/ZnO Schottky diode on the Zn-polar face of bulk ZnO obtained at a temperature of 298 K. I_{te} representing the fit to the thermionic model.

From Fig. 5.2.1 and Fig. 5.2.2, the *I-V* characteristics reveal mainly thermionic emission at room temperature. This good rectification behaviour of the Schottky diodes has been attributed to the cleaning procedure used prior to contact deposition, i.e. the boiling of the samples in hydrogen peroxide. Surface treatment of the ZnO sample is important in

improving the rectifying contact quality (increase barrier height, reduce the reverse leakage current, and achieve an ideality factor approaching unity) [1]. However, there are not much detailed reports to explain explicitly the effect of the H_2O_2 on the surface and structure of the ZnO samples. Several explanations such as good surface morphology, removal of C and OH contamination, and reduction in surface conductivity have been proposed [2].

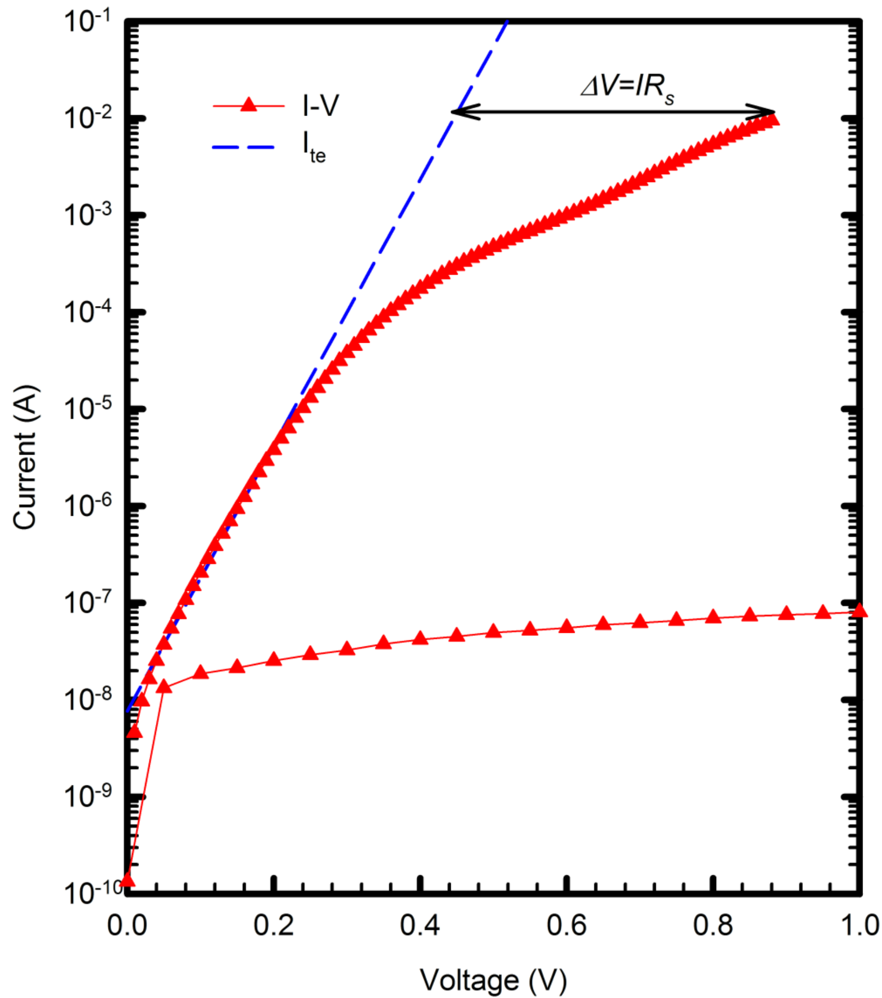

Fig.5.2.2: General I-V characteristics of the as-deposited Au/ZnO Schottky diode on the Zn-polar face of bulk ZnO. The characteristics have been obtained at a temperature of 298 K.

The mechanisms behind contact quality are still controversial and not well understood [1]. The effect of H_2O_2 on the ZnO samples was speculated by Kim *et al.* [3] as a method of reducing the deep level defects which could be some Zn interstitials and oxygen vacancies which are known to serve as donors [4]. Chen *et al.* [5] suggested that boiling hydrogen peroxide to temperatures as high as 100˚C causes it to dissociate, forming some oxygen radicals, which in turn react with the bulk ZnO, filling vacancies as well as forming some other ZnO molecules and reducing the net carrier concentration. In this study, the effects of

hydrogen peroxide treatment have been explained as completing the dangling bonds caused by surface termination on the Zn-polar face leading to the completion of the lattice and reducing the surface states. This in turn improves the quality of the metal-semiconductor contact as Fermi level pinning is reduced leading to a large barrier height.

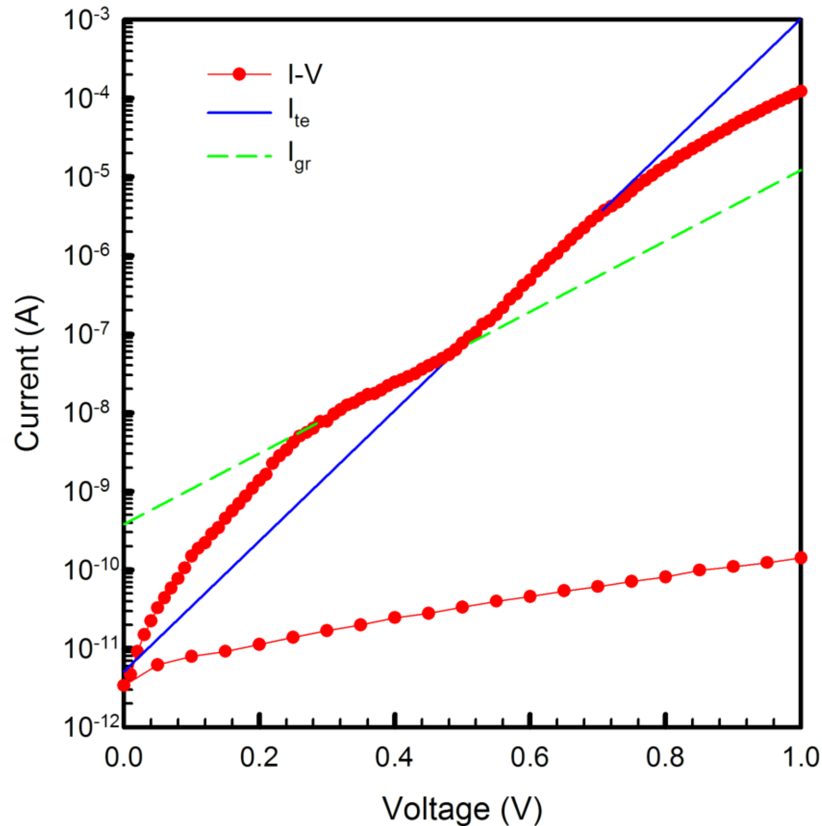

Fig.5.2.3. I-V characteristics of the Pd/ZnO Schottky contacts deposited on the O-polar face. Measurements performed at 298 K.

The *I-V* characteristics of Fig.5.2.3 and Fig.5.2.4 reveal the existence of generation/recombination current at room temperature at voltages ≤ 0.5 V as in the curve marked I_{gr}. Thermionic emission starts to dominate at voltages above 0.5 V. This unusual trend of generation/recombination at room temperature has been explained as the effect of the existence of an insulative oxide layer on the surface of the ZnO sample due to H_2O_2 treatment [6]. Due to the presence of the oxide layer, at low voltages, carriers won't be having enough energy to go over the barrier, so in an attempt to tunnel through the barrier, they are trapped by holes within the depletion region, leading to the formation of a generation /recombination current. At voltages above 0.5 V, carriers have enough energy to cross over the barrier, thus contributing to thermionic emission current indicated as I_{te}.

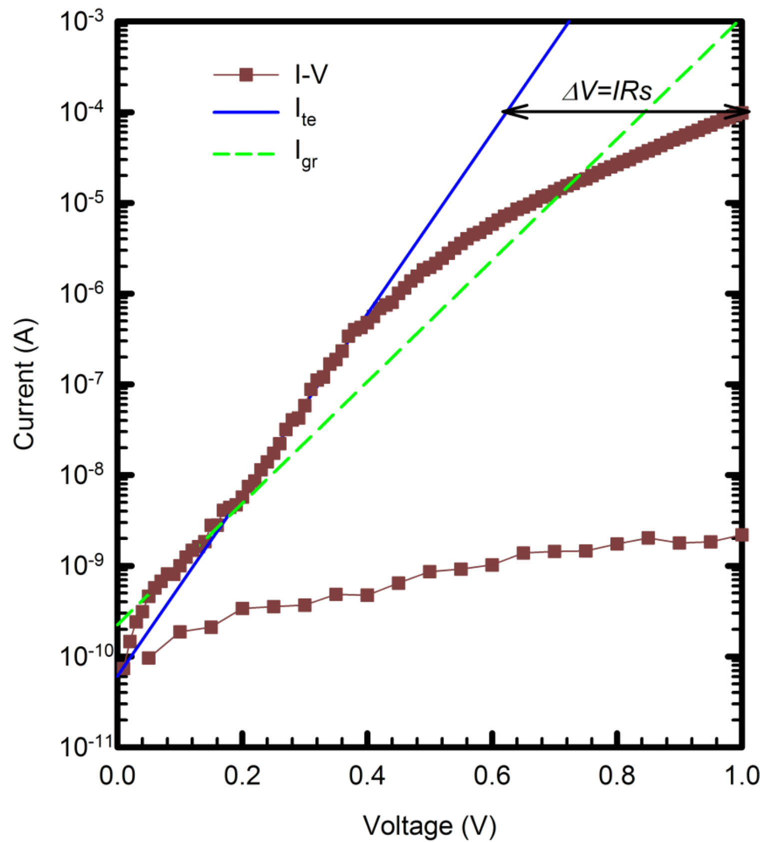

Fig. 5.2.4: I-V characteristics of the Au/ZnO Schottky contacts deposited on the O-polar face. Measurements performed at 298 K.

5.2.1.1: The ideality factor.

The values of the ideality factors, *n* were calculated from the slopes of Fig. 5.2.1, 5.2.2, 5.2.3 and 5.2.4 by making use of equation (3.4.19), assuming pure thermionic emission, i.e. using curves labelled I_{te}. Results obtained for the selected best diodes are given in Table 5.1.1.

Table. 5.1.1: Ideality factors obtained on the selected (low and almost constant leakage currents and low series resistance) metal Schottky contacts deposited on the ZnO polar faces.

Material	Face	Ideality factor, *n*
Palladium (Pd)	Zn-polar	1.26
	O-polar	2.04
Gold (Au)	Zn-polar	1.23
	O-polar	1.69

The Pd Schottky contacts deposited on the Zn-polar face produced ideality factors ranging from 1.03 – 1.55 with the contacts on the O-polar face giving values ranging from 1.51 –

2.65, while the Au contacts on the Zn-polar gave ideality factors ranging from 1.25 – 2.13 and contacts on the O-polar face yielding values in the range 1.28 – 2.65.

5.2.1.2: Series resistance.

The deviation of the *log (I)-V* curve from linearity at high currents is given by $\Delta V = IR_s$ [7], where R_s is the series resistance which can be obtained as,

$$R_s = \frac{\Delta V}{I} \tag{5.2.1}$$

From the four selected diodes, the series resistance values have been obtained as in Table 5.2.2.

Table 5.2.2: Series resistance values obtained on the selected best (low and almost constant leakage currents and low series resistance) Schottky contacts.

Metal	Face	Series Resistance, $R_s(\Omega)$
Palladium (Pd)	Zn-polar	42
	O-polar	210
Gold (Au)	Zn-polar	44
	O-polar	883

Since the series resistance depends on the bulk wafer resistivity and quality of contacts [7], the high series resistance values obtained on the O-polar face is due to the existence on an insulative oxide layer [6]. However, the large value of the resistance obtained on the Au contact is due to the poor adhesion of the metal to the surface of the semiconductor. Since the contacts were annealed after deposition, the Zn-polar face Schottky contacts yielded low resistance due to the annealed ohmic contact on the O-polar face, ensuring a low contact resistance. For the O-polar face Schottky contacts, the ohmic contacts were also annealed but the Schottky contact quality might have increased the resistance because no annealing was performed after Schottky contact deposition. Fig. 5.2.5 illustrates the effects of different ohmic contacts on the series resistance of a Schottky diode. The Schottky contacts with the indium gallium eutectic as an ohmic contact limits the forward current at 1 V to approximately 1×10^{-3} A, while the Schottky contact with an annealed metal composition allows a current as large as 1×10^{-2} A to flow through the device at 1 V. The IV curve deviates from linearity at low voltages, approximately 0.3 V for the contacts with InGa as the ohmic contact while for the contact with annealed metals, the curve deviates from linearity at

approximately 0.4 V. This is due to a large series resistance effect provided by the InGa ohmic contact.

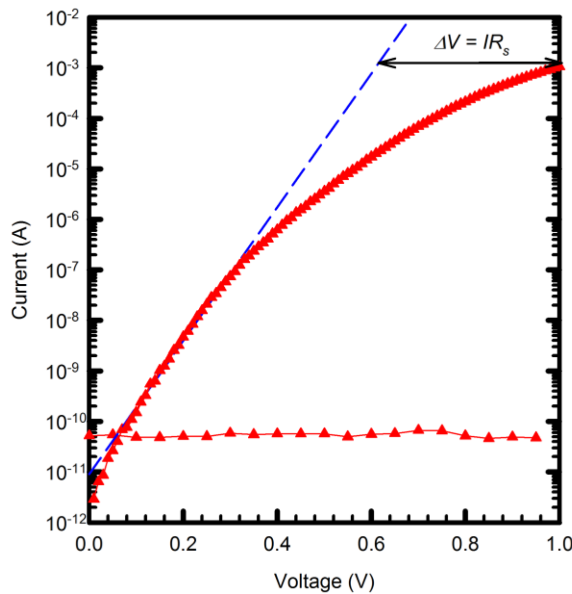

Fig 5.2.5a: Pd/ZnO Schottky contact with InGa eutectic as ohmic contact.

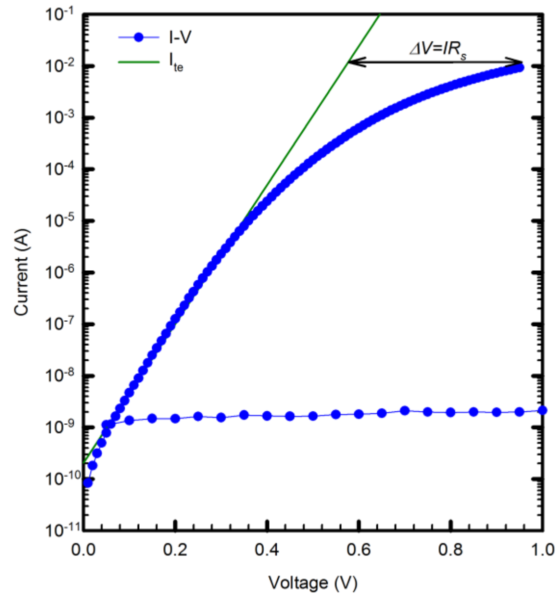

Fig 5.2.5b: Pd/ZnO Schottky contact with an annealed Ti/Al/Pt/Au ohmic contact.

5.2.1.3: Saturation current

The saturation current, usually referred to as the reverse saturation current, defines the maximum current that is expected to flow through the device at zero bias due to the thermal agitation of charge carriers. This value is obtained as the intercept on the current axis when $V= 0$. The saturation current values obtained are listed below.

Table 5.2.3: Saturation current values obtained from the selected (low and almost constant leakage currents and low series resistance) Schottky contacts.

Metal	Face	Saturation Current, I_s (A)
Palladium (Pd)	Zn-polar	1.07×10^{-9}
	O-polar	5.13×10^{-10}
Gold (Au)	Zn-polar	9.01×10^{-8}
	O-polar	1.05×10^{-9}

The saturation current values obtained on the O-polar face are an order of magnitude smaller than the ones obtained on the Zn-polar face for both the palladium and gold contacts. This can be explained by the fact that carriers recombine with holes as they try to cross the barrier

due to thermal agitation contributing to the generation/recombination current component hence reducing the thermionic saturation current values.

5.2.1.4: Barrier height determination

The *I-V* barrier height can be determined from Fig. 5.2.1, 5.2.2, 5.2.3 and Fig. 5.2.4 by assuming pure thermionic emission, i.e. carriers that have enough energy to go over the barrier. In this case, the barrier height obtained is the zero bias barrier height where the saturation current is used in equation (3.4.17). With A^{*}=32 $AK^{-2}cm^{-2}$ and area, $A = 2.83 \times 10^{-3} cm^{2}$, the zero bias barrier height values were obtained as in Table 5.3.

Table 5. 4: Zero bias barrier height values obtained from the I-V characteristics of the selected best Schottky contacts.

Metal	Face	Barrier Height (eV)
Palladium (Pd)	Zn-polar	0.80
	O-polar	0.90
Gold (Au)	Zn-polar	0.71
	O-polar	0.84

After using the same H_2O_2 treatment method, Gu *et al.* [2] observed barrier heights ranging from 0.35 - 0.65 eV for Au/ZnO Schottky diodes. Kim *et al.* [3] reported an *I-V* barrier height of 0.89 eV for the Pt Schottky contacts to ZnO also after H_2O_2 treatment. A barrier height of 0.68 eV for Pd contacts to ZnO has been reported by Sze [8]. The barrier height obtained using this method indicates a strong dependence on saturation current values. The determination of barrier heights using this method gives a clear indication of carriers contributing to the current flow, i.e. carriers with enough energy to surpass the barrier.

5.2.1.5: Reverse leakage current

A good Schottky (rectifying) contact must allow a very small or negligible current to flow in the reverse bias. Reverse leakage current values obtained From Fig. 5.2.1 and 5.2.2 are shown in Table 5.2.5. The values for the Zn-polar face Schottky contacts show some saturation (i.e. it is independent of the applied voltage), i.e. it’s nearly ideal, while the leakage current on the O-polar face is increasing with applied voltage (Fig. 5.2.3 and Fig. 5.2.4).

Table 5.2.5: Reverse leakage current at V= -1 V for the selected best (low and almost constant leakage currents and low series resistance) contacts (Figs. 5.2.1 – 5.2.4).

Metal	Face	Reverse leakage current, I_r(A)
Palladium (Pd)	Zn-polar	2.19×10^{-9}
	O-polar	1.42×10^{-10}
Gold (Au)	Zn-polar	9.02×10^{-8}
	O-polar	1.02×10^{-9}

The characteristic obtained on the Zn-polar face (Fig. 5.2.2.1 and Fig. 5.2.2), i.e. the saturation of the reverse leakage current indicates that the effects of an interfacial layer are less pronounced, while that on the O-polar face (Fig. 5.2.3 and Fig 5.2.4), as speculated can be due to the presence of an interfacial layer whose effects are highly pronounced. Another possibility could be due to the electric field dependence of the barrier height and the tunnelling effect. These deviations of the reverse leakage current from saturation have been explained by Rhoderick [9].

5.2.2: Conclusions.

The *I-V* characteristics obtained on the M/ZnO Schottky contacts reveal the presence of generation recombination at room temperature for contacts deposited on the O-polar face (Figs. 5.2.3 and 5.2.4), while for contacts deposited on the Zn-polar face (Figs. 5.2.1 and 5.2.2), the main transport mechanism is thermionic emission at room temperature. Pd has proved to be the better material for Schottky contacts to ZnO as it yields high barrier heights and low reverse leakage currents, which are voltage independent (Fig. 5.2.1). The ideality factor values obtained from the Pd contacts on the Zn-polar face range from 1.03-1.55 at room temperature. The measured barrier heights also range from 0.75-0.90 eV at room temperature. For Pd contacts on the O-polar face, the ideality factors and barrier heights were obtained in the ranges 1.51 - 2.65 and 0.68 - 0.90 eV at room temperature, respectively. Au contacts to ZnO on the Zn polar face yielded ideality factors ranging from 1.25 - 2.13, and *I-V* barrier heights ranging from 0.59 - 0.84 eV at room temperature. For the Au contacts deposited on the O-polar face, the ideality factor ranges from 1.28 - 2.65 while the *I-V* barrier heights range from 0.66 - 1.06 eV at room temperature. Samples with annealed and alloyed ohmic contacts produce Schottky contacts with low series resistance while the ones with un-

annealed contacts produce high series resistance contacts as shown in Fig 5.5. A detailed analysis on the Schottky contacts deposited on the Zn-polar and O-polar faces of ZnO is given in the publication at the end of this section.

References

[1] Q. L. Gu, C. C Ling, X. D. Chen, C. K. Cheng, A. M. C.Ng, C. D.Beling, S. Fung, A. B. Djurisic, and L. W Lu, Appl Phys Lett. 90, 122101 (2007).

[2] E. Gu. S. Tuzemen, B. Kihc, and C. Coskun, J. Phys: Condes. 19 (2007).

[3] S. H. Kim, H-Ki Kim, T-Yeon Seong, Appl Phys Lett. 86, 112101(2005).

[4] D. C. Look, J. W. Hemsky, and J. R. Sizelove, Phys Rev Lett. 82, 2552 (1999).

[5] Y. Chen, F. Giang, L. Wang, C. Mo, Y. Pu, and W. Fang, J. Cryst. Growth 268, 71 (2004)

[6] W. Mtangi, F.D. Auret, C. Nyamhere, P. J. Janse van Rensburg, M. Diale, A. Chawanda, Phys. B., 404, 1092 (2009).

[7] D. K. Schroder, Semiconductor material and device characterization, 3rd Ed. Wiley & sons, Inc., Hoboken, New Jersey, (2006).

[8] S. M. Sze, K. Kwok, Physics of Semiconductor devices 3rd Ed., John Wiley & sons, USA, (2007).

[9] E. H. Rhoderick, Metal-Semiconductor contacts, 1st Ed., Clarendon Press, Oxford, (1988).

UNIVERSITEIT VAN PRETORIA
UNIVERSITY OF PRETORIA
YUNIBESITHI YA PRETORIA

Publications.

pss-Header will be provided by the publisher

Review copy – not for distribution

(pss-logo will be inserted here by the publisher)

On the electrical properties of Pd and Au Schottky contacts deposited on the O-polar and Zn - polar faces of bulk grown single Crystal ZnO

W. Mtangi *, J. M. Nel, F. D. Auret, A. Chawanda, C. Nyamhere, P. J. Janse van Rensburg, M. Diale

Department of Physics, University of Pretoria, Pretoria 0002, South Africa

Received ZZZ, revised ZZZ, accepted ZZZ
Published online ZZZ (Dates will be provided by the publisher.)

PACS 61.50.Ah, 67.30.hp, 82.65.tr, 68.47.Fg, 68.47.Gh.

* Corresponding author: e-mail wilbert.mtangi@up.ac.za, Phone: +27 12 420 2684, Fax: +27 12 362 5288

We report on the electrical behaviour of the palladium(Pd) and gold (Au) Schottky contacts deposited on the Oxygen-polar (O-polar) and Zinc-polar (Zn-polar) faces of the bulk grown single crystal ZnO. Room temperature *I-V* measurements carried out have revealed the presence of generation/recombination on the Schottky contacts deposited on the O-polar face and predominantly thermionic emission on the Zn-polar face. Schottky contacts deposited on the Zn-polar face have yielded low ideality factors and low series resistances as compared to the contacts on the O-polar face. A reverse leakage current independent of the applied voltage has been observed on the Zn-polar face contacts.

Copyright line will be provided by the publisher

1 Introduction With its high exciton binding energy of 60 meV, its wide bandgap and excellent radiation hardness, ZnO has attracted the attention of many researchers as it can be used considerably in optoelectronic applications. The first Schottky contacts to ZnO were reported by Mead in 1965 [1]. Since then, an increasing amount of research has been carried out using different metals as Schottky contacts. In the majority of the reported work, the contacts have produced high leakage currents and in many cases, proved to be completely ohmic. Reported barrier heights on these contacts are in the range 0.6-0.8 eV [2]. Majority of reports have indicated the dependence of the contact quality on the cleaning procedures other than on the metal work functions [3]. Fabrication of stable Schottky contacts to ZnO has been a problem since in the early research [1] and still remains a challenge [4] even in the current research despite numerous investigations. Though cleaning procedures where in the earlier research, organic solvents have been used [4] , and of late the contact quality has reportedly been improved by the use of oxidising treatment where etching using acids has been employed [5]. Polarity of the ZnO samples is also another factor that can affect Schottky contact quality to ZnO. Since ZnO has a high iconicity and a wurtzite structure with a lack of inversion symmetry along the c-axis, it produces a large spontaneous polarization with bound sheet charges of opposite sign occurring at the Zn-polar and O-polar faces [6]. It is expected that the O-polar face and the Zn-polar face of bulk grown ZnO produce contacts of different qualities and properties. This is because of the termination of the different faces. During the process of termination, electronic configurations different from the bulk material and from each other are formed, creating incomplete covalent bonds, rendering the two faces different properties. Electronic band structure from the bulk to the vacuum is also expected to vary with the polarity of the faces. This in turn will affect the nature of the surface during chemical treatment as the two faces etch differently, and consequently the metal-surface chemical reactions are bound to differ. Allen et al [7] reported a significant effect of the polarity on the Pd and Pt Schottky contacts deposited on bulk single crystal ZnO purchased from Cermet Inc. Polarity effects were also observed in highly rectifying planar silver oxide diodes where the contacts deposited on the Zn-polar face yielded a barrier height which is 130 meV larger than the ones deposited on the O-polar face [6]. In this paper, we report on the polarity effect observed on the palladium (Pd) and gold (Au) Schottky contacts deposited on both the Zn-polar face and the O-polar face of the bulk grown single crystal ZnO samples using room temperature *I-V* measurements.

2 Experiment Undoped n-type ZnO bulk crystals of orientation (0001) and double side polished obtained from Cermet Inc were used in this study. The samples were degreased in acetone for 5minutes in the ultrasonic bath, methanol for another 5 minutes in the ultrasonic bath and

Copyright line will be provided by the publisher

finally boiled in hydrogen peroxide for 3 minutes. After treatment with the peroxide, the samples were blown dry with nitrogen gas. Ohmic contacts of composition Ti/Al/Pt/Au with thicknesses 20/80/40/80 nm were electron-beam deposited on the O-polar face for two samples and the Zn-polar face on the other two under vacuum with a pressure below 1×10^{-6} Torr were then deposited. The samples were then annealed in argon ambient for 30 minutes at a temperature of 200°C. Palladium and gold Schottky contacts with a diameter of 0.6 mm were finally resistively deposited on the samples under a vacuum of below 1×10^{-5} Torr. Room temperature *I-V* measurements were then performed.

Table 1. Electrical parameters extracted from the current-voltage characteristics of the metal Schottky contacts at room temperature.

Face	Metal	Ideality factor, n	Barrier Height (eV)	Series Resistance, Rs (Ω)	Current at V = -1 V (A)
Zn-polar	Pd	1.26	0.80	42	2.19×10^{-9}
	Au	1.23	0.71	44	9.02×10^{-8}
O-polar	Pd	2.04	0.90	210	1.42×10^{-10}
	Au	1.69	0.84	883	1.02×10^{-9}

3 Results and discussions

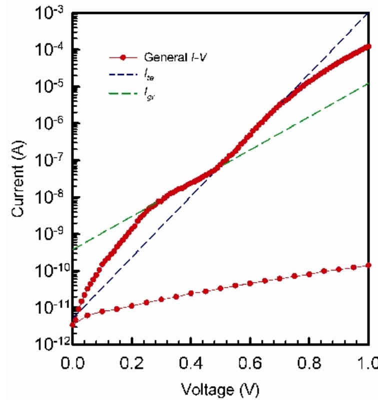

Fig. 1: Current voltage characteristics of the Pd/ZnO Schottky contact deposited on the O-polar face.

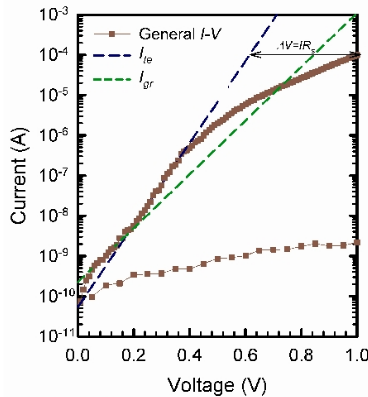

Fig. 2: Current voltage characteristics of the Au/ZnO Schottky contact deposited on the O-polar face.

Fig. 1 and Fig. 2 show the semilogarithmic *I-V* characteristics of the Pd and Au Schottky contacts deposited on the O-polar face of the bulk grown single crystal ZnO, respectively. The plots show the same characteristics at low and high voltages in the forward bias but only differ in the deviation from linearity at high voltages which is due to the effects of series resistance. The curves indicate the dominance of generation/recombination at low voltages [8], i.e. below 0.5 V. The experimental data for both Fig. 1 and Fig. 2 can be fitted to two distinct linear regions, I_{te} and I_{gr}. Fitting a straight line, I_{te} to the region that resembles thermionic emission current, i.e. the intermediate region using the equation,

$$I = AA^{*}T^{2}\exp\left(\frac{-\phi_B}{kT}\right)\left\{\exp\left[\frac{q\left(V-IR_s\right)}{nkT}\right]-1\right\} \quad (1),$$

where A^* is the effective Richardson constant, A is the Schottky contact area, ϕ_B is the barrier height, T the Kelvin temperature, k the Boltzmann constant, and R_s the series resistance, the ideality factor n can be obtained from,

$$n = \frac{q}{kT}\frac{dV}{d\left(\ln I\right)} \quad (2)$$

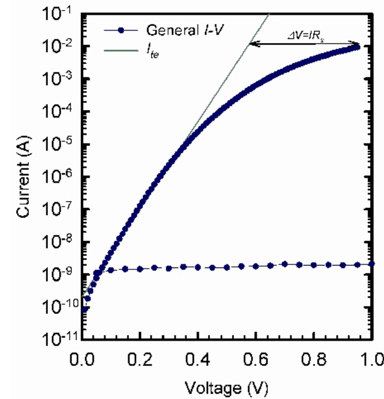

Fig. 3: Current voltage characteristics of the Pd/ZnO Schottky contact deposited on the Zn-polar face.

Copyright line will be provided by the publisher

Fig. 3 shows the semilogarithmic *IV* characteristics of the Pd Schottky contacts deposited on the Zn-polar face. The curves reveal that thermionic emission is the dominant transport mechanism. The data can fit to a single linear region by making use of equation (1) and the ideality factor can also be obtained from equation (2). The deviation in linearity at high voltages is due to the effects of series resistance.

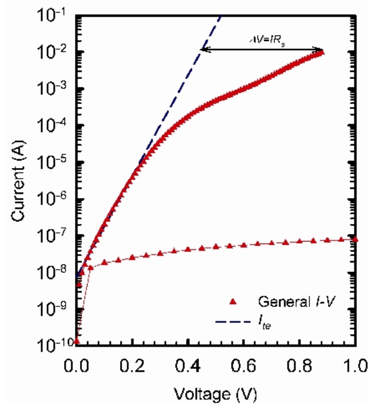

Fig. 4: Current voltage characteristics of the Au/ZnO Schottky contact deposited on the Zn-polar face.

Table 1 shows the parameters obtained by fitting the experimental data to a pure thermionic model. The ideality factors obtained for the contacts deposited on the Zn-polar face are lower than for the contacts on the O-polar face as shown in Table. 1. Furthermore, the Schottky contacts on the O-polar face have high barrier heights as compared to the one on the Zn-polar face. High series resistance values have also been measured for the contacts on the O-polar face with gold contacts yielding the largest resistance. The large series resistance for the Au contacts has been attributed to the poor adhesion of the metal to the semiconductor surface during fabrication. The observed differences can be attributed to the difference in the surface and chemical structures of the two terminated faces. Since the two faces differ in chemical structures, it is expected that they form different chemical bonds during cleaning and hence produce contacts of different qualities with the same metal. As it is speculated that boiling hydrogen peroxide produces some oxygen radicals that react with the surface of the ZnO sample [9], one would expect the Zn-terminated face to form a different structure from the O-terminated face, after reacting with the radicals. In completing the dangling bonds on the terminated faces, the Zn face is expected to form some ZnO molecules, while the oxygen face complete the covalent bonds with another oxygen atom rendering the difference in the properties (electronic, chemical and structural) of the faces. In other words, the Zn-polar face completes its lattice on the surface by reacting with the radicals as was suggested by Gu et al [9]. This brings about the difference in the quality of the Schottky contacts formed after metal deposition [10]. We speculate that the O-polar face forms an insulative layer because of the completion of the O-dangling bonds by oxygen atoms leading to the generation/recombination of carriers as they tunnel through the barrier at low voltages. As the voltage increases, carriers gain enough energy to cross over the barrier and thus thermionic emission current starts to dominate, while generation recombination vanishes. Allen et al [6] also revealed the difference in the Schottky barrier height for the contacts deposited on the polar faces of a ZnO sample obtained from the same supplier with the barrier height on the Zn-polar face being greater than the one on the O-polar face by 130meV. It can be said that the Zn-polar face forms the best contacts compared to the O-polar face since the contact resistance obtained for the Pd and Au contacts is low. Since the series resistance depends on the bulk wafer resistivity and contact resistance [11], the high series resistance obtained on the O-polar face can be attributed to the existence of an interfacial layer which causes poor chemical bonding between the metal and semiconductor since the contacts were prepared using the same method. Au Schottky contacts to both the O-polar and Zn-polar faces have high series resistance compared to the Pd Schottky contacts. This is because of the observed poor adhesion of the Au to the semiconductor surfaces.

4. Conclusion Results from the electrical properties of the Schottky contacts deposited on the Zn-polar and O-polar faces of bulk grown single crystal ZnO have shown a very strong dependence on polarity effects. The O-polar face has shown the dominance of generation/recombination at low voltages and at room temperature while the current transport mechanism for the Zn-polar face is predominantly thermionic emission. The leakage current for the contacts deposited on the Zn-polar face is almost constant with an increase in voltage while that for the O-polar face increases with the increase in voltage. The difference in Schottky contact quality can be attributed to the difference in the surface and chemical structures of the faces. Also the chemical reactions resulting in the formation and breaking of the bonds at the surface might have contributed to the good quality of the contacts on the Zn-polar face. We conclude that the Zn-polar face is the best for Schottky contact fabrication on bulk single crystal ZnO as it produces contacts with low ideality factors and series resistances together with a leakage current which is almost independent of the applied voltage. Also Pd forms a better contact to ZnO compared to Au.

Acknowledgements The authors would like to thank the South African National Research Foundation (NRF) for the financial assistance.

Copyright line will be provided by the publisher

UNIVERSITEIT VAN PRETORIA
UNIVERSITY OF PRETORIA
YUNIBESITHI YA PRETORIA

References

[1] C. A. Mead, Phys. Lett. 1965,18, 218
[2] Ü. Özgür, Ya. I. Alivov, C. Liu, A. Teke, M. A. Reshchikov, S. Doğan, V. Avrutin, S.J. Cho, and H. Morkoç J. Appl. Phys. 98 2005 041301
[3] A. Y. Polyakov, N. B. Smirnov, E. A. Kozhukhova, V. I. Vdovin, K. Ip, Y. W. Heo, D. P. Norton and S. J. Pearton. : Appl. Phys. Lett., 2003, Vol. 83. 1575
[4] H. L. Mosbacker, Y. M. Strzhemechny, B. D. White, P. E. Smith, D. C. Look, D. C. Reynolds, C. W. Litton, L. J. Brillson.: Appl. Phys. Lett., 2005, Vol. 87. 012102.
[5] W. Mtangi, F. D. Auret, C. Nyamhere, P. J. Janse van Rensburg, M. Diale, A. Chawanda, Phys. B., 2009, 404, 1092-1096
[6] M. W. Allen, P. Miller, J. B. Metson, R. J. Reeves, M. M. Alkaisi, S. M. Durbin. : Mater. Res. Soc. Symp. Proc. , 2007, Vol. 957. 0957-K09-03.
[7] M. W. Allen, M. M. Alkaisi and S. M. Durbin.: Appl. Phys. Lett., 2006, Vol. 89. 103520.
[8] E. H. Rhoderick, Metal-Semiconductor contacts, 1st Ed., Clarendon Press, Oxford, (1988).
[9] E Gu, S. Tuzemen, B. Kilic, C. Coskun.: J. Physics: Condens. Matter, 2007, Vol. 19. 196206.
[10] Tung, R. T. : Phys. Rev. B, 1992, Vol. 45. 13509.
[11] Schroder, Dieter K. *Semiconductor material and device characterization, 3rd Edn.* New Jersey : John Wiley and Sons, Inc., 2006.

Copyright line will be provided by the publisher

5.3: Temperature dependent IV measurements on ZnO Schottky Barrier Diodes.

Generally, the *I-V* characteristics of Schottky barrier diodes vary with temperature. This is because of the different current transport mechanisms which dominate under different temperature conditions. This section gives an outline of the temperature dependence of the parameters extracted and discussed in section 5.2 using Pd Schottky contacts only.

5.3.1: The general IV characteristics.

Palladium Schottky contacts deposited on the Zn-polar face indicate strong temperature dependence (Fig.5.3.1). A large deviation from the ideal Schottky behaviour is observed in the low temperature regions (60 -140 K) where the effects of generation recombination and other current transport mechanisms are highly pronounced. Above 180 K, thermionic emission starts to dominate as generation/recombination current decreases.

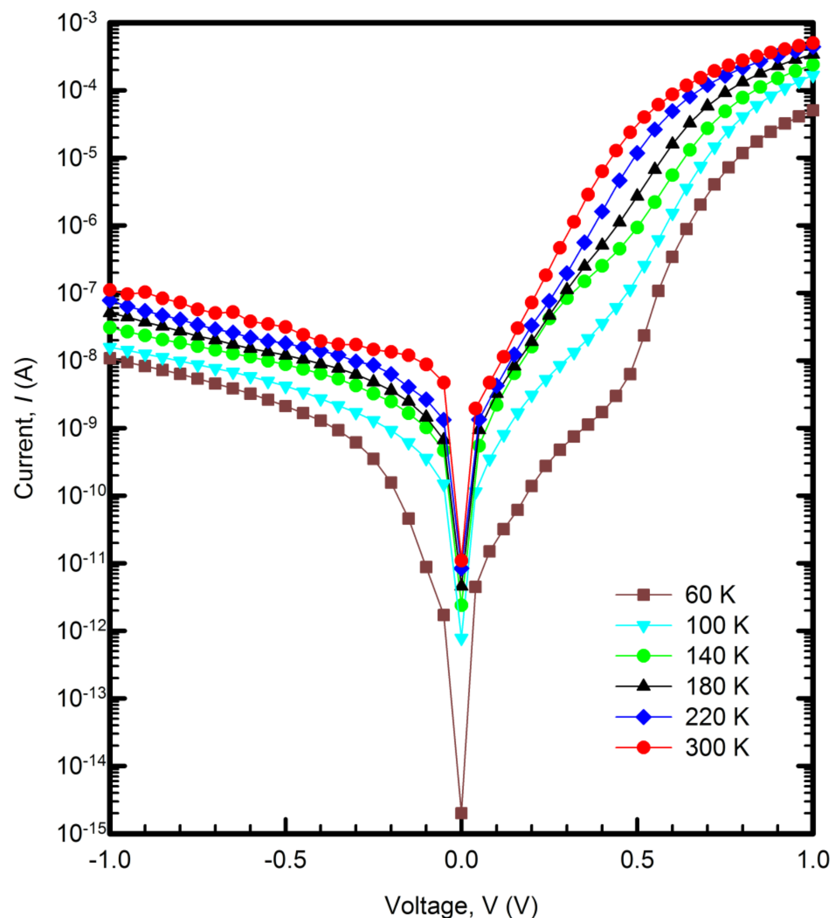

Fig. 5.3.1: Temperature dependent I-V semilogarithmic plot for the as-deposited Pd/ZnO Schottky diode in the 60-300 K range. Contacts were deposited on the Zn-polar face.

At 300 K, thermionic emission is the dominant mechanism present. Within the high temperature region (180-300 K), increasing series resistance with temperature is the only factor affecting the *I-V* characteristics.

According to the results of Fig.5.3.2, the curves show two linear bias regions within the entire temperature range (60 – 300 K). The lower bias region can be fitted to generation/recombination, while the intermediate region gives the thermionic emission. The upper parts of the curves which show some deviation from linearity define the series resistance of the contacts. For high temperatures, the effects of generation/recombination are observed to affect the curves at low forward bias conditions.

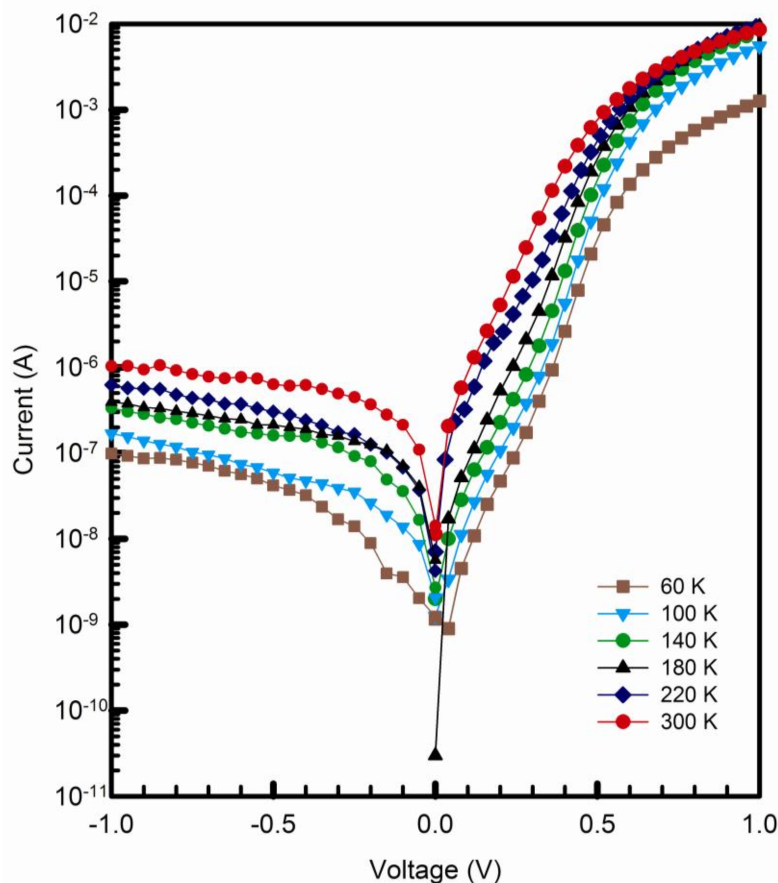

Fig. 5.3.2: Semilogarithmic I-V plot of the Pd/ZnO Schottky contacts deposited on the O-polar face of bulk ZnO.

Fig.5.3.3 gives a detailed analysis of the dependence of generation/recombination on applied voltage and temperature. The 60 K curve reveals that generation/recombination affects the diode at voltages ≤ 0.3 V, while for the 300 K temperature curve; generation/recombination is seen to affect the contacts at voltages ≤ 0.2 V. This can be explained by the fact that at high temperatures, under a certain given bias, the emission rate of carriers increases causing a

corresponding increase in the generation/recombination saturation current. At low temperatures, since carriers have low energy, a higher voltage has to be applied to excite carriers before they start contributing to the thermionic emission current.

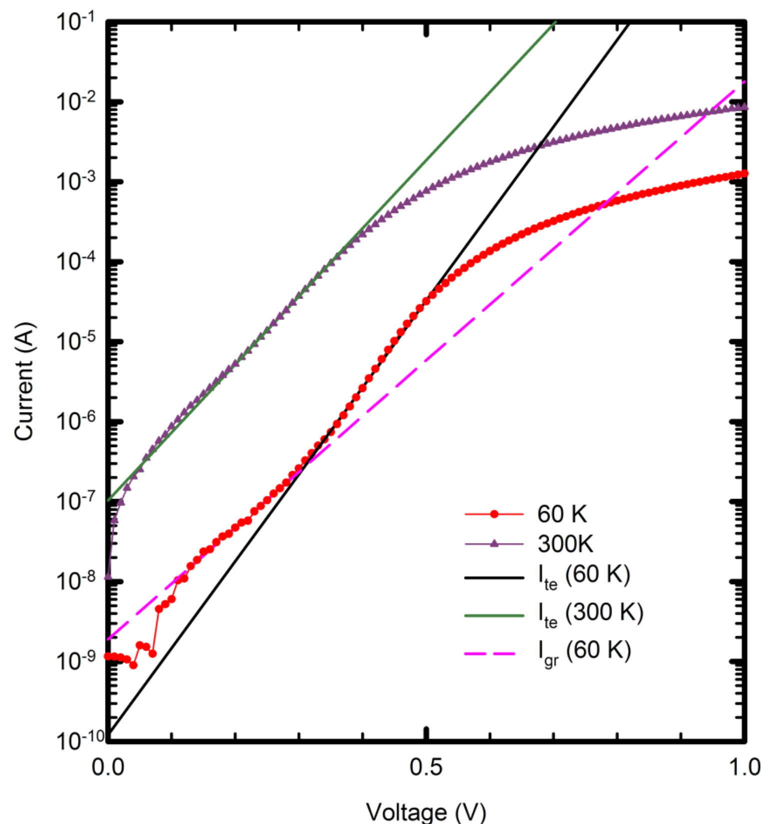

Fig.5.3.3: Forward bias IV curves at 60 K and 300 K temperature curves illustrating the current transport mechanisms taking place on the Pd/ZnO contacts deposited on the O-polar face in more detail.

5.3.2: Temperature dependence of the ideality factor.

The variation of the ideality factor for palladium Schottky contacts deposited on the Zn-polar and O-polar face is shown in Fig.5.3.4. The ideality factor on the Zn-polar face indicates an increase with temperature up to a temperature of 180 K whereafter an increase in temperature results in a decrease in ideality factor. This trend can be said to be unusual as one would expect the ideality factor to decrease with an increase in temperature as all the other current transport mechanisms will be vanishing and thermionic emission will dominate. This trend was also observed by Lu and Mohammed [1] in Al_xGaN_{1-x} diodes. This type of variation has been explained by Tung [2] as due to the so-called T_o anomaly. Within the 180-300 K temperature range, there is little variation of the ideality factor with temperature as the ideality factor varies between 1.7 and 2 with the lowest being 1.77 at 300 K.

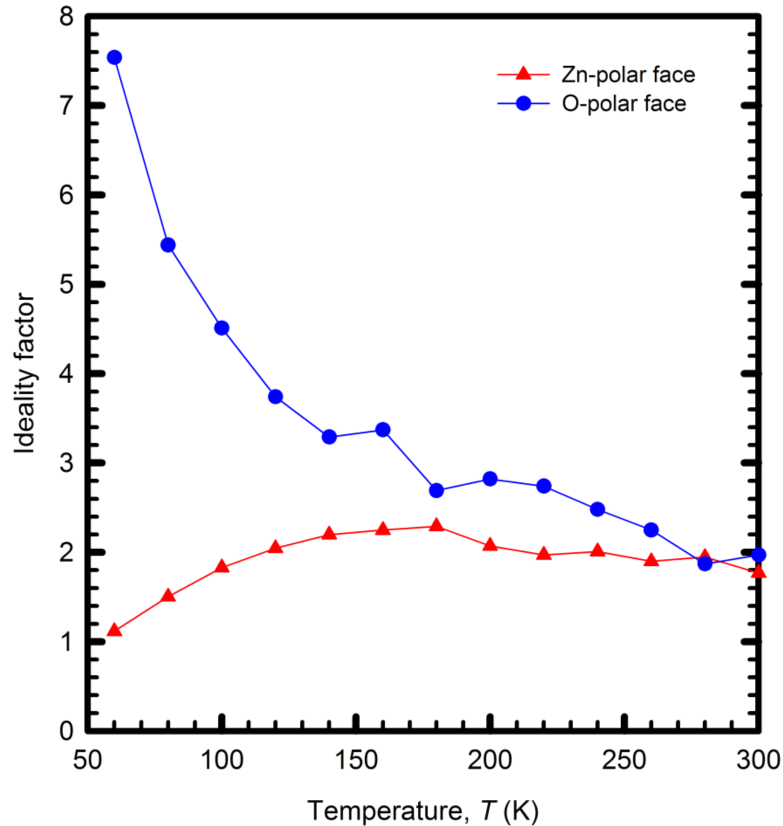

Fig.5.3.4: Variation of ideality factor with temperature for the palladium Schottky contacts to ZnO in the 60-300 K temperature range. Triangles representing the Zn-polar face, circles for the O-polar face.

The contacts can be said to be stable within this temperature range. The decrease in ideality factor within this region with the smallest value being obtained at 300 K indicates a decrease in the generation/recombination and dominance of the thermionic emission current.

On the O-polar face, the ideality factor decreases with increasing temperature, with the largest value being 7.55 at 60 K. This is the most expected trend as the diode deviates much from the ideal thermionic behaviour since we have many processes taking place within the low temperature region that affect the diode. Within the 60-140 K temperature range, the n values obtained indicate the presence of other mechanisms other than generation/recombination and thermionic emission. The large values of ideality factor at low temperatures can also be attributed to the potential drop in the interfacial layer and presence of excess current through the interfacial states between the semiconductor/insulator layers [3]. At 180 K, the ideality factor drops sharply to 2.69. Upon a further increase in temperature, the ideality factor drops slightly, but remains between 2 and 3 for the temperature range 180-300 K. This decrease in ideality factor indicates the subsiding effects of the generation/recombination with increase in temperature.

5.3.3: Temperature dependence of series resistance.

The variation of the series resistance with temperature is revealed in Fig.5.3.5a and Fig.5.3.5b.

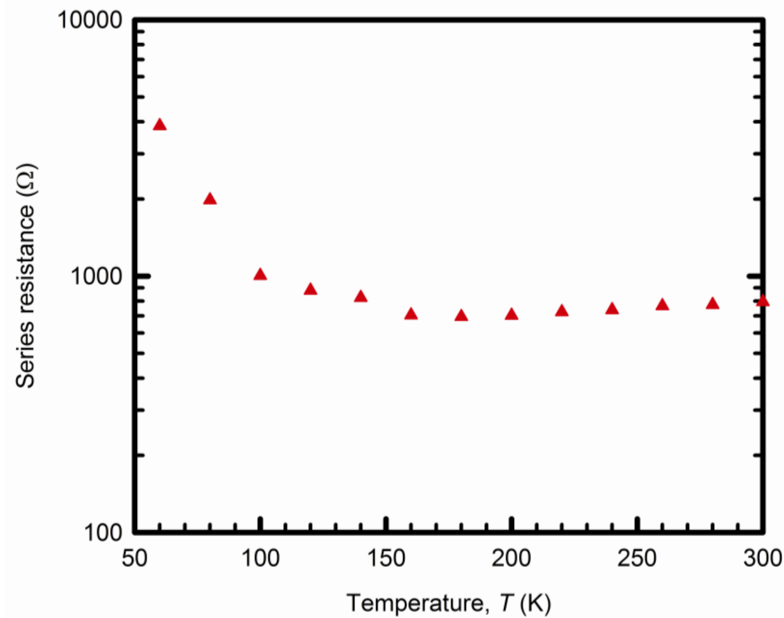

Fig.5.3.5a: Semilogarithmic series resistance temperature plot to show the variation of series resistance with temperature for the selected Pd/ZnO Schottky diode on the Zn-polar face in the temperature range 60-300 K, with indium as ohmic contacts.

Fig.5.3.5a and Fig.5.3.5b indicate a decrease in series resistance of the selected Schottky contacts to ZnO with increase in temperature. The highest value was recorded at 60 K for both the O-polar and Zn-polar face Schottky contacts. This is due to an increase in bulk resistivity as discussed in section 5.1.1.1. The high series resistance obtained on the Zn-polar face can be attributed to the bonding using silver paint [4].The series resistance shows a slight increase with temperature after 180 K for both the samples.

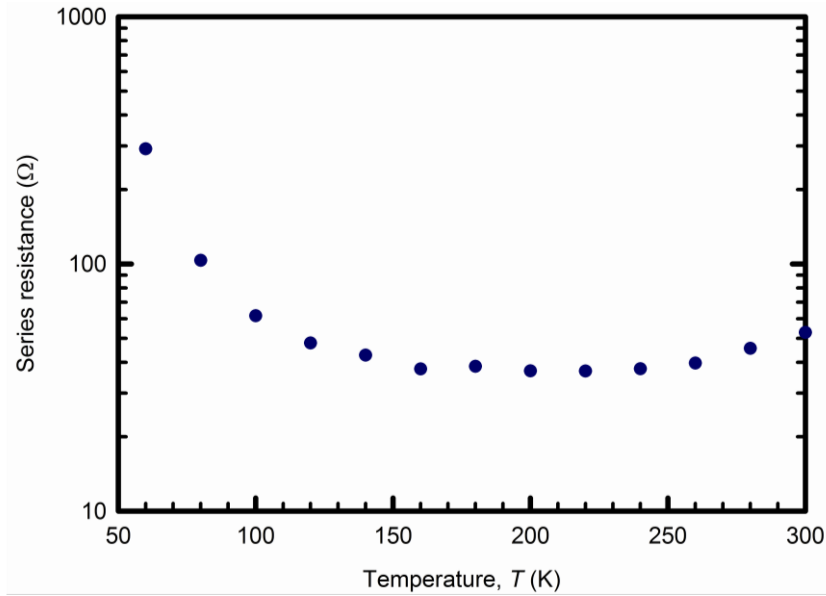

Fig.5.3.5b: Variation of series resistance with temperature for the selected Pd/ZnO Schottky diode on the O-polar face in the temperature range 60-300 K.

This trend can be related to the bulk resistivity of the samples as found from the Hall measurements, where a transition in the conductivity occurs at 180 K [5], i.e. an increase in conductivity with temperature was noted up to a temperature of 180 K then a decrease was observed with an increase in temperature. See section 5.1.1.1 for a detailed Hall results discussion.

5.3.4: Temperature dependence of the saturation current.

The saturation current values obtained as the intercept on the current axis define the current flowing through the device at zero bias voltage. Fig.5.3.6 illustrates an increase in saturation current with temperature for contacts on both the Zn-polar and O-polar faces. This can be explained by the fact that at low temperatures, carriers will be frozen out, and few will be able to contribute to the current flow. This could also be due to scattering of carriers due to the ionized impurities at low temperatures. As the temperature increases, thermal agitation of carriers increases, thereby increasing the amount of current flowing through the device. On the Zn-polar face, at temperatures higher than 180 K, the saturation current is significantly larger than at lower temperatures and it can be concluded that the saturation current is dependent on temperature. Its temperature dependence can be summarised by the equation,

$$I_s = AA^*T^2 \exp\left(-\frac{q\phi_b}{kT}\right) \tag{5.3.1}$$

Thus the device can be said to be stable in the 180 K-300 K temperature range.

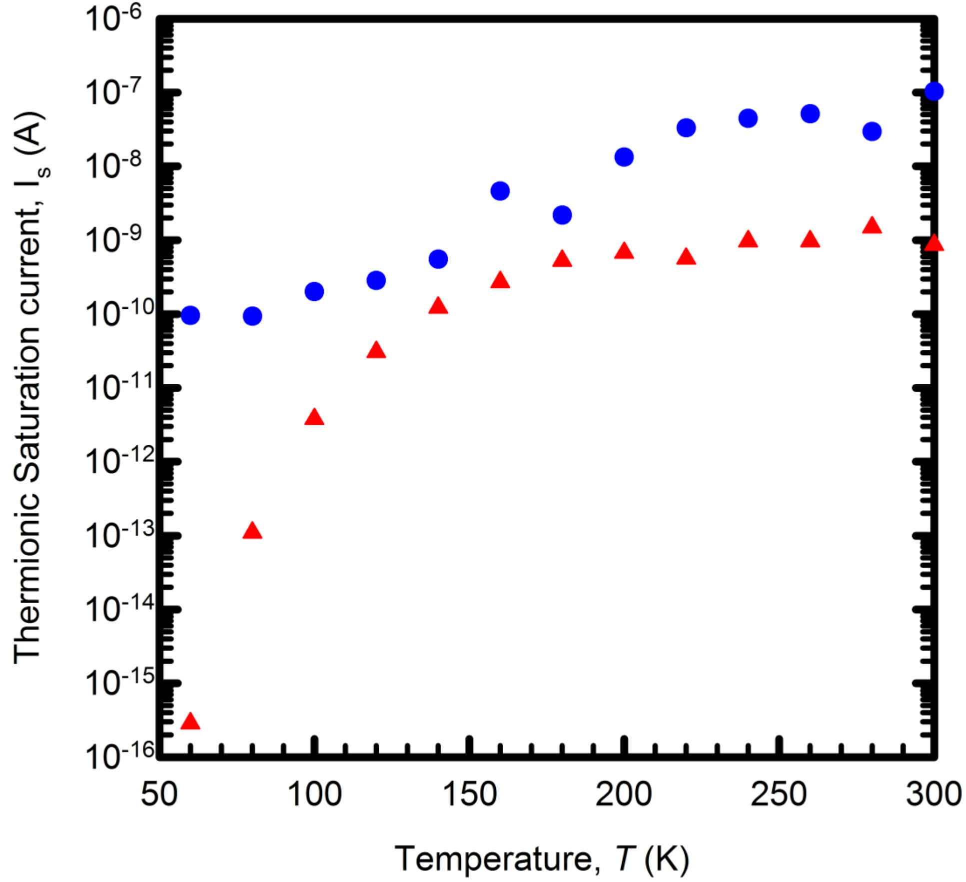

Fig.5.3.6: Temperature dependence of saturation current in the 60-300 K temperature range. Triangles indicate the saturation current on the Zn-polar face and circles represent the O-polar face saturation current.

5.3.5: Temperature dependence of the *I-V* barrier height.

The measured I-V barrier height on the Zn-polar face at every temperature is larger than the SBH of the O-polar face for the selected diodes shown in Fig.5.3.7. Previous studies of the temperature dependent SBHs were based on a comparison with the theory of Tersoff [6] who predicted a SBH,

$$q\Phi_p = \frac{1}{2}\left(E_G - \frac{\Delta}{3}\right) + \delta_m \tag{5.3.2}$$

for a metal on a p-type semiconductor. E_G is the semiconductor direct bandgap, Δ is the spin orbit splitting, and δ_m is an adjustable parameter that depends on the metal. According to equation (5.3.3), the temperature dependence of the SBHs should be controlled by the variation of the bandgap, E_G. Linearising the temperature dependence of the bandgap a linear behaviour of the SBHs is expected in the form,

$$\Phi_{n,p}(T) = \Phi_{n,p}(T=0) + \alpha_{\Phi}^{n,p} T \tag{5.3.3}$$

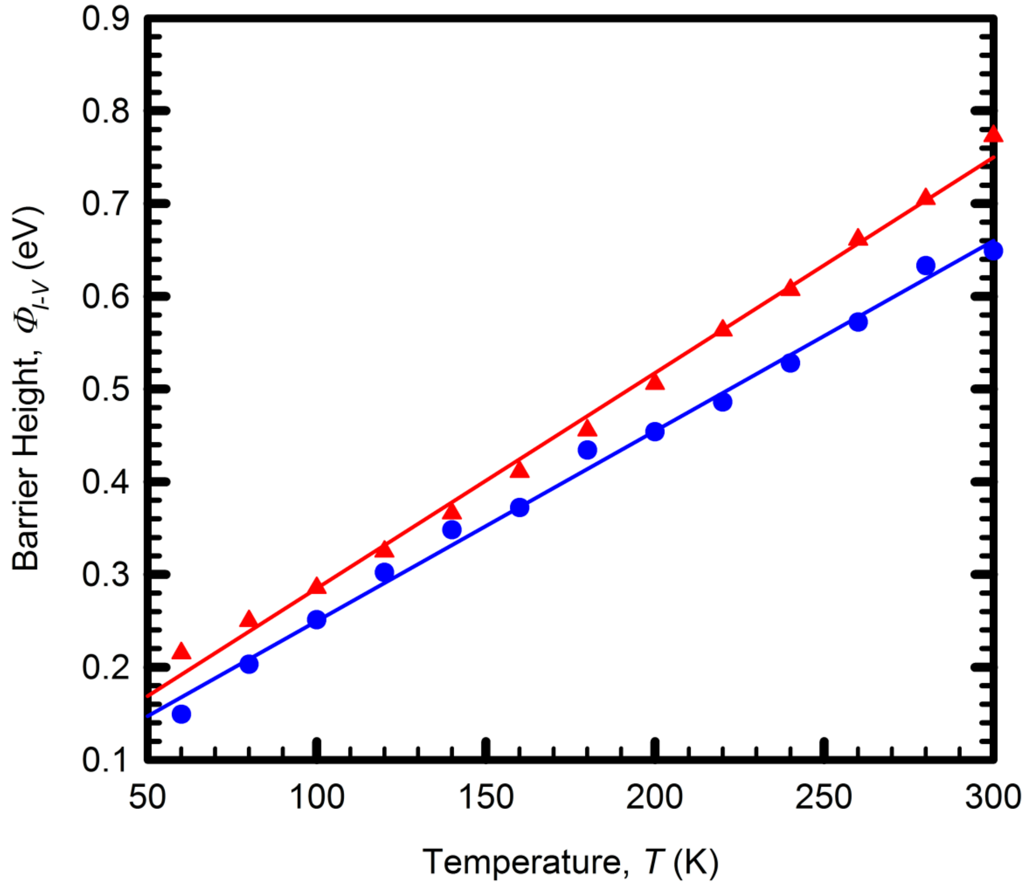

Fig.5.3.7: Variation of I-V barrier height with temperature for the palladium Schottky contacts to ZnO in the 60-300 K temperature range. Triangles represent the Zn-polar face; circles the O-polar face.

From equation (5.3.3), it is expected that the barrier height decreases with an increase in temperature, with a temperature coefficient given by [7]

$$\alpha_{\Phi}^{n,p} = \frac{d\Phi_{n,p}}{dT} = \alpha_{\Phi,Tersoff} = \frac{1}{2}\frac{dE_G}{dT} \tag{5.3.4}$$

Since the *I-V* barrier height depends on the saturation current values, this trend can be explained by the fact that at low temperatures, charge carriers have low energy to cross over the barrier and very little current at zero bias flows through the diode. As the temperature increases, carriers now gain enough energy to surpass the energy barrier, causing a large current to flow and hence a reduced potential barrier. However, the measured barrier height on the selected diodes on the Zn-polar and O-polar face increases with temperature. The increase in barrier height has been observed and explained by other researchers [8, 9, 10, 11] on Si and n-GaAs. The reason for this observation is not clear as different explanations have been given. Several theoretical models with pinning of the Fermi level by electronic states

being the most favoured one [8] have been used. It is suggested that Fermi level pinning is by metal induced gap states (MIGS) [6] or defect states at the interface [12]. For Fermi level pinning by MIGS, the temperature dependence of the barrier height is governed by the temperature dependence of the energy gap implying the barrier height must decrease with temperature. If the Fermi level pinning is due to interface defects, their ionization entropy would control the dependence of the barrier height on temperature [8]. Revva *et al.* [13] however suggested that the ionization entropy of the interface defects depend weakly on temperature and hence the temperature coefficient of the SBH should be nearly zero. Another explanation for the observed increase in barrier height with temperature is the existence of laterally extended SBH inhomogeneities at the MS interface in which the electron transport can be treated by the parallel conduction model [14, 8]. Under this situation, the current flowing through the barrier is assumed to be the sum of all the individual currents, I_i flowing through individual patches, each of its own area A_i and Schottky barrier height, Φ_i [8]:

$$I(V) = \sum I_i = A^* T^2 \left[\exp\left(\frac{qV}{kT}\right) - 1 \right] \sum \exp\left(\frac{-q\Phi_i}{kT}\right) A_i \tag{5.3.5}$$

In this case, the current will be dominated by the low barrier regions. In this study, since the value of the temperature coefficients obtained from Fig.5.3.7 for the Zn-polar and O-polar face are 52.6 meVK^{-1} and 44.5 meVK^{-1}, respectively, Fermi level pinning cannot explain the temperature dependence of the observed barrier heights. Thus the temperature dependence of barrier height can be explained by the lateral inhomogeneities of the SBH.

5.3.6: Determination of the effective Richardson constant for ZnO.

The Richardson constant for ZnO has been calculated from the saturation current values assuming that the Schottky barrier height of the Pd/ZnO Schottky contacts is non-homogeneous. By using equation (5.3.2) a linear plot shown in Fig. 5.3.7, was obtained in the (60-160 K) temperature range. For the insert, linearity was restored by multiplying the $\ln\left(I_s/T^2\right)$ by the ideality factor as was suggested by Schroder [15]. The apparent Richardson constant, A^* was obtained as 8.60×10^{-9} AK^{-2}cm^{-2} in the 60-160 K temperature range and 5.19×10^{-15} AK^{-2}cm^{-2} in the 180-300 K using equation (5.3.3). Gu *et al.* [16] and Sheng *et al.* [17] also calculated the value of A^* on Ag/ZnO SBDs in the high temperature ranges, 200-500 K and 265-340 K and obtained the values as 0.248 and 0.15 AK^{-2}cm^{-2}, respectively. It should be noted that the value of A^* depends on contact quality, saturation current [5] and temperature as different values have been obtained for different temperature ranges even with

the same metals. Values of the Richardson constant that deviate from the theoretical values have also been calculated by some researchers on other materials. Dokme *et al.* [18] calculated the Richardson constant, A^* for Al/p-Si SBD and obtained it as 1.3×10^{-4} AK^{-2}cm^{-2} in the temperature range 150-375 K compared to the theoretical value of 32 AK^{-2}cm^{-2}.

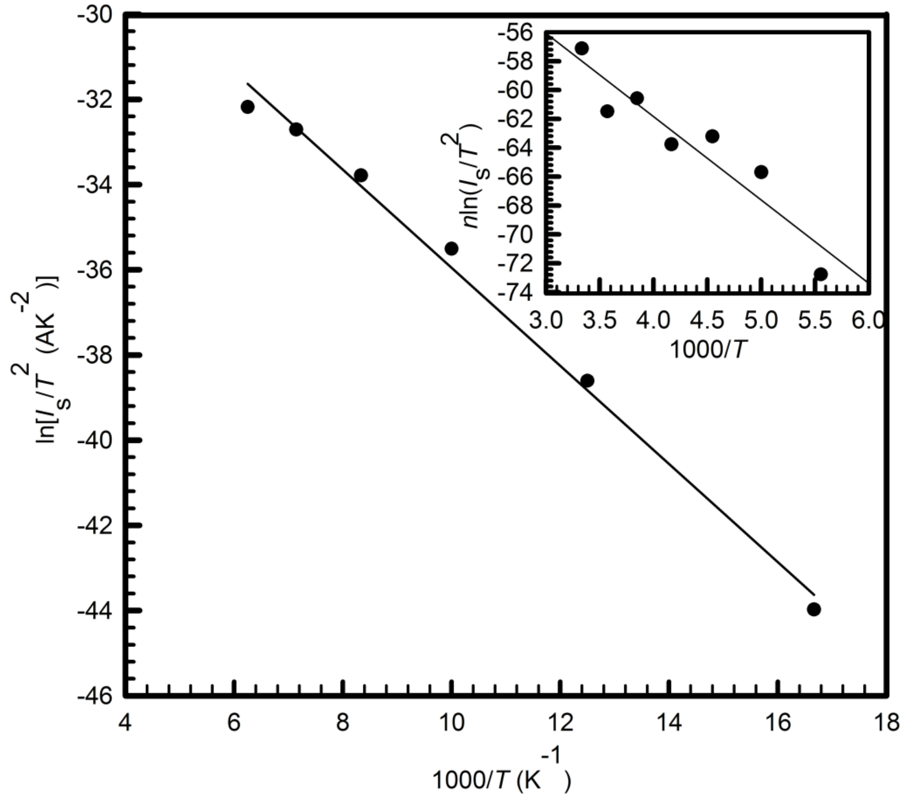

Fig. 5.3.7: The Richardson plot, ln[I_s/T^2] *versus 1000/T for the Pd/ZnO SBD in the 60-160 K temperature range. The insert shows the nln*[I_s/T^2] *in the 180-300 K temperature range where n is the ideality factor.*

Barrier inhomogeneity has been suggested as the cause for the deviation of the value of A^* from the theoretical value [18, 19]. The existence of high and low barrier areas at the contact mainly due to the formation of different oxide layer thicknesses between the metal and semiconductor influences the flow of the current through the contact. Due to the potential fluctuations at the interface, diode current will flow through the low barrier areas in the potential distribution. To get a value of A^* closer to the theoretical value of 32 AK^{-2}cm^{-2}, barrier inhomogeneities correction needs to be performed as outlined in section 3.4.3.1. After barrier height inhomogeneities correction, a corrected value of the Richardson constant called the effective Richardson constant, A^{**} has been obtained as 167 AK^{-2}cm^{-2} from Fig. 5.3.8.

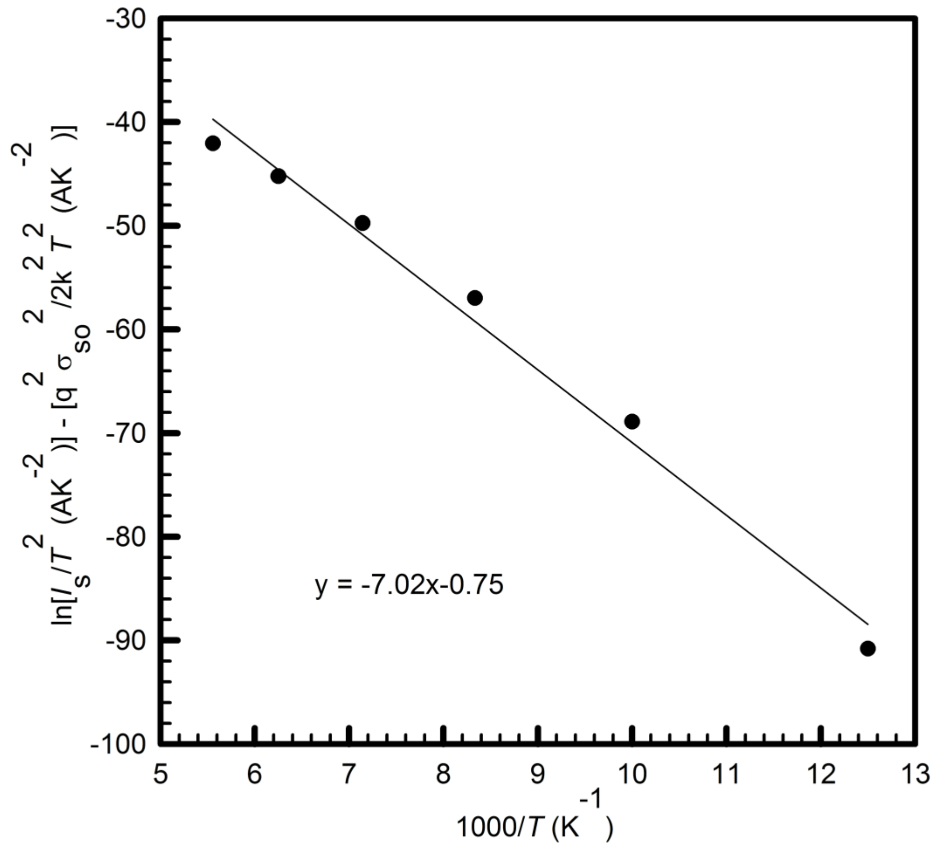

Fig. 5.3.8: Modified Richardson plot according to the Gaussian distribution of barrier heights.

5.3.7: Conclusions.

The Pd Schottky contacts on ZnO have very strong temperature dependences as revealed by the *I-V* characteristics of Fig.5.3.1 and 5.3.2. This temperature dependence has affected the parameters extracted from these curves. On the O-polar face, generation recombination has even shown its effects at room temperature. At low temperatures, generation recombination and other mechanisms play a role in the transport of carriers across the barrier. The ideality factor shows a strong dependence on temperature on the O-polar face. The *I-V* barrier height shows a trend that disagrees with the negative temperature coefficient of the II-VI compound semiconductor material, an effect explained by the inhomogeneities of the barrier. The series resistance of the diodes decreases with an increase in temperature and has been correlated to the resistivity and hence conductivity of the bulk semiconductor material. In the determination of the effective Richardson constant, barrier inhomogeneities correction needs to be effected in order to get a value closer to the known theoretical value. The publication at the end of this section gives detailed analysis on the temperature dependence of the IV results.

References

[1] C. Lu, S. N. Mohammed, Appl. Phys. Lett. 89, 162111, (2006)

[2] R. T. Tung, Phys. Rev. B. 45, 13509, (1992)

[3] S. Karatas, S. Altindal, Sol. Stat. Electron., 49, 1052, (2005).

[4] W. Mtangi , J. M. Nel, F. D. Auret, A. Chawanda, C. Nyamhere, P. J. Janse van Rensburg, M. Diale, with Phys. Stat. Sol.

[5] W. Mtangi, F.D. Auret, C. Nyamhere, P. J. Janse van Rensburg, M. Diale, A. Chawanda, Phys. B., 404, 1092 (2009).

[6] J. Tersoff, Phys. Rev. Lett. 52, 465, (1984)

[7] J. H. Werner, H. H. Guttler, J. Appl. Phys. 73.(3) (1993)

[8] R. Singh, S. K. Arora, R. Tyagi, S. K. Agarwal and D. Kangilal, Bull. Mater. Sci., 23, 6, (2000)

[9] J. Tersoff, Phys. Rev. B. 32,6968 (1985)

[10] J. Osvald, Micro. Eng. 86 117-120 (2009).

[11] H. Korkut, N. Yildirim, A. Turut, H. Dogan, Mater. Sci. & Eng. B 157, 48 (2009)

[12] J. Bardeen, Phys. Rev. B, 71, 717, 1947.

[13] P. Revva, J. M. Langer, M. Missous, A. R. Peaker, J. Appl. Phys. 74, 416, (1993)

[14] R. T. Tung, Appl. Phys. Lett. 58 (24), (1991)

[15] D. K. Schroder, Semiconductor material and device characterization, 3rd Ed. Wiley & sons, Inc., Hoboken, New Jersey, (2006).

[16] E. Gu. S. Tuzemen, B. Kihc, and C. Coskun, J. Phys: Condes. 19 (2007).

[17] H. Sheng, N. W. Emanetoglu, S. Muthukumar, B. V. Yakshinskiy, S. Feng and Y. Lu, Electronic Mat. 32, 9, (2003).

[18] I. Dokme, S. Altindal, M. M. Bulbul, Appl. Surf. Sci., 252, 7749 (2006)

[19] H. von. Wenckenstern, G. Biene, R. A. Rhaman, E. M. Kaidashev, H. Hochmuth, M. Lorenz, M. Grundmann, Appl. Phys. Lett. 88, 2835, (2006).

UNIVERSITEIT VAN PRETORIA
UNIVERSITY OF PRETORIA
YUNIBESITHI YA PRETORIA

Publications.

Physica B 404 (2009) 1092–1096

Contents lists available at ScienceDirect

Physica B

journal homepage: www.elsevier.com/locate/physb

Analysis of temperature dependent $I-V$ measurements on Pd/ZnO Schottky barrier diodes and the determination of the Richardson constant

W. Mtangi *, F.D. Auret, C. Nyamhere, P.J. Janse van Rensburg, M. Diale, A. Chawanda

Department of Physics, University of Pretoria, Pretoria 0002, South Africa

A R T I C L E I N F O

Article history:
Received 12 September 2008
Received in revised form
25 October 2008
Accepted 12 November 2008

PACS:
71.55.−i
72.10.Bg
72.20.Jv
79.40.+z

Keywords:
Schottky contacts
Electrical characterization
Richardson constant
Barrier inhomogeneities
Barrier height
DLTS

A B S T R A C T

Temperature dependent current–voltage ($I-V$) and Hall measurements were performed on Pd/ZnO Schottky barrier diodes in the range 20–300 K. The apparent Richardson constant was found to be 8.60×10^{-9} A K^{-2} cm^{-2} in the 60–160 K temperature range, and mean barrier height of 0.50 eV in the 180–300 K temperature range. After barrier height inhomogeneities correction, the Richardson constant and the mean barrier height were obtained as 167 A K^{-2} cm^{-2} and 0.61 eV in the temperature range 80–180 K, respectively. A defect level with energy at 0.12 eV below the conduction band was observed using the saturation current plot and (0.11 ± 0.01) eV using deep level transient spectroscopy measurements.

© 2008 Elsevier B.V. All rights reserved.

1. Introduction

In determining the Schottky barrier height, Φ_b of metal/semiconductor contacts, general $I-V$ and capacitance–voltage ($C-V$) measurements are usually employed at room temperature, which use the assumption that only thermionic emission is responsible for the flow of electrons across the potential barrier. In this paper, we have assumed that other current transport processes also contribute towards the movement of electrons within the depletion region and across the barrier in Schottky contacts, to determine the barrier height. The equations usually used for the determination of the barrier height according to Schroder [1], indicate the dependence of the barrier height on the saturation current, I_s:

$$\Phi_b = \frac{kT}{q} \ln \frac{AA^*T^2}{I_s} \tag{1}$$

where A^* is the effective Richardson constant, A is the Schottky contact area, I_s is the saturation current, k the Boltzmann constant and T is the Kelvin temperature, assuming pure thermionic emission over the barrier, such that,

$$I = I_s \left\{ \exp\left(\frac{qV}{kT}\right) - 1 \right\} \tag{2}$$

This approximation factors out the effect of the series resistance, R_s and the ideality factor, n. The barrier height determined using this method is for zero bias [1]. There usually exists uncertainity because of using an incorrect value of A^* [1]. The Richardson constant has a tendency of varying with temperature, and so there is need to know the actual value of the constant in a range of temperatures, which the barrier height is being evaluated. Different values of the Richardson constant have been obtained by different researchers [2–6] using different temperature ranges. Since A^* appears in the 'ln' term in Eq. (1), an error of two would mean the value of Φ_b will be affected by a factor of 0.7 kT/q [1]. Incorporating other current transport mechanisms, to make the diode non-ideal, i.e. $n>1$, the series resistance and the ideality factor, n need to be factored into Eq. (2) [7]:

$$I = I_s \exp\left[\frac{q(V - IR_s)}{nkT}\right] \left\{ 1 - \exp\left(-\frac{[q(V - IR_s)]}{kT}\right) \right\} \tag{3}$$

* Corresponding author. Tel.: +27 74 1874157; fax: +27 12362 5288.
E-mail address: Wilbert.Mtangi@up.ac.za (W. Mtangi).

0921-4526/$ - see front matter © 2008 Elsevier B.V. All rights reserved.
doi:10.1016/j.physb.2008.11.022

where

$$I_s = AA^*T^2 \exp\left(\frac{-q\Phi_b}{kT}\right) \quad (4)$$

Eq. (3) is commonly used in computing the values of I_s and Φ_b providing $n \leqslant 1.1$ [1]. When thermionic emission is no longer the only dominant mechanism or the series resistance is too large, the ideality factor n increases. By extrapolating the semi-logarithmic plot of the general $I-V$ relationship, I_s is obtained as the intercept on the vertical axis, acceptable when the pure thermionic emission vanishes and therefore no physical interpretation in calculating Φ_b from Eq. (4) is justified [7]. Another type of error arises when choosing the linear range from the semi-logarithmic $I-V$ relationship plot. Since the series resistance influences the upper limit while the lower part is affected by other current transport mechanisms, especially for structures with high barrier heights Φ_b, they push the interval limit up, thus reducing the linear region [7], making it slightly impossible to fit the experimental $I-V$ curves within a wide temperature range. Gu et al. [2], and Sheng et al. [4] performed temperature dependent $I-V$ measurements on the Ag/ZnO Schottky diodes in the higher temperature ranges (200–500 K) and (265–340 K), and obtained the effective Richardson constant to be 0.248 and 0.15 A K^{-2} cm^{-2}, respectively. Grossner et al. [8] performed some measurements on the Pd/ZnO Schottky diodes and revealed the stability of the Schottky barrier diode (SBD) in the temperature range 130–340 K. In this study, analysis of the temperature dependence of the hydrogen peroxide treated Pd/ZnO SBD and calculation of the effective mean barrier height Φ_b, the Richardson constant A^*, the modified Richardson constant A^{**} and the thermal activation energy of a defect in the ZnO sample in the temperature range (20–300 K) has been performed.

2. Experimental procedure

Undoped ZnO samples from Cermet Inc. were used in this study. Temperature dependent Hall measurements were carried out using a Helium cryostat in the temperature range 60–330 K on a hydrogen peroxide treated sample. Prior to the deposition of the ohmic and Schottky contacts, the sample was degreased in acetone, methanol and boiled in hydrogen peroxide at 100 °C for 3 min. After treatment with the peroxide, they were blown dry using nitrogen gas. Ohmic contacts with the composition of Ti/Al/Pt/Au with thicknesses 20/80/40/80 nm were deposited on the oxygen polar face in the electron-beam at a pressure of approximately 1×10^{-6} Torr. The samples were then annealed in Argon ambient at a temperature of 200 °C for 30 min. Palladium contacts with an area $A = 2.83 \times 10^{-3}$ cm^2 were then fabricated on the Zn-polar face of the ZnO samples in the resistive evaporation system under a vacuum of approximately 1×10^{-5} Torr. Bonding of thin gold wires was carried out on the Pd Schottky contacts using silver paint. The silver paint was also used on the O-polar face to provide for the ohmic contacts, and the samples were attached to gold plated ceramic plates. Temperature dependent $I-V$ measurements were carried out in a He cryostat in the range 20–300 K. Deep level transient spectroscopy (DLTS) measurements were finally carried out in the temperature range 20–330 K.

3. Results and discussion

From Fig. 1, the curves obtained for the $I-V$ measurements indicate a very strong temperature dependence of the Pd/ZnO Schottky diodes. These characteristics deviate from ideality at low

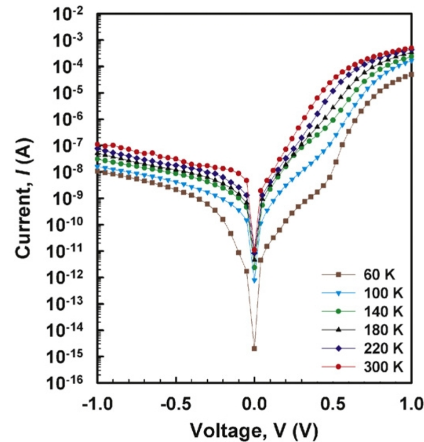

Fig. 1. (Color online) Temperature dependent $I-V$ semi logarithmic plot for the as-deposited Pd/ZnO Schottky diode in the 60–300 K range.

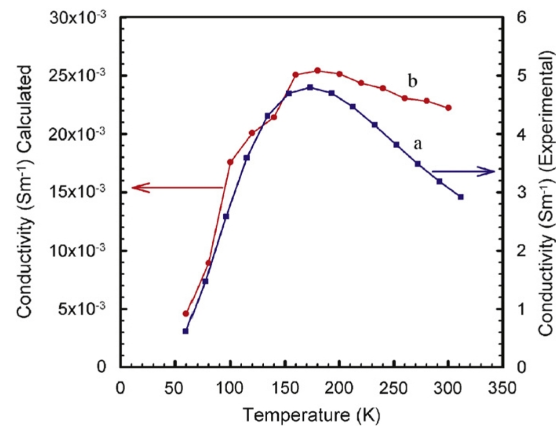

Fig. 2. (Color online) Conductivity–temperature variation of ZnO: (a) is the plot obtained from the Hall measurement results and (b) is the plot obtained from calculations, using Eq. (6).

temperatures (20–140 K), which may be due to the effect of other current transport processes like the generation-recombination of carriers in the space charge region [9] and tunneling of electrons through the barrier. At temperatures above 140 K, thermionic emission becomes the dominant process. In the 160–300 K temperature range, the diode is characterized by an increasing series resistance with temperature. This series resistance is correlated to the resistivity of the ZnO material and therefore to the intrinsic electron carrier concentration. The series resistance increases with a decrease in temperature, i.e. below 160 K. The resistivity, ρ of a material can be related to the conductivity by the equation [2]

$$\rho = \frac{1}{q\mu_n n} = \frac{1}{\sigma} \quad (5)$$

where μ_n is the electron mobility, and n is the electron carrier concentration. Fig. 2 shows an increase in conductivity with temperature up to 160 K, which justifies the increase in series resistance with a decrease in temperature as well as a decrease in

conductivity with increase in temperature above 160 K. On the same graph, we have plotted a curve using the calculated values from the series resistance, using the equation,

$$\rho = \frac{AR}{l} \tag{6}$$

where A is the Schottky contact cross sectional area, R is the series resistance and l is the thickness of the sample. These two curves are in agreement as they both show the same trend. The only difference is in the magnitude of the values, i.e. the conductivity obtained from Hall measurements is larger than that obtained using the calculated series resistance. The low conductivity in the curve where the series resistance was used to calculate the resistivity could be due to the presence of a back ohmic contact. The possible existence of the insulative oxide layer between the metal and semiconductor could have also contributed to the high resistivity of the diode. Another possibility for low conductivity could be the contact area, which was large as the diameter of the contact was used compared to the Hall measurement technique where very small contacts are used. Fig. 3 shows a plot of barrier height and ideality factor as a function of temperature. The ideality factor increases with temperature from 60 to 160 K. Lu and Mohammad [10] also observed this trend in Al_xGaN_{1-x} diodes. At 180 K, the ideality factor starts to decrease up to 300 K where it is approximately 1.77. This type of variation might be due to the so-called T_0 anomaly as explained by Tung [11]. The barrier height has also shown some temperature dependence with the highest value being 1.02 eV at a temperature of 60 K. As the temperature increases, the barrier height starts to decrease until it becomes almost constant in the 180–300 K temperature range, where thermionic emission is dominant. This trend is the most expected, as at low temperatures, charge carriers would not be having enough energy to surpass the barrier and some lose their energy during collisions when they undergo recombination-generation and hence they see a large barrier. After 160 K, majority charge carriers gain enough energy as they are excited over the potential barrier and start contributing to the current flowing through the semiconductor and hence they see a reduced barrier. Since thermionic emission is the dominant current transport process and the diode exhibits the same characteristics in the 180–300 K-temperature range, with little variation in the ideality factor, we can say the diode is stable in this temperature range.

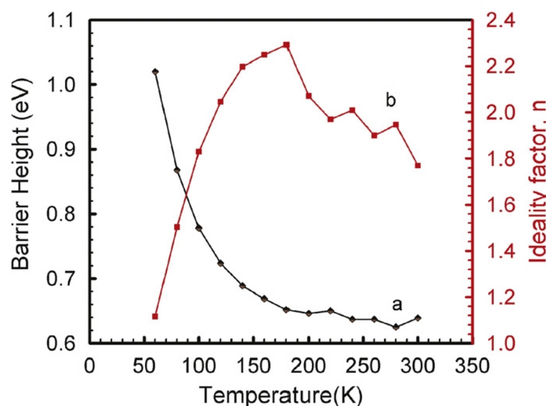

Fig. 3. Barrier height (a) and ideality factor (b) as a function of temperature in the temperature range (60–300 K) for the as-deposited Pd/ZnO Schottky diode.

3.1. The Richardson constant

The transition in the characteristics of the diode at 160 K, has affected the linearity of the curve for the Richardson plot in the temperature range 180–300 K and so we have managed to fit the curve in the 60–160 K temperature range as shown in Fig. 4, which is a linear fit of Eq. (4). The insert of Fig. 4, is a Richardson plot for the temperature range 180–300 K. The diode shows high dependence of ideality factor on temperature, which distorted the linearity of the plot. Linear restoration of the plot in the 180–300 K region was performed by multiplying $\ln(I_s/T^2)$ by the ideality factor, n as suggested by Schroder [1]. The apparent Richardson constant was calculated as 8.60×10^{-9} and $5.19 \times 10^{-15}\,\mathrm{A\,K^{-2}\,cm^{-2}}$ for the 60–160 and 180–300 K temperature ranges, respectively, from the plots of Fig. 4. Dokme et al. [3] calculated the value of the effective Richardson constant for Al/p-Si SBD in the temperature range 150–375 K and found it to be $1.3 \times 10^{-4}\,\mathrm{A\,K^{-2}\,cm^{-2}}$. The gradient of the insert of Fig. 4, yielded an effective barrier height of 0.50 eV. The deviation of the Richardson constant from the theoretical value, $32\,\mathrm{A\,K^{-2}\,cm^{-2}}$ is explained by some researchers [3,6] as an effect of the barrier inhomogeneity of the contact, meaning that it consists of high and low barrier areas at the interface mainly due to the formation of different oxide layer thicknesses between the metal and the semiconductor. Due to these potential fluctuations at the interface, the current of the diode will flow preferentially through the lower barriers in the potential distribution [12].

3.2. Barrier height inhomogeneities

We have corrected the barrier height inhomogeneities, to obtain a modified value of the Richardson constant, closer to the known value of $32\,\mathrm{A\,K^{-2}\,cm^{-2}}$. The analysis of the barrier height inhomogeneities was also suggested and performed by Dokme et al. [3] and Karadeniz et al. [12]. Usually, the barrier height obtained under the flat band condition is considered to be a real fundamental quantity which assumes that the electrical field is zero. This eliminates the effect of image force lowering that would affect the $I-V$ characteristics and removes the influence of lateral inhomogeneity [3]. In addressing the observed abnormal deviation from classical thermionic emission theory, some researchers [13,14] have considered a system of discrete regions of low barrier imbedded in a higher background uniform barrier. These behaviors can be explained by assuming that the distribution of the barrier heights is a Gaussian distribution of barrier heights with a mean value $\bar{\Phi}_b$ and standard deviation σ_s, which can be

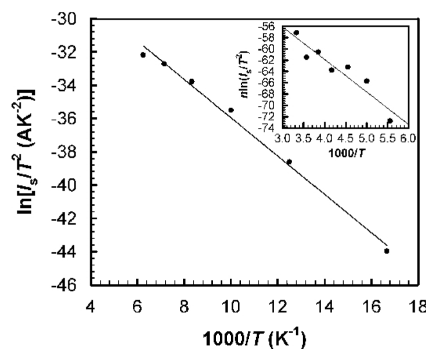

Fig. 4. Richardson plot, $\ln(I_s/T^2)$ versus $1000/T$, for the Pd/ZnO SBD in the temperature range 60–160 K. The insert shows the $n[\ln(I_s/T^2)]$ versus $1000/T$ variation for the ZnO/Pd SBD in the temperature range 180–300 K.

given by [13,15,16]

$$P(\Phi_b) = \frac{1}{\sigma_s\sqrt{2\pi}}\exp\left[-\frac{(\Phi_b)-\bar{\Phi}_b}{2\sigma_s^2}\right] \quad (7)$$

where $1/\sigma_s\sqrt{2\pi}$ is the normalization constant of the Gaussian barrier height distribution. The total $I(V)$ across a Schottky diode containing a barrier inhomogeneities can be expressed as [3]

$$I(V) = \int_{-\infty}^{+\infty} I(\Phi_b, V)P(\Phi_b)\,d\Phi_b \quad (8)$$

where $I(\Phi_b, V)$ is the current at a bias V for a barrier of height based on the ideal thermionic emission–diffusion (TED) theory and $P(\Phi_b)$ is the normalized distribution function giving the probability of accuracy for barrier height. Substituting Eq. (3) for $I(\Phi_b, V)$ and Eq. (7) for $P(\Phi_b)$ in Eq. (8), we obtain the current, $I(V)$ through the Schottky barrier at a forward bias V but with a modified barrier as [3]

$$I(V) = I_s\exp\left(\frac{qV}{n_{ap}kT}\right)\times\left[1-\exp\left(-\frac{qV}{kT}\right)\right] \quad (9)$$

with

$$I_s = AA^{**}T^2\exp\left(-\frac{q\Phi_{ap}}{kT}\right) \quad (10)$$

where n_{ap} and Φ_{ap} are the apparent ideality factor and apparent barrier height at zero bias, respectively, given by [18]

$$\Phi_{ap} = \bar{\Phi}_b(T=0) - \frac{q\sigma_{so}^2}{2kT} \quad (11)$$

$$\left(\frac{1}{n_{ap}}-1\right) = \rho_2 - \frac{q\rho_3}{2kT} \quad (12)$$

We need to assume that the mean Schottky barrier height $\bar{\Phi}_b$ and σ_s are linearly bias-dependent on Gaussian parameters, such that $\bar{\Phi}_b = \bar{\Phi}_{b0} + \rho_2 V$ and standard deviation $\sigma_s = \sigma_{so} + \rho_3 V$, where $\bar{\Phi}_{b0}$ is the barrier height at temperature $T = 0$ K, ρ_2 and ρ_3 are voltage coefficients which may depend on temperature, quantifying the voltage deformation of the barrier height distribution [17,18]. The temperature dependence of σ_s is small and therefore can be neglected [19]. The decrease of zero-bias barrier height is caused by the existence of the Gaussian distribution and the extent of influence is determined by the standard deviation itself [3,12]. The existence of the barrier inhomogeneities affects the current transport of electrons across the Schottky barrier. Since at low temperatures, charge carriers have very low energies to surpass the energy barrier, tunneling of electrons is the dominant process. Due to the fact that the barrier is non homogeneous, further tunneling through the low barrier areas leads to the deviation of the barrier height from the value that could be obtained for a uniformly distributed barrier at the metal–semiconductor interface. A linear fit for the apparent ideality factor, which obeys Eq. (12), has been obtained as in Fig. 5; in the low temperature region as the Gaussian distribution effect is common at low temperatures [12]. The fitting of the experimental data using Eq. (4) or (10)gives the value of the apparent barrier height, which should obey Eq. (11). Our fitted data to Eq. (11), yielded a value of $\bar{\Phi}_{b0}$ as 0.529 eV and $\sigma_{so} = 0.066$ V from the intercept and slope respectively. The lower the value of σ_{so}, the more homogeneous the barrier height is and the better the diode rectifying performance. The ideality factor plot only produced a linear fit for the low temperature values, i.e. 80–180 K as the Schottky diode shows a transition in the ideality factor, series resistance and barrier height at 160 K. For this particular fit, the voltage coefficients were obtained as $\rho_2 = -0.769$ V and $\rho_3 = -0.0057$ V from the intercept and gradient, respectively. The linear behavior of the ideality factor fit in the 80–180 K temperature range shows the voltage deformation of the Gaussian distribution of the Schottky barrier height in this range.

3.3. The modified Richardson plot

The Richardson plot can now be modified by combining Eqs. (10) and (11) such that,

$$I_s = AA^{**}T^2\exp\left[-\frac{q\bar{\Phi}_{ap}}{kT} + \frac{q^2\sigma_{so}^2}{2k^2T^2}\right] \quad (13)$$

and

$$\ln\left(\frac{I_s}{T^2}\right) - \left(\frac{q^2\sigma_{so}^2}{2k^2T^2}\right) = \ln(AA^{**}) - \frac{q\bar{\Phi}_{ap}}{kT} \quad (14)$$

where A^{**} is the modified Richardson constant. A plot of the modified $\ln(I_s/T^2) - (q^2\sigma_{so}^2/2k^2T^2)$ versus $1000/T$ yields a straight line with the slope giving the mean barrier height and the intercept giving the modified Richardson constant as shown in Fig. 6. The graph has been plotted for the 80–180 K temperature range as the ideality factor plot produced a linear fit in this region, denoting the voltage deformation of the Gaussian distribution of the barrier heights [12]. The 60 K temperature curve could not be used, because it was difficult to obtain a reliable saturation current value from it. The modified Richardson constant has been obtained as 167 A K^{-2} cm^{-2} and a mean barrier height of 0.61 eV. Karadeniz et al. [12] and Dokme et al. [3] also used the same method and obtained a modified Richardson constant of 12.89 and 40.08 A cm^{-2} K^{-2} for Ag/p-SnS and Al/p-Si Schottky diodes, respectively.

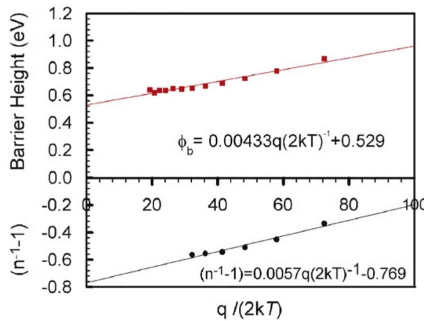

Fig. 5. (Color online) Zero-bias apparent barrier height and ideality factor versus $q/(2kT)$ curves of the Pd/ZnO Schottky diode according to the Gaussian distribution of the barrier heights.

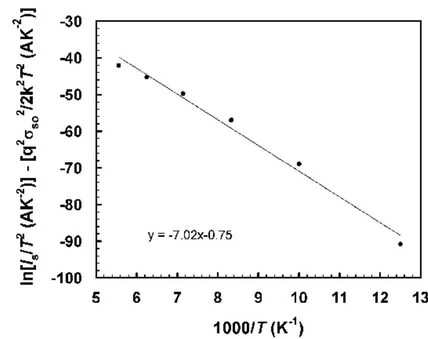

Fig. 6. Modified Richardson plot for the Pd/ZnO Schottky diode according to the Gaussian distribution of barrier heights.

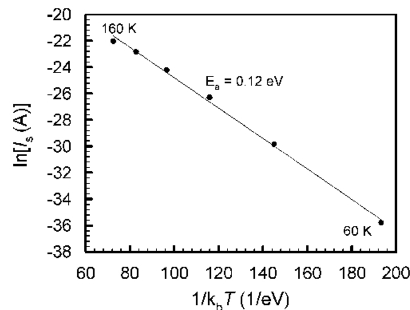

Fig. 7. Saturation current plot for the Pd/ZnO sample in the temperature range 60–160 K.

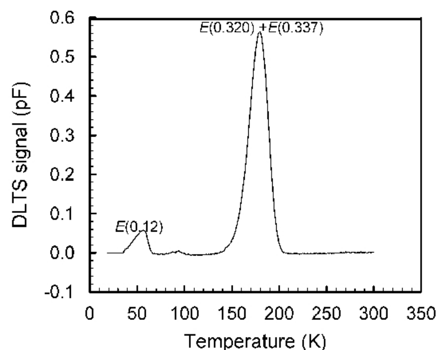

Fig. 8. DLTS signal for the as-deposited hydrogen peroxide treated Pd/ZnO Schottky diode. This spectra was measured at quiescent reverse bias of −2 V, filling pulse of $V_p = 0$ V and rate window of 80 s^{-1}.

3.4. Saturation current plot

Following the conclusion deduced from the characteristics of the curves of Fig. 1, a saturation current plot in the temperature range 60–160 K using the equation [2,7],

$$I_s = I_{oo} \exp\left(\frac{-E_a}{k_b T}\right) \quad (15)$$

has been plotted as in Fig. 7, to find the activation energy of the defect that traps the carriers causing the generation–recombination current to dominate. I_s is the saturation current measured at different temperatures, E_a is the activation energy of the defect, k_b is the Boltzmann constant. The activation energy was obtained as the gradient of the linear fit to Eq. (15) with a value of 0.12 eV as in Fig. 7. DLTS measurements have revealed the presence of two prominent peaks, with the main peak consisting of two energy levels, 0.320 and 0.337 eV below the conduction band as shown in the spectra of Fig. 8. The low temperature peak has an energy level (0.11 ± 0.01) eV below the conduction band. This peak has shown a strong dependence on the electric field as its energy varies from 0.10 eV at low electric fields to 0.12 eV at high electric fields. Auret et al. [20] observed a defect level with almost the same energy level ($E_a = 0.12$ eV) to the latter in a ZnO sample grown by the vapor phase technique, whose origins are not specified yet. This peak is also asymmetric as the capacitance drops sharply at low temperatures as was also observed by Auret et al. [20], which is possibly the effect of carrier freeze out.

4. Conclusion

ZnO has shown a temperature dependent behavior in a wide temperature range. Within this range, below 160 K, generation–recombination has proved to be the dominant current transport mechanism. For the temperature range 180–300 K, thermionic emission is the dominant transport mechanism and the diode is highly stable as shown by the ideality factor, which varies little with temperature. In this temperature range, ZnO has revealed a barrier height that is independent of temperature. The apparent Richardson constant, A^* for ZnO has been found to be 8.60×10^{-9} and 5.19×10^{-15} A K^{-2} cm^{-2} in the 60–160 and 180–300 K temperature ranges, respectively. A^* has shown a strong dependence on the metal–semiconductor contact quality and saturation current. From the modified Richardson plot, the modified Richardson constant, A^{**} has been obtained as 167 A K^{-2} cm^{-2} in the 80–180 K temperature range and a mean barrier height of 0.61 eV. In determining A^{**}, barrier inhomogeneities needs to be taken into consideration to obtain a more accurate value. The cleaning procedure used in this particular study has proved to be the best for ZnO as good diodes with very low reverse leakage currents and high rectification properties were obtained as was also revealed by Gu et al. [2].

Acknowledgment

We would like to thank the South African National Research Foundation for the financial support.

References

[1] D.K. Schroder, Semiconductor Material and Device Characterization, second ed., Wiley, New York, 1998.
[2] E. Gu, S. Tuzemen, B. Kilic, C. Coskun, J. Phys.: Condens. Matter 19 (2007) 196206.
[3] I. Dokme, S. Altindal, M.M. Bulbul, Appl. Surf. Sci. 252 (2006) 7749.
[4] H. Sheng, S. Muthukumar, N.W. Emanetoglu, Y. Lu, Appl. Phys. Lett. 80 (2005) 2132.
[5] K. Ip, Y.W. Heo, K.H. Baik, D.P. Norton, S.J. Pearton, S. Kim, J.R. LaRoche, F. Ren, Appl. Phys. Lett. 84 (2004) 5133.
[6] H. von Wenckenstern, G. Biene, R.A. Rahman, E.M. Kaidashev, H. Hochmuth, M. Lorenz, M. Grundmann, Appl. Phys. Lett. 88 (2006) 2835.
[7] D. Donoval, M. Barus, M. Zdimal, Solid State Electron. 34 (1991) 1365.
[8] U. Grossner, S. Gabrielsen, T.M. Borseth, J. Grillenberger, A.Y. Kuznetsov, B.G. Svensson, Appl. Phys. Lett. 85 (2004) 259.
[9] S. M Sze, Physics of Semiconductor Devices, second ed., Wiley, New York, 1981.
[10] C. Lu, S.N. Mohammad, Appl. Phys. Lett. 89 (2006) 162111.
[11] R.T. Tung, Phys. Rev. B 45 (1992) 13509.
[12] Ş. Karadeniz, M. Şahin, N. Touğluoğlu, H. Şafak, Semicond. Sci. Technol. 19 (9) (2004) 1098.
[13] JŞ. Altindal, S. Karadeniz, N. Touğluoğlu, A. Tataroglu, Solid-State Electron. 47 (2003) 1847.
[14] R.F. Schmitsdorf, T.U. Kampen, W. Mönch, Surf. Sci. 324 (1995) 249.
[15] J.H. Werner, H.H. Güttler, Appl. Phys. 69 (1991) 1522.
[16] Y.P. Song, R.L. Meirhaeghe, W.H. Laflere, F. Cardon, Solid State Electron. 29 (1986) 663.
[17] S. Zhu, R.L. Van Meirhaege, C. Detavernier, F. Cardon, G.P. Ru, X.P. Qu, B.Z. Li, Solid State Electron. 44 (2000) 663.
[18] A. Gümüş, A. Türüt, N. Yalçin, J. Appl. Phys. 91 (2002) 245.
[19] M.K. Hudait, S.P. Venkateswarlu, S.B. Krupanidhi, Solid State Electron. 45 (2001) 133.
[20] F.D. Auret, S.A. Goodman, M. Hayes, M.J. Legodi, H.A. van Laarhoven, D.C. Look, J. Phys.: Condens. Matter 13 (2001) 8989.

5.4: CV measurements on ZnO Schottky Barrier Diodes.

As has been discussed in section 3.5.1, low capacitance values have been measured from the Pd and Au Schottky contacts deposited on the O-polar face at room temperature. An ac voltage with a frequency of 1 MHz has been superimposed on a reverse dc bias in the range −1 to 0 V. The capacitance produced on the MS junction depends on how the charge distribution within the system adjusts itself under an applied bias [1], hence it is a differential capacitance. However, it has been pointed out that if the charge density changes uniformly, the differential capacitance has no simple meaning because the fields and field increments are not the same [1]. The interpretation of the measured effective differential capacitance can be simplified by assuming that the space charge density in most of the barrier region remains unchanged [1]. For a classical Schottky barrier with the space charge density fixed at $\rho = eN_D$, except near the barrier edge, with an externally applied ripple voltage, the charge separation becomes well defined yielding a dynamic capacitance. Obtained values of capacitance for the selected diodes are discussed in the following sections.

5.4.1: CV characteristics of M/ZnO Schottky diodes.

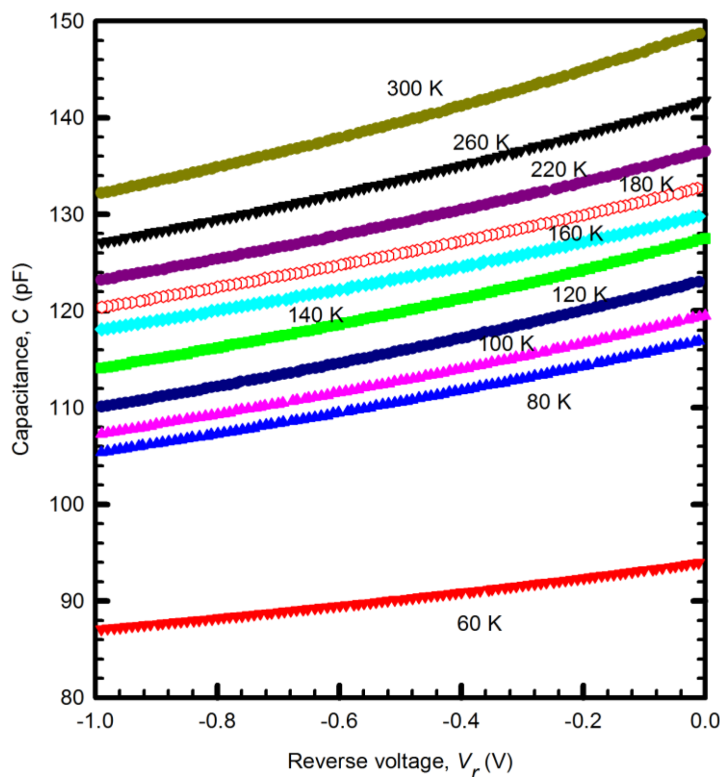

Fig. 5.4.1: Variation of capacitance with reverse voltage in the 60 – 300 K temperature range for the Pd/ZnO Schottky contacts.

For any applied bias, at a constant temperature as illustrated in Fig. 5.4.1, the capacitance increases with decreasing bias. The variation of capacitance with bias, taking the MS contact to resemble a parallel plate capacitor must satisfy equation (3.5.9). This is expected as in the forward bias mode, the Fermi level in the semiconductor moves up, pushing the energy bands upwards and hence collapsing the depletion width. Also at a constant bias, the capacitance increases with temperature, also shown in Fig. 5.4.1. This variation must satisfy the relationship [1],

$$C = A\sqrt{\frac{q\varepsilon N_d}{2(V+V_D)}} \tag{5.4.1}$$

where, C is the capacitance, A is the Schottky contact area, ε is the semiconductor permittivity, q the electronic charge, N_d, the carrier density, V the applied voltage and V_D the intercept on the voltage axis, for a semiconductor with completely ionized donors. At low temperatures, more of the charge carriers are bound to their donor atoms implying that less donors will be ionized, thus N_d will be small. As the temperature increases, the Fermi level moves downwards causing an increase in the number of ionized donors and hence an increase in the ionized donor concentration, N_d. Thus the capacitance increases. Very low capacitance values are measured at 60 K as we are approaching the freeze out region. This will be discussed further in section 5.4.1.3.

5.4.1.1: The built-in potential.

By bringing the metal Fermi level into equilibrium with the semiconductor Fermi level, a region depleted of charge carriers in the semiconductor is formed. Due to the existence of positive and negative charges on either side of the depletion region, a parallel plate capacitor is formed where the depletion region acts as a dielectric. An electric field will be created at the MS junction because of the polarity of the junction. The induced electric field induces a voltage on the MS contact called the built-in voltage. This built-in voltage is extracted from the voltage intercept of the $1/C^2$ versus V plots and is related to the built-in potential by,

$$V_I = V_{bi} + \frac{kT}{q} \tag{5.4.2}$$

The built-in potential is usually approximated to the voltage intercept since the term kT/q is very small compared to the voltage intercept. The values of the built-in potential obtained from the $1/C^2$ versus V plots are shown as a function of temperature in Fig. 5.4.2.

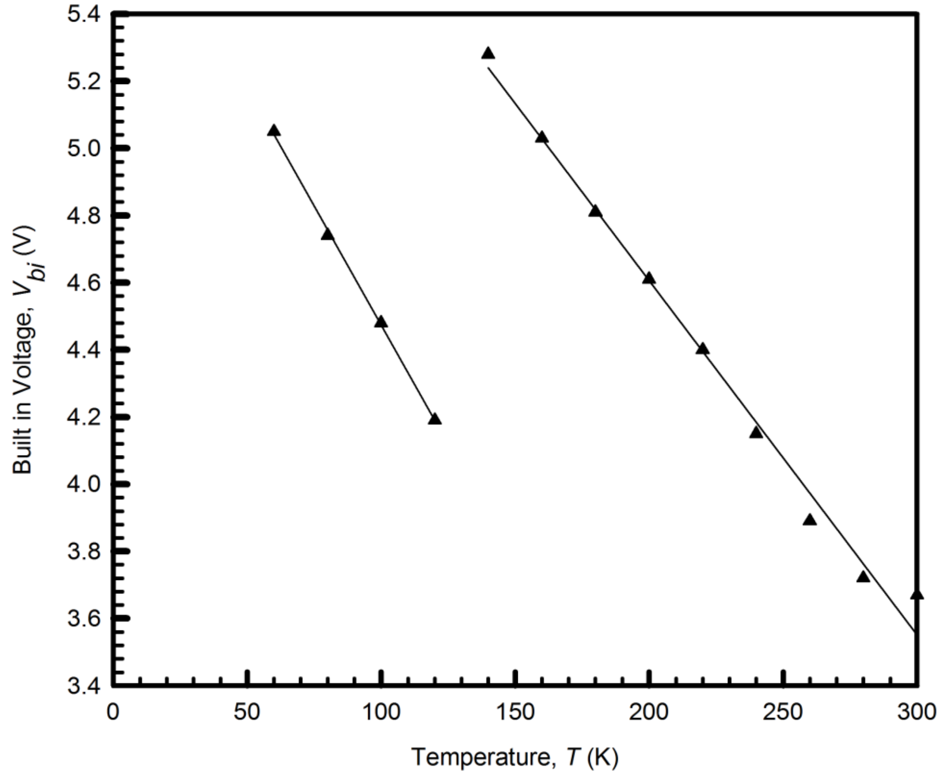

Fig. 5.4.2: Variation of built-in voltage with temperature for the 60-300 K range.

The graph indicates a linear relationship between the built in potential and temperature. However there is a discontinuity at 120 K making it possible to fit the data in two regions, 60 – 120 K and 140 – 300 K. This discontinuity has been attributed to a defect that affects capacitance determination between 120 K and 140 K [2] as shown on the capacitance temperature curve of Fig. 5.4.7. The measured values of the built-in potential are larger than the energy gap of ZnO. This could be due to existence of an inversion layer with high charge density that causes the maximum electric field in the space charge region to attain high values even with moderate doping concentrations [3]. The electric field strength within this system is obtained by solving Poisson's equation relating the charge density and the electrostatic potential [4],

$$\frac{d^2\psi}{dx^2} = -\frac{\rho}{\varepsilon_s} \qquad (5.4.3),$$

which by integration, and assuming no force and electric potential in the bulk of the semiconductor yields [4],

$$\varepsilon_{\max}^2 = \frac{2q}{\varepsilon_s}\left\{N_d\left(V_d - \frac{kT}{q}\right) + \frac{p_s kT}{q}\left[1 - \exp\left(\frac{-qV_d}{kT}\right)\right] + \frac{kTN_d}{q}\exp\left(\frac{-qV_d}{kT}\right)\right\} \qquad (5.4.4)$$

where p_s is the hole concentration at $x = 0$, V_d is equal to the surface potential. For a barrier height that is too large, such that the surface is strongly p-type, the term involving p_s is negligible, and if $qV_d/kT >> kT$ the exponential term in the coefficient of N_d can be ignored, so that to a good approximation,

$$\varepsilon_{\max}^2 = \frac{2q}{\varepsilon_s}\left\{N_d\left(V_d - \frac{kT}{q}\right)\right\} \tag{5.4.5}$$

5.4.1.2: Determination of the barrier height.

The barrier height has been determined by making use of equation (3.5.17) in the 60 – 300 K temperature range. The measured barrier heights are large compared to the energy gap of ZnO. Barrier heights greater than the energy gap of the semiconductor have been measured by Chi *et al.* [3] for NiGe/n-Ge Schottky contacts, Dos Santos *et al.* [5] for the Schottky contacts deposited on PbSe, where the barrier height was obtained to be twice as large as the energy gap and by Walpole and Nill [6] on PbTe and InAs. This has been explained as an effect of an inversion layer. As has been highlighted in section 5.4.1.1, the inversion layer affects the built-in potential values, and since the barrier height strongly depends on the built-in potential, it is also affected indirectly. An analysis of the effect of the inversion layer has been presented by Walpole *et al.* [6] on p-type PbTe and InAs.

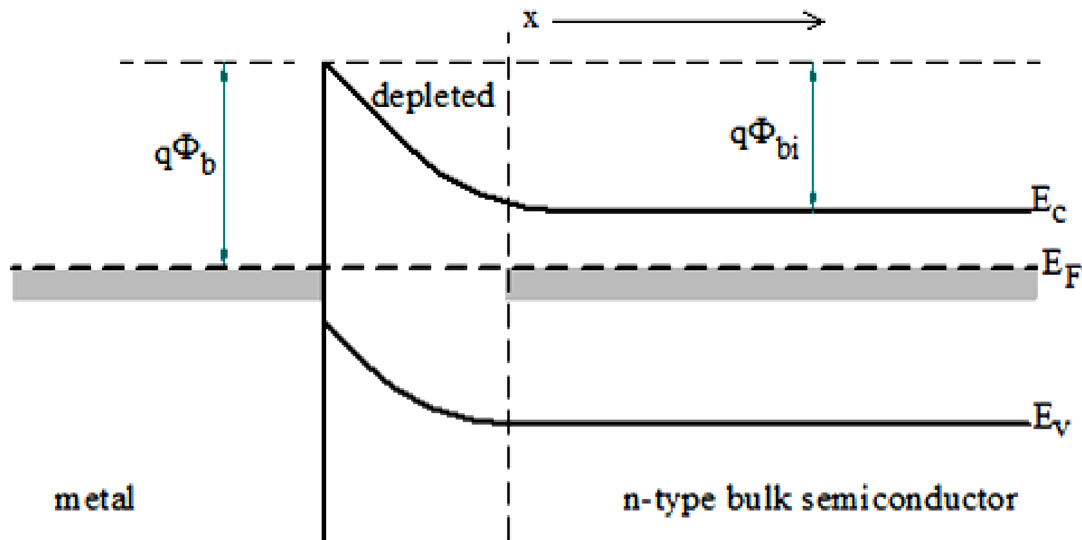

Fig. 5.4.3a: Energy bands versus distance x for a metal semiconductor contact without an inversion layer, Φ_b representing the barrier height and Φ_{bi} the built-in potential.

At equilbrium, the energy bands between a metal and semiconductor with no applied bias appears as in Fig. 5.4.3a. An inversion layer is usually formed when the Fermi level at the

electrode interface approaches the band edge level of mobile minority carriers with increasing potential across the depletion layer as in shown in Fig. 5.4.3b.

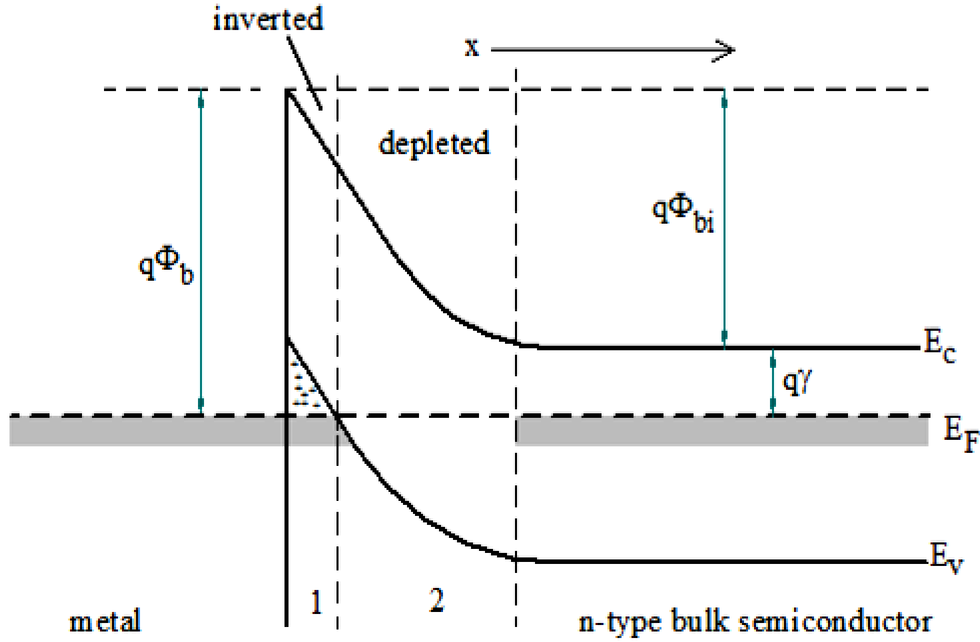

Fig. 5.4.3b: Energy bands versus distance x for a metal semiconductor cantact with an inversion layer.

The total charge per unit area in the bulk semiconductor, taking the metal semiconductor interface as the origin is given by,

$$Q_T = \int_0^{\infty} \rho(x)dx \tag{5.4.6}$$

Part of this charge, Q_D is due to the presence of charged donors within the depleted and inverted regions which are not neutralized by electrons and the remainder of the charge Q_h is due to holes in the inverted region supplied by the current entering the metal electrode which also supplies the incremental charge on the metal, similar to the case for a Schottky diode with $q\phi_b > E_G$ [7]. The capacitance measured is given by $C = AdQ_D/dV$ with $Q_D = qN_d x_d$ where x_d is the depletion layer width. By subdividing the depletion layer into two regions, i.e. $x < x_i$ for region 1 and $x_i < x < x_d$ for region 2, the capacitance is given by [7],

$$C \cong qAN_d dx_i/dV + \left[\frac{q\varepsilon_s\varepsilon_0 N_d}{2(\phi_b - \gamma - V - U(x_i) - kT/q}\right] \tag{5.4.7}$$

where γ is the energy difference between the Fermi level and the conduction band, V is the applied voltage, $U(x_i)$ is the electric potential at a point, x_i. The modification of the capacitance value also affects the measured barrier height.

5.4.1.3: Depth Profiling.

By making use of the depth profile technique, the donor concentration has been obtained in the 60 – 300 K temperature range as the gradient of the $1/C^2$ versus V plots. Fig. 5.4.4 and Fig. 5.4.5 show the $1/C^2$ versus V plots obtained at 60 K and 300 K, respectively.

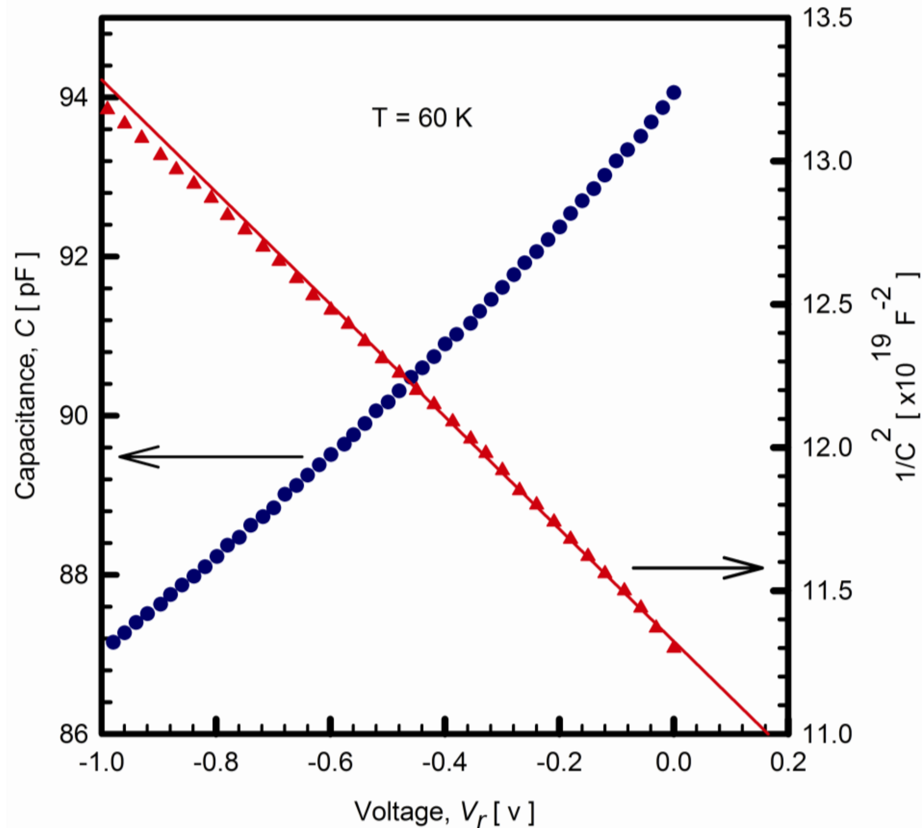

Fig. 5.4.4: Variation of $1/C^2$ with applied reverse voltage (red triangles) to determine the donor concentration measured at 60 K.

The experimental data show a deviation from linearity at low voltages for the 60 K plot. This shows a decrease in carrier concentration as we move deep into the bulk of the semiconductor [1]. This also shows incomplete donor ionization at low temperatures. The 300 K temperature plot (Fig. 5.4.5) shows linearity in the data in the whole voltage range. This indicates complete donor ionization at this particular temperature [1]. Fig. 5.4.6 shows the measured donor concentration as a function of temperature. At low temperatures, the donor concentration is low and increases with increasing temperature. This can be explained by the fact that at low temperatures, the carriers are bound to their donor atoms i.e. fewer of the donor atoms are ionized and with increasing temperature more of the donor atoms are ionized [8]. There is however a sudden increase in donor concentration between 120 K and 140 K. This has been explained as an effect of a defect that fills up with carriers at low temperatures and releases (empties) at high enough temperatures, affecting capacitance determination.

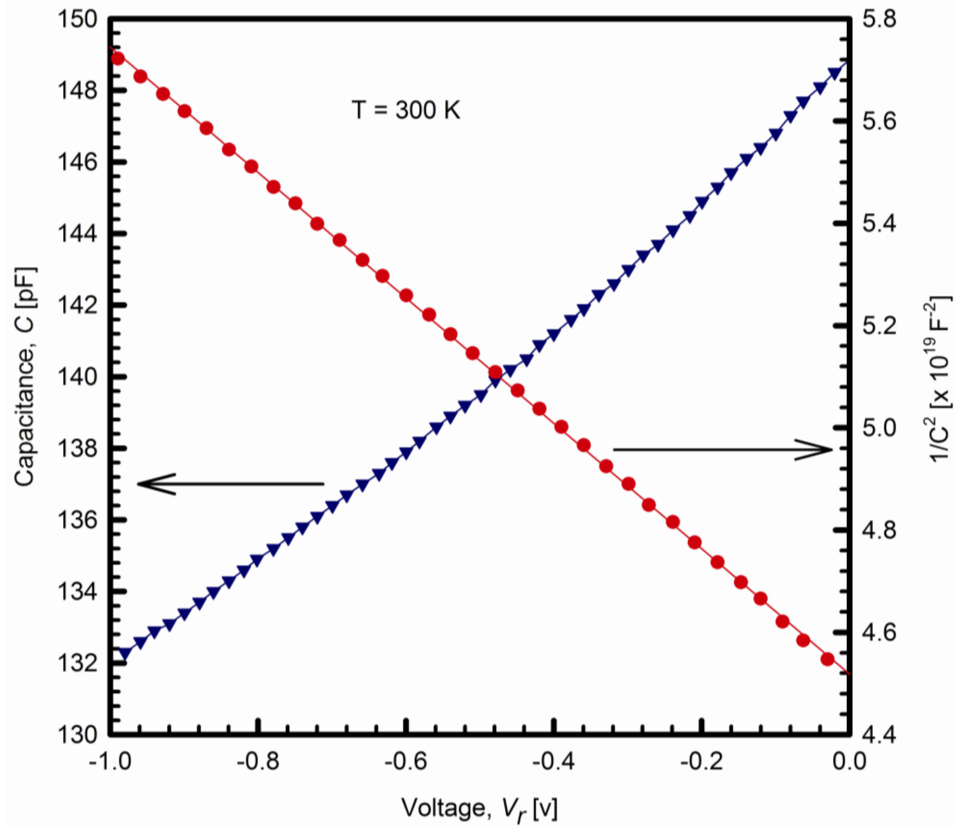

Fig. 5.4.5: Variation of $1/C^2$ with applied reverse voltage (red circles) to determine the donor concentration, N_d measured at 300 K.

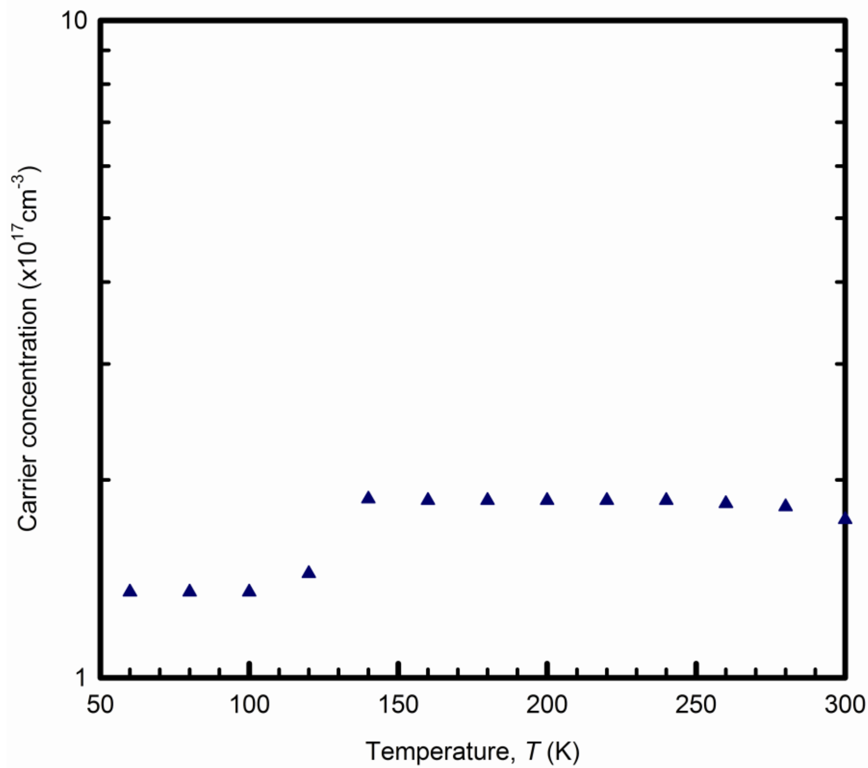

Fig. 5.4.6: Semilogarithmic carrier concentration temperature plot showing the variation of donor concentration, N_d with temperature for the Pd/ZnO Schottky diodes.

Fig. 5.4.7 shows the capacitance temperature plot measured on the palladium Schottky contacts. The plot indicates the freeze out region below 50 K. At 120 K there is a sudden increase in capacitance, followed by a gradual increase in capacitance until 300 K.

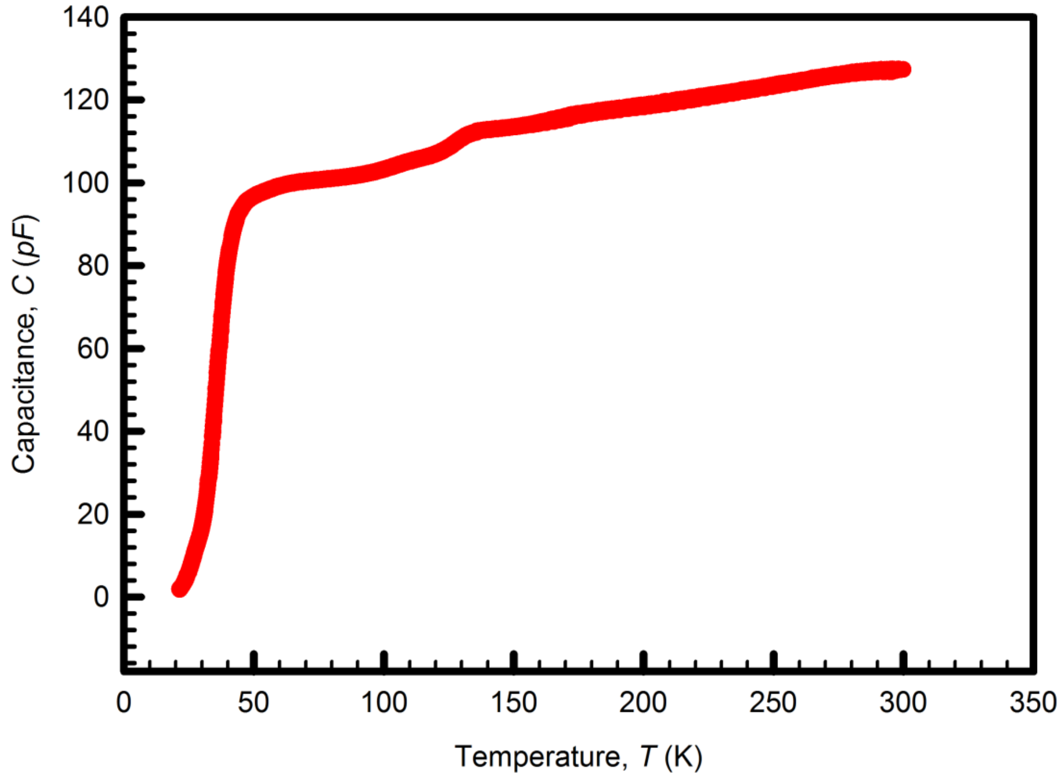

Fig. 5.4.7: Capacitance-temperature variation measured at a reverse bias voltage of -2 V and frequency of 1MHz.

5.4.2: Temperature dependence of CV barrier height.

The dependence of the barrier height on temperature is of vital importance as the SBH controls the electronic properties of devices. Measurements performed on the Pd/ZnO contacts indicate a decrease in barrier height with increasing temperature as in Fig. 5.4.8. The variation of the barrier height with temperature has enabled us to fit two linear regions to the barrier height values i.e. the first region being linear from 60 K to 120 K and the second being linear from 140 K to 300 K yielding equations of the form,

$$\phi_{C-V}(T_{60-120}) = \phi(T=0) + \alpha_1 T \quad (5.4.8)$$

where α_1 is the temperature coefficient of the semiconductor in the 60 K-120 K temperature range which was obtained as -13.6 meVK^{-1}, and

$$\phi_{C-V}(T_{140-300}) = \phi(T=0) + \alpha_2 T \quad (5.4.9)$$

where α_2 is the temperature coefficient in the 140 K-300 K temperature range which was obtained as -9.93 meVK^{-1}. At low temperatures, charge carriers will have very low energies to cross over the barrier and thus they "experience" a large barrier. With increasing temperature, carriers now have enough energy and thus they experience a reduced barrier. This variation of SBH with temperature is expected, as it follows the negative temperature coefficient of the II-VI semiconductor material [9].

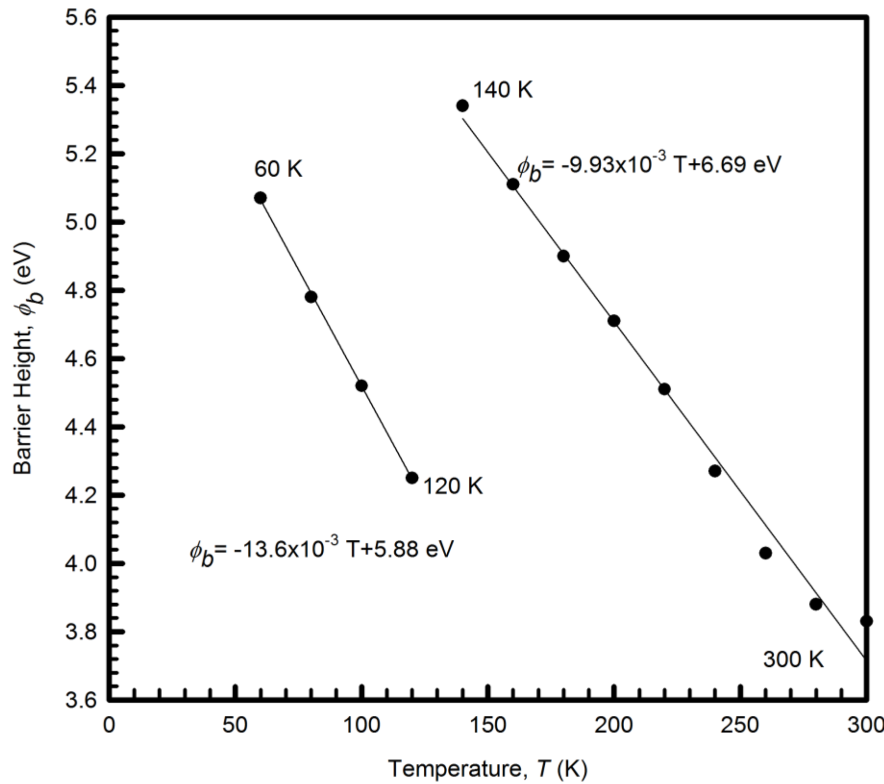

Fig. 5.4.8: Variation of Schottky barrier height with temperature.

5.4.3: Conclusions.

Capacitance voltage characteristics of palladium Schottky contacts on ZnO have been successfully determined. The variation in capacitance with temperature has been attributed to the movement of the Fermi level and donor ionization, while the variation of capacitance with applied bias has been related to the variation of the depletion width. Capacitance measured across the MS interface is affected by the nature of the interface, with traps and without traps. The CV technique can be used to determine the properties of the MS interface. The values of the built-in potential and the barrier height indicate the effect of the minority carriers on the capacitance voltage measurements. This effect has been explained in terms of the existence of an inversion layer located closer to the surface of the semiconductor. ZnO has a negative temperature coefficient as has been revealed by the variation of the barrier

height with temperature. The CV technique has also been successfully used to determine the donor concentration of the Schottky contacts. The variation of the donor concentration with temperature has been explained by the complete ionization of donors at high temperatures and incomplete ionization at low temperatures. A detailed analysis of the temperature dependence of barrier heights is discussed in the publication at the end of this particular section.

References

[1] H. K. Heinisch Semiconductor contacts, Claredon Press, Oxford, (1994).

[2] W. Mtangi, F. D. Auret, C. Nyamhere, P. J. Janse van Rensburg, A. Chawanda, M. Diale, J. M. Nel and W. E. Meyer, Phys. B. 404, 4402 (2009).

[3] Z. Chi, R. T. P. Lee, S. J. and Chua J. Appl. Phys. 97, 113706. (2005).

[4] E. H. Rhoderick, Metal-Semiconductor contacts, 2nd Edn. Oxford (1988)

[5] O. Dos Santos, V. Mathet, C. Fau, S. Charar and M. Averous, Sol. Stat. Electron. 39, 813- (1996).

[6] J. N. Walpole and K. W. Nill, J. Appl. Phys. 42, 13, (1971).

[7] H. B. Yao, D. Z. Chi, R. Li, S. J. Lee, D. L. Kwong, Appl. Phys. Lett. 89, 242117,(2006).

[8] S. M. Sze, Physics of Semiconductor devices ,Willey, New York, (1981).

[9] B. G. Yacobi, Semiconductor Materials: An Introduction to basic principles, Springer, (2003).

UNIVERSITEIT VAN PRETORIA
UNIVERSITY OF PRETORIA
YUNIBESITHI YA PRETORIA

Publications.

ARTICLE IN PRESS

Physica B ∎ (∎∎∎∎) ∎∎∎–∎∎∎

Contents lists available at ScienceDirect

Physica B

journal homepage: www.elsevier.com/locate/physb

The dependence of barrier height on temperature for Pd Schottky contacts on ZnO

W. Mtangi *, F.D. Auret, C. Nyamhere, P.J. Janse van Rensburg, A. Chawanda, M. Diale, J.M. Nel, W.E. Meyer

Physics Department, University of Pretoria, Pretoria 0002, South Africa

ARTICLE INFO

PACS:
71.55.−I
72.10.Bg
72.20.Jv
79.40.+z

Keywords:
Barrier height
DLTS
Capacitance
Traps

ABSTRACT

Temperature dependent current–voltage (*I–V*) and capacitance–voltage (*C–V*) measurements have been performed on Pd/ZnO Schottky barrier diodes in the range 60–300 K. The room temperature values for the zero bias barrier height from the *I–V* measurements (Φ_{I-V}) was found to be 0.52 eV and from the *C–V* measurements (Φ_{C-V}) as 3.83 eV. From the temperature dependence of forward bias *I–V*, the barrier height was observed to increase with temperature, a trend that disagrees with the negative temperature coefficient for semiconductor material. The *C–V* barrier height decreases with temperature, a trend that is in agreement with the negative temperature coefficient of semiconductor material. This has enabled us to fit two curves in two regions (60–120 K and 140–300 K). We have attributed this behaviour to a defect observed by DLTS with energy level 0.31 eV below the conduction band and defect concentration of between 4×10^{16} and 6×10^{16} cm^{-3} that traps carriers, influencing the determination of the barrier height.

© 2009 Elsevier B.V. All rights reserved.

1. Introduction

ZnO is a group II–VI compound semiconductor with a wide and direct bandgap (3.37 eV at room temperature). Due to its large exciton binding energy of about 60 meV, which makes it highly efficient in excitonic emission, it has attracted much attention in researchers as it can also be used in ultraviolet and blue-range optoelectronic devices, including lasers [1]. It also has superior electronic parameters such as high breakdown voltage, high electron saturation velocity [2], high thermal conductivity [3] and high radiation tolerance [4], which are better than those of the classical semiconductors, such as Si and GaAs, and is also comparable with the wide band gap semiconductors, like SiC and GaN [5]. Good rectifying ZnO Schottky contacts have been difficult to achieve since the cleaning procedure of the ZnO samples prior to contacts deposition plays a major role. Due to this effect, studies on the quality of the metal/ZnO structures have been of considerable interest to researchers. The performance and reliability of the metal-semiconductor (MS) device is influenced by the quality of the contact between the metal and the semiconductor. This is because the Schottky barrier height of the MS device is given by the mismatch between the energy levels of the majority charge carriers across the metal-semiconductor interface [6]. The Schottky barrier height (SBH) is of vital importance as it controls the electronic transport across the MS interface. Under different conditions of temperature and bias, the barrier height tends to vary as was observed by Karatas and Altindal [7] in GaAs Schottky barrier diodes. At times the barrier height (BH) measured using different techniques also tends to differ, though slightly. The performance of the MS device is also dependent on the formation of an insulative layer, which can strongly influence the device characteristics [7]. Device characteristics can also be influenced by the interface states which can lead to a large deviation from the ideal behaviour as they modify the nature of the barrier. The barrier height calculated at room temperature usually assumes the transport of carriers across the barrier to be thermionic, ignoring the effects of other current transport processes. The temperature dependence of barrier height has been studied by several researchers with conflicting results [8]. We have studied the variation of the barrier height by performing some temperature dependent *I–V* and *C–V* measurements on Pd/ZnO Schottky barrier diodes in the temperature range 60–300 K.

2. Experiment

Undoped n-type ZnO samples were used in this study. The samples were degreased in acetone for 5 min in an ultrasonic bath, then methanol for another 5 min in the ultrasonic bath and finally boiled in hydrogen peroxide for 3 min. After treatment with

* Corresponding author.
E-mail address: wilbert.mtangi@up.ac.za (W. Mtangi).

0921-4526/$ - see front matter © 2009 Elsevier B.V. All rights reserved.
doi:10.1016/j.physb.2009.09.022

Please cite this article as: W. Mtangi, et al., Physica B (2009), doi:10.1016/j.physb.2009.09.022

the peroxide, the samples were blown dry with nitrogen gas. Ohmic contacts of composition Ti/Al/Pt/Au and thicknesses of 20/80/40/80 nm were then deposited on the Zn-polar face in an electron beam deposition system under a vacuum of approximately 1×10^{-6} Torr. Annealing at a temperature of 200 °C under argon ambient was performed for 30 min. Schottky contacts with a diameter of 0.6 mm were then resistively evaporated on the O-polar face under a vacuum of approximately 1×10^{-5} Torr. Current–voltage (I–V) and capacitance–voltage (C–V) measurements were then performed in a closed cycle helium cryostat in the temperature range 60–330 K. Finally, DLTS measurements were performed in the same 20–300 K temperature range.

3. Results and discussion

In a case where an interfacial layer exists at the Schottky contact between the metal and semiconductor, the relationship between the applied voltage, V and current, I is given by [9],

$$I = I_0\left[\exp\left(\frac{qV}{nkT}\right)-1\right] \quad (1)$$

where n is the ideality factor, k is the Boltzmann constant, T is the Kelvin temperature and I_0 the reverse saturation current defined by,

$$I_0 = AA^*T^2\exp\left(-\frac{q\phi_{b0}}{nkT}\right) \quad (2)$$

where A is the Schottky contact area, A^* is the effective Richardson constant, $\phi_{b0}(=\phi_{I-V})$ is the zero bias barrier height. The ideality factor has been included to take into account the effects that cause deviation from ideality, i.e. $n\neq1$. Fig. 1 shows the semilogarithmic plot of the forward I–V characteristics of the Pd/ZnO Schottky barrier diodes in the temperature range 60–300 K. The 60–260 K curves indicate two regions where straight lines can be fitted by making use of Eq. (1). The lower part of the curves yield the generation recombination as the intercept on the current axis when the applied bias is zero while the intermediate part yields the thermionic emission current, I_0 extrapolated to the current axis when the applied voltage is zero. From the values of the I_0 obtained as intercepts after extrapolating the intermediate region to the current axis, the zero bias barrier height, ϕ_{I-V} was calculated from the relationship,

$$\phi_{I-V} = \frac{kT}{q}\ln\frac{AA^*T^2}{I_0} \quad (3)$$

with $A^*=32\,\text{AK}^{-2}\,\text{cm}^{-2}$. The resulting barrier heights from Eq. (3) are plotted as a function of temperature in Fig. 2. The observed trend is an increase in zero bias barrier height with temperature which disagrees with the negative temperature coefficient of II–VI semiconductor material [10]. The same trend of an increase in zero bias barrier height with temperature was previously observed on GaAs Schottky contacts [11,7] and Si Schottky contacts [12]. The ideality factor, n was obtained from the gradient of the linear region of the I–V plots at different temperatures, i.e.

$$n = \frac{q}{kT}\frac{\partial V}{\partial(\ln I)} \quad (4)$$

Fig. 2 indicates a decrease of n with increasing temperature from 7.55 (at 60 K) to 1.77 (at 300 K). This can be attributed to the change in the current transport process from generation recombination and other mechanisms at very low temperatures, i.e. 60–160 K to only generation recombination at the intermediate temperatures (180–260 K) and thermionic emission from 280 to 300 K. This is in agreement with what was suggested by [13]. Fig. 3 shows the variation of barrier height obtained from C–V measurements, Φ_b with temperature. The barrier height was obtained from [13],

$$\phi_{Bn} = V_i + V_n + \frac{kT}{q} - \Delta\phi \quad (5)$$

where V_n is the depth of the Fermi level below the conduction band, given by,

$$V_n = \frac{E_C-E_F}{q} = \frac{kT}{q}\ln\left(\frac{N_C}{N_D}\right) \quad (6)$$

V_i is the built in potential which is obtained as the intercept on the voltage axis of the linear C–V relationship plot of an intimate

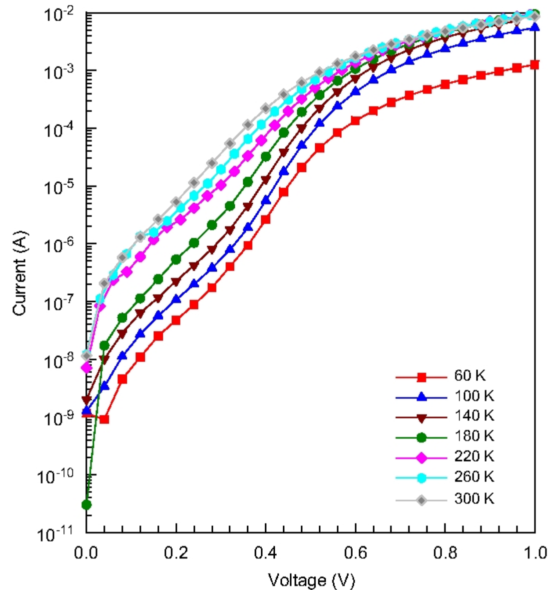

Fig. 1. Semilogarithmic current–voltage (I–V) characteristics as a function of temperature, T.

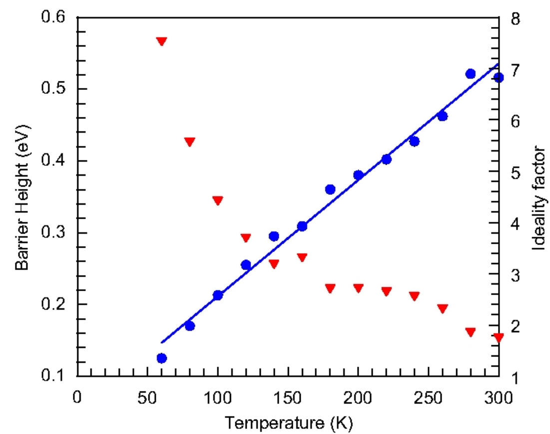

Fig. 2. I–V barrier height and ideality factor versus temperature, T.

Please cite this article as: W. Mtangi, et al., Physica B (2009), doi:10.1016/j.physb.2009.09.022

ARTICLE IN PRESS

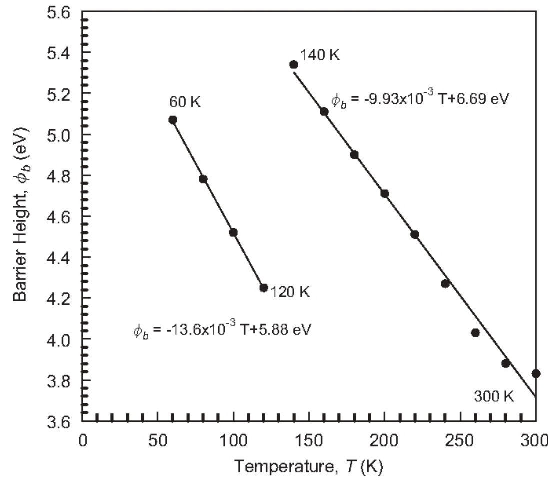

Fig. 3. Capacitance–voltage (C–V) barrier height, $\Phi_{C\text{–}V}$ versus temperature, T.

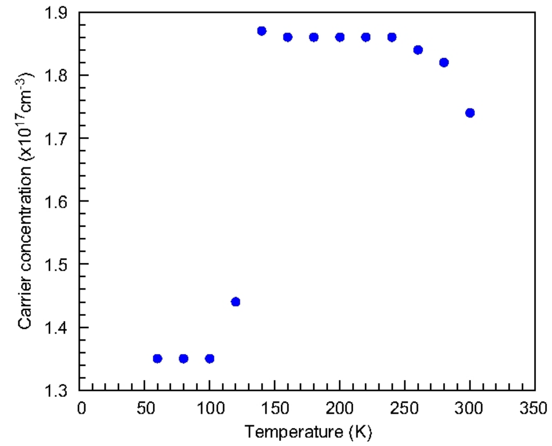

Fig. 4. Carrier concentration versus temperature, T.

Schottky barrier assuming a uniformly doped material, given by [14],

$$\frac{1}{C^2} = \frac{2V}{A^2 q \varepsilon_s N_D} \quad (7)$$

where N_D is the impurity concentration obtained as the gradient of the C^{-2} versus V plot, A is the Schottky contact area and ε_s is the semiconductor dielectric constant. The intercept on the voltage axis was found to be large, of the order of 5.05 V (at 60 K) to 3.67 V (at 300 K). This influenced the values of the measured C–V barrier heights to yield values larger than the energy gap, E_g of ZnO = 3.37 eV at room temperature. Such large barrier heights, larger than the energy gap of semiconductor material have been observed by Chi et al. [15] on NiGe/n-Ge Schottky contacts, Dos Santos et al. [14] on the Schottky contacts deposited on PbSe, where the barrier height was obtained to be twice as large as the energy gap and Walpole and Nill (1971) on PbTe and InAs [16]. This behaviour of the barrier heights being larger than the band gap energy has been explained by some researchers [14,15], as being due to the existence of an inversion layer with high charge density that causes the maximum electric field in the space charge region to attain high values even with moderate doping concentrations [15]. The variation of the barrier height with temperature has enabled us to fit two linear regions to the barrier height values i.e. the first region being linear from 60 to 120 K and the second being linear from 140 to 300 K yielding equations of the form,

$$\phi_{C-V}(T_{60-120}) = \phi(T=0) + \alpha_1 T \quad (8)$$

where α_1 is the temperature coefficient of the semiconductor in the 60–120 K temperature range which was obtained as $-13.6\,\text{meV}\,\text{K}^{-1}$, and

$$\phi_{C-V}(T_{140-300}) = \phi(T=0) + \alpha_2 T \quad (9)$$

where α_2 is the temperature coefficient in the 140–300 K temperature range which was obtained as $-9.93\,\text{meV}\,\text{K}^{-1}$. The variation of carrier concentration with temperature in Fig. 4 also shows a sudden increase in carrier concentration from 120–140 K. We propose that the discontinuity resulting in the two distinct linear regions has been caused by a defect within the ZnO material which was observed using deep level transient spectroscopy (DLTS) at an energy level of 0.31 eV below the conduction band

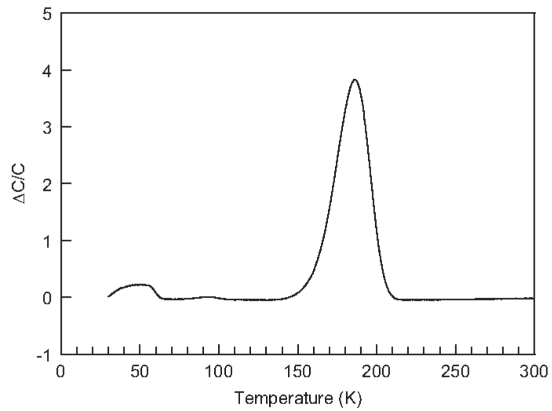

Fig. 5. DLTS signal for the as-deposited Pd/ZnO Schottky diode. This spectra was measured at quiescent reverse bias of −2 V, filling pulse of V_p = 0 V and rate window of 80 s^{-1}.

with a trap concentration of between 4×10^{16} and $6 \times 10^{16}\,\text{cm}^{-3}$ as shown in Fig. 5. This defect traps carriers at low temperatures, i.e. it fills up at low temperatures and releases them at high temperatures causing the variation of the measured capacitance and hence a difficulty in obtaining the barrier height in the 120–130 K temperature range. The capacitance transient causes a sudden change in carrier concentration between 120 and 140 K.

4. Conclusion

The barrier height of Pd Schottky contacts on ZnO from the I–V measurements, Φ_{I-V} has shown an increasing trend with an increasing temperature a trend that disagrees with the negative temperature coefficient of semiconductor material. From the C–V measurements, the variation of the barrier height Φ_{C-V} with temperature agrees well with the negative temperature coefficient of semiconductor material. The temperature coefficients have been

Please cite this article as: W. Mtangi, et al., Physica B (2009), doi:10.1016/j.physb.2009.09.022

UNIVERSITEIT VAN PRETORIA
UNIVERSITY OF PRETORIA
YUNIBESITHI YA PRETORIA

ARTICLE IN PRESS

calculated as $-13.6\,\mathrm{meV\,K^{-1}}$ (60–120 K) and $-9.93\,\mathrm{meV\,K^{-1}}$ (140–300 K). The barrier height that is larger than the band gap energy from C–V measurements is due to the presence of an "inversion layer" in the semiconductor closer to the metal that modifies the electric field, influencing the junction capacitance and hence the value of the built in potential on the voltage intercept.

Acknowledgement

This work has been made successful through the financial support from the South Africa National Research Foundation.

References

[1] E. Gur, S. Tuzemen, B. Kilic, C. Coskun, J. Phys. Condes. 19 (2007).
[2] J.D. Albrecht, P.P. Ruden, S. Limpijumnong, W.R.L. Lambrecht, K.F.J. Brennan, Appl. Phys. 86 (1999) 6864.
[3] D.I. Flourescu, L.G. Mourokh, F.H. Pollak, D.C. Look, G. Cantwell, X.J. Li, Appl. Phys. 91 (2002) 890.
[4] C. Coskun, D.C. Look, G.C. Farlow, J.R. Sizelove, Semicond. Sci. Technol. 19 (2004) 752.
[5] H. Morkoc, S. Strite, G.B. Gao, M.E. Lin, B. Sverdlov, M.J. Burns, Appl. Phys. 76 (1994) 1363.
[6] R.T. Tung, Mat. Sci. Eng. 35 (2001) 1.
[7] S. Karatas, S. Altindal, Sol. Stat. Elect. 49 (2005) 1052.
[8] E.H. Rhoderick, Metal-Semiconductor Contacts, 2nd ed., Oxford University Press, Oxford, 1988.
[9] H.C. Card, E.H. Rhoderick, J. Phys. D 4 (1971) 1589.
[10] B.G. Yacobi, Semiconductor Materials: An Introduction to Basic Principles, Springer, Berlin, 2003.
[11] A. Gumus, A. Turut, N. Yalcin, J. Appl. Phys. 91 (2002).
[12] J.H. Werner, H.H. Guttler, J. Appl. Phys. 73 (3) (1993).
[13] S.M. Sze, Physics of Semiconductor Devices, Wiley, New York, 1981.
[14] O. Dos Santos, V. Mathet, C. Fau, S. Charar, M. Averous, Sol. Stat. Electron. 39 (1996) 813.
[15] D.Z. Chi, R.T.P. Lee, S.J. Chua, J. Appl. Phys. 97 (2005) 113706.
[16] H.K. Henisch, Semiconductor Contacts, Clarendon Press, Oxford, 1994.

Please cite this article as: W. Mtangi, et al., Physica B (2009), doi:10.1016/j.physb.2009.09.022

Chapter 6: Conclusions

ZnO has been successfully characterized electrically by use of different techniques. The measured TDH data fitted well to a model with two s-like donors and one acceptor on the as-received melt grown ZnO samples. The two donors have been explained to be Zn_i related or hydrogen complex related and Al related. The mobility peak for the as-received samples has been measured as 1250 cm^2/Vs. After hydrogen peroxide treatment, the peak mobility increased to about 1400 cm^2/Vs. Surface conduction has proved to be dominant in the low temperature region, influencing the determination of the surface donor concentration at low temperatures. However, a model has been used to calculate accurately the surface donor volume concentrations at low temperatures.

Annealing studies of the hydrogen peroxide treated ZnO samples indicate the increase in surface conduction with increase in annealing temperature. Surface donor volume concentrations have been shown to increase with an increase in annealing temperature. The peak mobility for these samples shows a decreasing trend with increasing annealing temperature. Further investigations need to be carried out to determine the effects of decreasing mobility with annealing, e.g. Rutherford Backscattering Spectroscopy, to check the effects of annealing on the crystalline structure of the samples.

Schottky contacts to ZnO were successfully fabricated after treatment with hydrogen peroxide. High orders of rectification have been observed at room temperatures for the Pd and Au Schottky contacts. An investigation carried out on the quality of the contacts formed by the two different metals reveals that Pd forms a better contact to ZnO, with a high rectification behaviour, low series resistance, low leakage currents and high barrier heights.

The Schottky contacts to ZnO have also revealed a strong dependence on temperature. At high temperatures, i.e. close to room temperature, the current transport mechanism has proved to be predominantly thermionic while at low temperatures, the contacts have shown the dominance of other mechanisms, other than pure thermionic emission. Current-voltage and capacitance-voltage techniques have been used to measure the barrier heights on the Schottky contacts. From the current voltage measurements, the barrier height has proved to be affected by barrier inhomogeneities leading to a trend in which the SBH increases with an

increase in temperature, a trend that disagrees with the negative temperature coefficient of the II-VI compound semiconductor material. The barrier heights obtained from the capacitance voltage measurements have revealed a decrease in barrier height with temperature, a phenomena which agrees well with the properties of the semiconductor material.

Schottky contacts to ZnO have also shown a strong dependence on the polarity of the ZnO material, with the Zn-polar face producing contacts of the best quality compared to the ones on the O-polar face as discussed in section 5.2 of chapter 5.

Concluding from the TDH results, annealing of Schottky contacts to ZnO at temperatures above 200°C can lead to a loss in the rectification behaviour as surface conduction will start to contribute to current flow. Further studies need to be carried out to investigate the effects of annealing on rectification behaviour of the Schottky contacts to ZnO. Also to characterize the deep level defects in ZnO, Deep Level Transient Spectroscopy (DLTS) measurements need to be performed on the Schottky contacts.